学位論文

Role of crossed ladder diagrams in the diquark Bethe-Salpeter equation

(ダイクォークのベーテ・サルペーター方程式における
交差型はしごダイアグラムの役割)

平成 27 年 12 月博士（理学）申請

東京大学大学院理学系研究科
物理学専攻
三嶋　剛

Abstract

We point out that the completely crossed ladder diagrams in diquark Green's function are enhanced due to their color factors. We perform a resummation of the completely crossed ladder diagrams with an arbitrary number of gluon-exchange, incorporating a simple model of dressed gluon propagator and dressed quark-gluon vertex. As a result of our analysis, we show that there is a bound-state solution to the diquark Bethe-Salpeter equation, which was thought to be absent previously. Some interpretations of our result in the context of phenomenological diquark models for baryons and exotic mesons are given, and our result turns out to be consistent with them.

We anticipate that the completely crossed ladder diagrams in the diquark Green's function will play a key role in the study of the infrared behavior of QCD.

This thesis is based on a paper collaborated with R. Jinno, and T. Kitahara "Diquark bound states with a completely crossed ladder truncation, " Phys. Rev. D91 (2015) 076011 [1].

Contents

1 Introduction **2**
- 1.1 Motivation . . . 2
- 1.2 Highlight and outline of this thesis . . . 4
- 1.3 Color, Spin, Flavor and Parity of Diquarks . . . 5
- 1.4 Hadron spectroscopy and diquark models . . . 6
  - 1.4.1 Baryon and diquark models . . . 6
  - 1.4.2 Meson and diquark models . . . 9

2 Functional approach to hadrons **12**
- 2.1 Baryon as a pole of three-quark Green's function . . . 12
- 2.2 Dyson-Schwinger equation and quark propagator . . . 15
- 2.3 Bethe-Salpeter equation and diquark . . . 21

3 Crossed ladder diagrams in the diquark Bethe-Salpeter equation **23**
- 3.1 Green's functions of two quarks in light of the 't Hooft limit . . . 24
  - 3.1.1 Double line notation in the diquark Green's function . . . 26
  - 3.1.2 Comment on the application of t' Hooft limit to the diquark . . . 28
  - 3.1.3 Color factors of various two-quark Green's functions in SU(3) QCD . . . 29
- 3.2 Application to the Munczek-Nemirovsky model . . . 32
  - 3.2.1 Finite fixed order truncations . . . 32
  - 3.2.2 Resummation of the completely crossed ladder diagrams . . . 41
  - 3.2.3 Interpretation of the results and discussion . . . 47

4 Summary **53**

A Kugo-Ojima confinement of diquarks **55**

Chapter 1

Introduction

1.1 Motivation

In 1964, Gell-Mann [2] and Zweig [3] independently proposed a model which is now called quark model to explain the observed mass spectra of mesons and baryons. Since then, the quark model has been a successful model in reproducing various hadronic phenomena. Its history is few years longer than that of Quantum Chromodynamics (QCD) [4, 5, 6, 7], and this means that some aspects of hadrons are well describable without knowing detailed dynamics of quark and gluon. Even today, baryon spectra including excited states are calculated only by the quark models, or more precisely, the constituent quark models.

Among various ideas in the quark model, one of the most important ones to explain the nature well is a strong correlation of two quarks inside hadron, namely, a concept of diquark correlation. It appeared at the very beginning of the quark model [2] and was applied to reproduce the observed baryon spectra by Ida, Kobayashi [8] and Lichtenberg, Tassie [9]. If we naively apply the quark model to baryon spectra, too much excited states are predicted. This is called "missing resonance problem" and not yet fully solved, but consideration of the strong diquark correlation is known to improve this long-standing problem. So far, the constituent quark models together with the diquark correlation seem to work very well, or at least, no other method can reproduce baryon spectra better than them.

Taking a look at resent progress of hadron physics, one of hot topics is the study of exotic hadrons, and the strong diquark correlation is also playing an essential role to describe the observed properties of exotic hadrons.

However, many things are left unknown when we treat the diquarks in terms of QCD. Current phenomenological successes are consequences of some assumptions about properties of diquark, but most of them are not derived from QCD. At present, they are just assumptions.

Ultimately we want to understand all of hadron phenomena based on QCD only, and to this end, understanding of the interaction between two quarks in the infrared region is demanded. One standard way to investigate such the diquark system is the use of Bethe-Salpeter equation, but there is very little knowledge about which kinds of diagrams to be included in the diquark Bethe-Salpeter kernel. In fact, it is controversial issue whether or not the diquark Bethe-Salpeter equation has a bound-state solution. The origin of the "abnormally strong force" between two quarks which

is needed to form the phenomenologically-preferred strong diquark correlation is also left to be a mystery.

The motivation of this thesis is summarized in the words by Lichtenberg [10], who is one of pioneers of this field:

> I hope that some time in the future, physicists will be able to calculate with non-perturbative QCD (or with some successor theory), and two-quark correlations (di-quarks) will be the output rather than the input.

We believe this thesis gives an essential progress toward the goal.

1.2 Highlight and outline of this thesis

The novelty of this thesis is a finding that the completely crossed ladder diagrams like

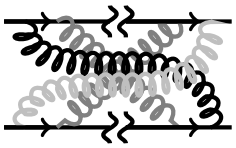

give a significant effect to the diquark Green's function. We show this fact in two ways: first, based on discussions in light of the 't Hooft limit, and second, based on explicit calculations using a simple model of dressed gluon propagator and dressed quark-gluon vertex.

Besides, we suggest that the diquark Bethe-Salpeter equation has a bound-state solution, which has been thought to be absent previously.

Outline

The rest of this chapter is devoted to an introduction of the diquarks in a phenomenological point of view. In §1.3, the diquark states are classified according to their symmetry and corresponding diquark operators are introduced. In §1.4, theoretical attempts to reproduce hadron spectra are reviewed with emphasis on the roles of diquarks.

In chapter 2, we review the studies of hadrons based on QCD with functional methods and introduce the diquark Bethe-Salpeter equation, which is the main subject of this thesis.

Chapter 3 is the main part of this thesis and is based on the work collaborated with R. Jinno and T. Kitahara [1]. In §3.1, we introduce the 't Hooft limit and apply it to the diquark Green's function. In §3.1.1, we find that all the completely crossed ladder diagrams of the diquark Green's function are the leading order of 't Hooft limit in contrast to the case of meson. In §3.1.2, we discuss the validity of results obtained under the 't Hooft limit, and in §3.1.3, we see the color-factor enhancement actually occurs in the case of $N_c = 3$. In §3.2, we solve the diquark Bethe-Salpeter equation with the Munczek-Nemirovsky model, and investigate whether or not it has a bound-state solution. In §3.2.1, we examine truncation schemes in which the completely crossed n-gluon exchange diagrams are included in the Bethe-Salpeter kernel up to n, and we find that the truncation schemes with finite n-gluon exchange are not sensible. In §3.2.2, we perform a resummation of the completely crossed ladder diagrams, and find that there is a bound-state solution in the diquark Bethe-Salpeter equation. In §3.2.3, we give interpretations and discussions of our result.

Finally, in chapter 4, we summarize this thesis.

Appendix A is devoted to a brief review of the BRST quantization of QCD and the Kugo-Ojima confinement mechanism, which are used in §3.2.3.

1.3 Color, Spin, Flavor and Parity of Diquarks

In this section, we classify possible diquark states in terms of their symmetries—color, spin, flavor, and parity. In the diquark system, an interchange of the two quarks should generate minus sign to the state, which is the product of symmetric factors of color, spin, flavor, and spacial excitation. The color representation of the diquark system is either anti-fundamental or sextet representation corresponding to the antisymmetric and symmetric state respectively. When we consider the three-flavor theory, it is convenient to use an enlarged symmetry group $\mathrm{SU}(6) \supset \mathrm{SU}_{\mathrm{spin}}(2) \otimes \mathrm{SU}_{\mathrm{flavor}}(3)$ to classify the states. The irreducible representations of diquark systems are

$$[6] \otimes [6] = [21]_{\text{symmetric}} \oplus [15]_{\text{antisymmetric}}, \tag{1.1}$$

where, in the $\mathrm{SU}_{\mathrm{spin}}(2) \otimes \mathrm{SU}_{\mathrm{flavor}}(3)$ representation,

$$[21]_{\text{spin-flavor}} = [0_{\text{spin}}, \bar{3}_{\text{flavor}}] \oplus [1_{\text{spin}}, 6_{\text{flavor}}], \quad [15]_{\text{spin-flavor}} = [1_{\text{spin}}, \bar{3}_{\text{flavor}}] \oplus [0_{\text{spin}}, 6_{\text{flavor}}]. \tag{1.2}$$

The symmetric factor of spacial excitation is $(-1)^\ell$ where ℓ is the relative orbital angular momentum. Parity of the system is the product of intrinsic parity and $(-1)^\ell$.

In this thesis, we consider the color anti-fundamental diquarks because they are the ones inside baryons. One important assumption in the diquark models which we will see in the next section (§1.4.1) is that only the spacial ground states ($\ell = 0$) are relevant. In other words, the spacial excitation is assumed to need large energy. Some indications of the large excitation energy from functional methods are available [11, 12, 13], and we accept this assumption when we review the phenomenology of diquarks in §1.4. Under these consideration, the only possible spin-flavor representation is $[21]_{\text{symmetric}}$ states, and the total parity is determined by the intrinsic parity only. Since the intrinsic parity of quark is set to be positive, the total parity of ground state diquark system is positive. We summarized the low-lying diquark states in Tab.1.1 with mesons for the sake of comparison.

The local operators of $[0_{\text{spin}}, \bar{3}_{\text{flavor}}]$ and $[1_{\text{spin}}, 6_{\text{flavor}}]$ diquark states are

$$\mathfrak{O}^{i\mathfrak{a}}_{qq0^+} = \epsilon^{ijk}\epsilon^{\mathfrak{abc}}\psi^{\mathrm{T}}_{j\mathfrak{b}} C\gamma_5 \psi_{k\mathfrak{c}}, \qquad \mathfrak{O}^{i\mathfrak{ab}\mu}_{\mathrm{qq}1^+} = \epsilon^{ijk}\left(\psi^{\mathrm{T}}_{j\mathfrak{a}} C\gamma^\mu \psi_{k\mathfrak{b}} + \psi^{\mathrm{T}}_{j\mathfrak{b}} C\gamma^\mu \psi_{k\mathfrak{a}}\right), \tag{1.3}$$

respectively, where i, j, k are the color indices, $\mathfrak{a}, \mathfrak{b}, \mathfrak{c}$ are the flavor indices, ϵ^{ijk} is the Levi-Civita tensor, and $C = -\mathrm{i}\gamma_0\gamma_2$ is the charge conjugate matrix. Throughout this thesis, the local composite operators like Eqs.(1.3) are considered to be the normal ordered operators.

Note that there is γ_5 in the scalar diquark operator and not in the axial-vector diquark operator contrary to the case with mesons. This is a consequence of the fact that quark and anti-quark has opposite intrinsic parity, or in other words, the charge conjugation operator has odd parity, if we assign parities for each operators. In another point of view, when we express the scalar diquark operator using the left-handed ψ_L and right-handed ψ_R operators, it becomes like $\psi_L\psi_L$ or $\psi_R\psi_R$ that is contrary to the case of pion $\sim \bar{\psi}_L\psi_R$. [See Tab.1.1.]

Table 1.1: The low-lying states of diquarks and mesons and their total angular momentum J and parity P.

	diquark		meson	
spin & chirality	singlet $(\psi_{\rm R}\psi_{\rm R})$	triplet $(\psi_{\rm L}\psi_{\rm R})$	singlet $(\bar{\psi}_{\rm L}\psi_{\rm R})$	triplet $(\bar{\psi}_{\rm R}\psi_{\rm R})$
$J^P(\ell=0)$	0^+	1^+	0^-	1^-
$J^P(\ell=1)$	1^-	$0^-, 2^-$	1^+	$0^+, 2^+$

1.4 Hadron spectroscopy and diquark models

In this section, we briefly review the current status of theoretical attempts to understand hadron spectra and introduce diquarks as key ingredients in some of these studies. The major methods to calculate hadron masses are perturbative QCD, lattice simulation and functional approach like the use of Bethe-Salpeter equation. At present, most of observed hadrons are reproduced with them, but some hadrons still remain to be done. The examples of those hadrons are exited baryons, tetraquarks and pentaquarks. The concept of diquark is important to investigate those hadrons.

In §1.4.1, we review baryon spectroscopy and explain the long-standing "missing resonance problem," discussing how the diquark improves this problem. We also comment on the recently observed pentaquarks and their relation to diquarks. In §1.4.2, we first review successful achievements to reproduce the conventional meson spectra. Next we consider exotic mesons which are not expressed as ordinary quark-antiquark bound states, and also consider diquark models for them.

1.4.1 Baryon and diquark models

The quark model was suggested originally to explain the mass spectra of mesons and baryons [2, 3], and even today, this is the best way to study baryon spectra including higher excited states. The lattice simulations become more and more powerful recently but restricted to the lower-lying baryons at present [14, 15, 16, 17, 18]. The functional approach, which will be explained in §2.1, is also attractive but restricted to the low-lying states [19, 20, 21, 22]. In the rest of this subsection, we consider the constituent quark model.

Using the spin-flavor representation, the irreducible representation of three-quark state is

$$[6]\otimes[6]\otimes[6] = [56]_{\rm symmetric}\oplus[70]_{\rm mixed}\oplus[70]_{\rm mixed}\oplus[20]_{\rm antisymmetric}, \tag{1.4}$$

where, in the $\mathrm{SU}_{\rm spin}(2)\otimes\mathrm{SU}_{\rm flavor}(3)$ representation,

$$[56]_{\rm symmetric} = [3/2_{\rm spin}, 10_{\rm flavor}]\oplus[1/2_{\rm spin}, 8_{\rm flavor}], \tag{1.5}$$

$$[70]_{\rm mixed} = [1/2_{\rm spin}, 10_{\rm flavor}]\oplus[3/2_{\rm spin}, 8_{\rm flavor}]\oplus[1/2_{\rm spin}, 8_{\rm flavor}]\oplus[1/2_{\rm spin}, 1_{\rm flavor}], \tag{1.6}$$

$$[20]_{\rm antisymmetric} = [3/2_{\rm spin}, 1_{\rm flavor}]\oplus[1/2_{\rm spin}, 8_{\rm flavor}]. \tag{1.7}$$

The spacial wave functions are also classified to be symmetric, mixed symmetric, antisymmetric and the combination of spin-flavor and spacial symmetry should be totally symmetric. This is the basic feature of the quark model.

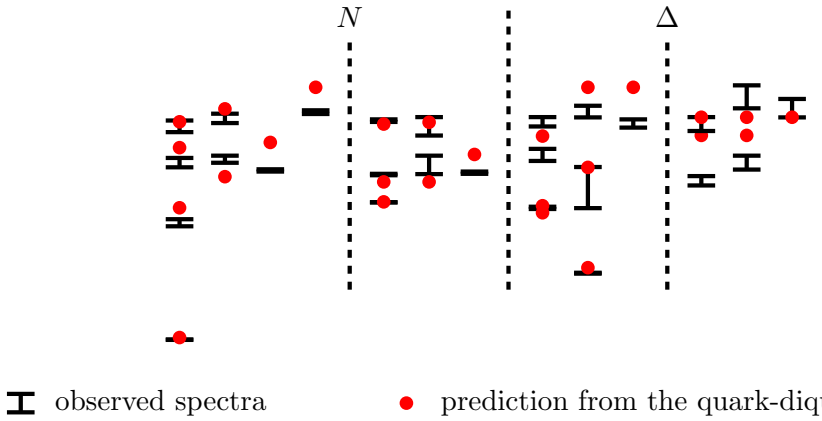

Figure 1.1: The baryon mass spectra calculated using a diquark-model [24], and that from Particle Data Group [26].

However, it is known that if we naively apply the quark model, too much excited states are predicted. This is called "missing resonance problem", and not yet fully solved. According to PDG2014 [23], only 14 states out of 45 predicted N states below 2.4 GeV are established, and 10 states are tentative. This problem was regarded seriously already in 1966, leading Ida and Kobayashi to suggest a diquark model as a partial solution to the problem [8].

The essential feature of the diquark models are the following: as stated in §1.3, we assume that only the diquarks of spacial ground states are relevant to baryon spectra. In this case, the spacial wave function can not be antisymmetric. Therefore, the spin-flavor antisymmetric state (1.7) disappears from the predicted baryon spectrum. Furthermore, the parity of baryon is determined as $(-1)^L$ where L is the orbital angular momentum of the quark-diquark system. This is because the intrinsic parity of the diquark ground state is positive. [See Tab.1.1.] Then the states with $L^P = 1^+, 2^-, ...$ disappear from the predicted baryon spectrum. Above two reductions are the major advantage of the diquark models, and in models with more concrete interactions, further reduction can be achieved. In one of the latest studies based on the constituent quark-diquark model, 14 N states are reproduced with 3 missing states, and 12 Δ, 10 Σ , 2 Ξ, 9 Λ states are reproduced with 0, 2, 2, 8 missing states respectively [24]. They consider one constituent quark and one constituent diquark, and the interaction between them is modeled with 11 parameters. In addition, the constituent quark mass and the constituent diquark mass are treated as fitting parameters. The resultant spectra is displayed in Fig.1.1 for the N and Δ sector. Is is also reported that if we restrict to the non-strange (N, Δ) sector below 2 GeV, the missing resonance problem can be fully solved in a similar method [25]. The above is a typical way to investigate the baryon spectra, but the discussion based on the specific constituent model seems to have large model dependence, so let us see the situation in a less model dependent way next.

In order to illustrate the effectiveness of diquark in a transparent way, we compare the non-strange baryon spectra calculated using their symmetry only [27] and that of Baryon Summary Table in PDG2014 [23] in Tab.1.2. In Ref.[27], the dynamics inside baryon is not specified, and a mass formula from various symmetry with 7 fitting parameters is derived. The Tab.1.2 shows that only 12 out of 33 predicted states are observed in the N-sector below 2 GeV. In the Δ-sector

Table 1.2: Comparison between the predicted mass spectrua [27] and the Baryon Summary Table of PDG2014 [23] in the N and Δ sector below 2 GeV. The masses are written in the unit of MeV. We use the notation in which $^2 8$ stands for $[1/2_{\rm spin}, 8_{\rm flavor}]$ of Eqs.(1.5), (1.6), (1.7), and $^4 8$ stands for $[3/2_{\rm spin}, 8_{\rm flavor}]$ of Eq.(1.6), and $^2 10$ stands for $[1/2_{\rm spin}, 10_{\rm flavor}]$ of Eq.(1.6), and $^4 10$ stands for $[3/2_{\rm spin}, 10_{\rm flavor}]$ of Eq.(1.5), and the subscripts are the total angular momentum. The brackets represent the spin-flavor representation and the orbital angular momentum. The blanks mean the missing states, and the states with parentheses are those disappear if we take into account the diquark correlation.

State	Predicted mass [27]	Observed state [23]						
$^2 8_{1/2}[56, 0^+]$	939	$N(939)$	$^2 8_{1/2}[70, 1^-]$	1566	$N(1535)$	$^2 8_{3/2}[70, 1^-]$	1566	$N(1520)$
$^4 8_{1/2}[70, 1^-]$	1680	$N(1650)$	$^4 8_{3/2}[70, 1^-]$	1680	$N(1700)$	$^4 8_{5/2}[70, 1^-]$	1680	$N(1675)$
$(^2 8_{1/2}[20, 1^+])$	1720		$(^2 8_{3/2}[20, 1^+])$	1720		$^2 8_{3/2}[56, 2^+]$	1735	
$^2 8_{5/2}[56, 2^+]$	1735	$N(1680)$	$(^2 8_{3/2}[70, 2^-])$	1875		$(^2 8_{5/2}[70, 2^-])$	1875	
$^2 8_{3/2}[70, 2^+]$	1875	$N(1900)$	$^2 8_{5/2}[70, 2^+]$	1875		$(^4 8_{1/2}[70, 2^-])$	1972	
$(^4 8_{3/2}[70, 2^-])$	1972		$(^4 8_{5/2}[70, 2^-])$	1972		$(^4 8_{7/2}[70, 2^-])$	1972	
$^4 8_{1/2}[70, 2^+]$	1972		$^4 8_{3/2}[70, 2^+]$	1972		$^4 8_{5/2}[70, 2^+]$	1972	
$^4 8_{7/2}[70, 2^+]$	1972		$^2 8_{1/2}[56, 0^+]$	1440	$N(1440)$	$^2 8_{1/2}[70, 1^-]$	1909	
$^2 8_{3/2}[70, 1^-]$	1909	$N(1875)$	$^2 8_{1/2}[70, 0^+]$	1710	$N(1710)$	$^4 8_{3/2}[70, 0^+]$	1815	$N(1720)$
$^2 8_{1/2}[56, 1^-]$	1866		$^2 8_{3/2}[56, 1^-]$	1866		$(^2 8_{1/2}[70, 1^+])$	1997	
$(^2 8_{3/2}[70, 1^+])$	1997		$^2 8_{1/2}[70, 1^-]$	1997		$^2 8_{3/2}[70, 1^-]$	1997	
$^4 10_{3/2}[56, 0^+]$	1232	$\Delta(1232)$	$^2 10_{1/2}[70, 1^-]$	1649	$\Delta(1620)$	$^2 10_{3/2}[70, 1^-]$	1649	$\Delta(1700)$
$^4 10_{1/2}[56, 2^+]$	1909	$\Delta(1910)$	$^4 10_{3/2}[56, 2^+]$	1909	$\Delta(1920)$	$^4 10_{5/2}[56, 2^+]$	1909	$\Delta(1905)$
$^4 10_{7/2}[56, 2^+]$	1909	$\Delta(1950)$	$(^2 10_{3/2}[70, 2^-])$	1945		$(^2 10_{5/2}[70, 2^-])$	1945	$\Delta(1930)$
$^2 10_{3/2}[70, 2^+]$	1945		$^2 10_{5/2}[70, 2^+]$	1945	$^{**}\Delta(2000)$	$^4 10_{3/2}[56, 0^+]$	1646	$\Delta(1600)$
$^2 10_{1/2}[70, 1^-]$	1977	$^{**}\Delta(1900)$	$^2 10_{3/2}[70, 1^-]$	1977	$^{**}\Delta(1940)$	$^2 10_{1/2}[70, 0^+]$	1786	$^*\Delta(1750)$

below 2 GeV, 9 out of 15 predicted states are confirmed and 4 states are regarded as "tentative" in PDG2014 [23]. Inclusion of the strange baryons makes the situation even worse. In the Tab.1.3, the mass spectra of the flavor octet $(N, \Sigma, \Lambda, \Xi)$ and decuplet $(\Delta, \Sigma^*, \Xi^*, \Omega)$ calculated in the same method are summarized [28], and their levels of evidence is illustrated by the single dagger (3- or 4- star status) and the double dagger (1- or 2- star status) in PDG2014 [23]. In the Tab.1.3, only 38 out of 128 predicted states are observed. This is the missing resonance problem. Note that the counting of states are different in Tab.1.2 and Tab.1.3 since the spin-multiplets are identified as a same state in the Tab.1.3 for simplicity. In any case, the major part of predicted baryon spectra is missing. Applying the two reductions explained above, the states with parentheses disappear.

To summarize this section, the excited baryon spectrum is not yet fully reproduced ("missing resonance problem"), but the consideration of diquark correlation improve the situation well.

pentaquark states

In July 2015, LHCb collaborations announced that they observed resonances corresponding to pentaquark states [29]. They analyzed the three body decay of Λ_b^0 baryon into $J/\psi\ K^-\ p$, and found resonances in the invariant mass of $J/\psi\ p$ channel. Soon after, many attempt to explain the pentaquark resonances using the diquark models appeared. At present, it is premature to conclude what kind of treatment is better, but it is worth noting that diquark models is playing important role [30, 31, 32, 33, 34, 35, 36, 37].

There is another pentaquark candidate which was announced to be observed in 2003 by LEPS collaboration [38]. The statistical significance of the peak was 4.6 σ, and later it became 5.1 σ

Table 1.3: The mass spectra of the flavor octet $(N, \Sigma, \Lambda, \Xi)$ and decuplet $(\Delta, \Sigma^*, \Xi^*, \Omega)$ baryon predicted using the symmetries of baryons [28]. The single daggered states are confirmed and the double daggered states are tentative in PDG2014 [23]. In this table, the spin-multiplets are identified as a same state, so the total angular momentum J is not specified explicitly. Other notation of the label of states are the same as that of Tab.1.2. The states with orange daggers are listed as observed states in PDG2014 but not in Ref.[28], which was published in 2000. The blanks mean the missing states, and the states with parentheses are those disappear in the diquark models.

State	N	Σ	Λ	Ξ	State	N	Σ	Λ	Ξ
$^2 8_J[56, 0^+]$	939 †	1170 †	1133 †	1334 †	$^2 8_J[70, 1^-]$	1563 †	1711 †	1686 †	1828 †
$^4 8_J[70, 1^-]$	1683 †	1822 †	1799 †	1932	$(^2 8_J[20, 1^+])$	1713	1849 ‡	1826 †	1957
$^2 8_J[56, 2^+]$	1737 †	1872 †	1849 †	1979	$^2 8_J[70, 2^+]$	1874 ‡	1999	1978	2100
$(^2 8_J[70, 2^-])$	1874 †	1999	1978	2100	$^4 8_J[70, 2^+]$	1975	2095 ‡	2074 †	2191
$(^4 8_J[70, 2^-])$	1975	2095 ‡	2074 †	2191	$^2 8_J[56, 0^+]$	1444 †	1604 †	1577 †	1727
$^2 8_J[70, 1^-]$	1909	2033 †	2012	2132	$^4 8_J[70, 1^-]$	2009	2127	2107	2222
$(^2 8_J[20, 1^+])$	2034	2150	2130	2244	$^2 8_J[70, 0^+]$	1683 †	1822 ‡	1799 †	1932
$^4 8_J[70, 0^+]$	1796 †	1926 ‡	1904	2030	$^2 8_J[56, 1^-]$	1847	1974 †	1952	2076
$^2 8_J[70, 1^-]$	1975	2095	2074	2191	$(^2 8_J[70, 1^+])$	1975	2095 ‡	2074	2191
$^4 8_J[70, 1^-]$	2072	2186	2167	2278	$(^4 8_J[70, 1^+])$	2072	2186	2167	2278
$(^2 8_J[20, 1^-])$	2096	2209	2190	2300					

State	Δ	Σ^*	Ξ^*	Ω	State	Δ	Σ^*	Ξ^*	Ω
$^4 10_J[56, 0^+]$	1246 †	1382 †	1524 †	1670 †	$^2 10_J[70, 1^-]$	1649 †	1755 †	1869	1989
$^4 10_J[56, 2^+]$	1921 †	2012 †	2112	2219	$^2 10_J[70, 2^+]$	1946 ‡	2037	2135	2242
$(^2 10_J[70, 2^-])$	1946 †	2037	2135	2242	$^4 10_J[56, 0^+]$	1660 †	1765 ‡	1878	1998
$^2 10_J[70, 1^-]$	1981 ‡	2070	2167	2272	$^2 10_J[70, 0^+]$	1764 ‡	1863 ‡	1970	2085
$^4 10_J[56, 1^-]$	2020	2107	2203	2306	$^2 10_J[70, 1^-]$	2044	2131	2225	2327
$(^2 10_J[70, 1^+])$	2044	2131	2225	2327					

[39]. Inspired by this observation, comprehensive studies of diquark models to reproduce this state have been done. [See Ref.[40].] Note that the latest publication by the member of the LEPS collaboration shows the significance of the signal reduces to 3.6-3.8 σ by incorporating new data set [41], The present status of other experiments are summarized in Ref.[42].

1.4.2 Meson and diquark models

There are various methods to study meson spectra depending on their mass scale. Among them, the most established one is the perturbative QCD calculation, which is valid for heavy quarkonium states. The prime example is bottomonium [43], which requires essentially only one fitting parameter ($\bar{m}_b$) and one input parameter ($\alpha_S(m_Z)$) to reproduce mass spectra. [See Fig.1.2.]

In the case of charmonium, the perturbative QCD calculation is applicable for some lower-lying charmonium states [44], but higher excited states turn out to be difficult to deal with so far because the relevant energy scale tends to be small and the convergence of coupling perturbation becomes worse. For those excited states, an effective potential model is applied, which possesses four fitting parameters including the charm quark mass [45].

In the above heavy quarkonium states, the masses of mesons are essentially expressed as "the pole masses of quark and antiquark + binding energy (potential energy)," and this potential picture gives us an intuitive understanding of the bound states.

However, when one or both of quarks are light like up, down and strange quark, the poten-

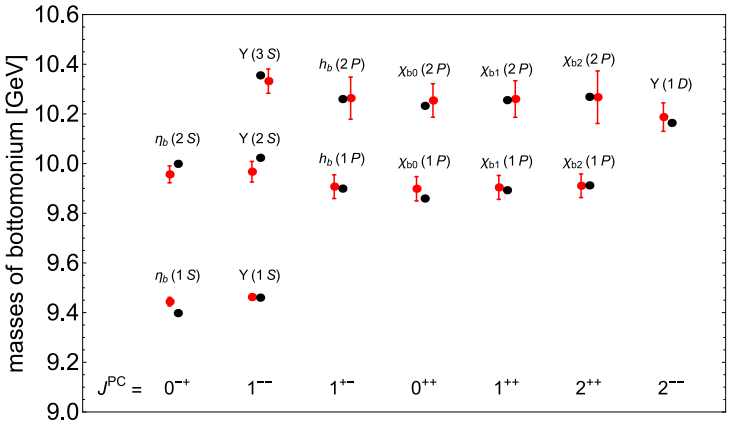

Figure 1.2: Comparison of the observed bottomonium spectra [23] (black bullets) and those calculated by the perturbative QCD [43] (red bullets). We set the theoretical uncertainties as the differences between the predictions at NNLO and those at NNNLO for each states. The experimental uncertainty is quite small and negligible here.

tial picture above is not available. In this case, the functional method is effective. For example, $\pi, \rho, a, b, \eta, \phi, f, K$ are rather well reproduced by the Dyson-Schwinger method together with the Maris-Tandy model [46]. Light-heavy mesons like D and B are also described in the same method, which possesses seven parameters including light quark masses [47]. Note that, the lattice simulations are also available for the low-lying light meson spectra [14] and charmonium spectra [48].

The above mesons are well understandable in the conventional picture of quark-antiquark bound states, but some observed mesons do not fit this description. Such states are called "exotic hadrons," and actually one of the hot topics in recent high energy physics phenomenology is the study of such exotic hadron. This is where the diquarks play an important role as effective degrees of freedom. In the remaining of this section, we briefly summarize the situation of some charmonium-like exotic mesons.

charmonium-like states

In 2003, a narrow charmonium-like state named $X(3872)$ was discovered by Belle [49], and later confirmed by CDF [50], BABAR [51], D0 [52], LHCb [53]. Its decay mode to $J/\psi\pi^+\pi^-$ containing the ρ-meson resonance indicates the $X(3872)$ has a component of iso-vector, which means it is not the usual charmonium-like state. A model to treat $X(3872)$ as a diquark-antidiquark bound state was proposed in 2004 [54], and many other studies have been following. The charged exotic state $Z_c(4430)^+$ discovered by Belle in 2009 [55], and by LHCb in 2014 [56] clearly shows its exoticness because it is charged. It is found that the diquark model can explain their decay pattern and the narrow width well, which are unnatural in meson-molecule models [57]. For example, if we consider a molecule composed of two charmed meson, the decay probability to J/ψ or $\psi(2S)$ should be small. This is because J/ψ and $\psi(2S)$ are relatively compact object, so the two charmed meson have to be close to each other in order to get sufficient overlap of their wave function, which is unlikely to occur in the usual meson models. However, in the observed decay of $X(3872)$, the mode to

$\psi(1S)$ not so suppressed and in the case of $Z(4430)$, its dominant decay mode is considered to be $\psi(2S)\pi^-$. When we consider a charmed diquark and a charmed anti-diquark as effective degrees of freedom, the dynamics can change drastically, resulting the fulfillment of observed decay pattern.

The diquarks discussed above in the context of exotic hadrons are usually the charmed diquarks, which are composed of a heavy quark and a light quark. Therefore the situation may be different form the diquarks composed of two light quarks, which are discussed in the context of usual baryons in §1.4.1. One marked difference is that the "pole mass" of these heavy-light diquarks seem to be rather accepted in an analogy of the pole mass of charm quark. In fact, most of the studies of diquark-antidiquark description of exotic mesons rely on the potential picture, in which the masses of mesons are expressed as "the pole masses + binding energy."

Some studies to determine the pole mass of charmed diquark using the QCD sum rule are available [58, 59]. The QCD sum rule is a relation between the spectral function and the imaginary part of correlation function, which is derived using the analyticity of these function. This method was invented in 1979 [60, 61], and has been a central tool to determine various parameters of QCD. Its application to diquark begun in 1989 [62, 63], and has been extended. The values determine by the sum rule are an important input to the phenomenological diquark models of exotic hadron.

In the QCD sum rule used in Refs.[58, 59], an assumption that the Green's function of the diquark has a pole, is crucial for the validity of their method. This point is closely related to what we will discuss in this thesis, namely, whether or not the diquark Green's functions has any poles. We will revisit this point later in §3.2.3.b.

Before closing this subsection, we would like to note that the artificial discrimination of the meson-molecule and the diquark-antidiquark bound states is not what is realized in the nature. Various states will mix together as long as their quantum numbers are the same, and after all, the observed energy-eigenstates are superposition of them. Therefore the meson-molecule pictures or the diquark-antidiquark pictures (or others) are just an approximation and nothing farther.

Chapter 2

Functional approach to hadrons

In this chapter, we review the studies of hadrons based on QCD with functional methods and introduce the diquark Bethe-Salpeter equation, which is the main subject of this thesis.

The original Lagrangian we consider in this thesis is

$$\mathcal{L} = -\frac{1}{4}F^a_{\mu\nu}F^{a\mu\nu} + \bar{\psi}(\mathrm{i}\not{\partial} - m)\psi - \partial^\mu B^a A^a_\mu + \frac{\xi}{2}B^a B^a - \mathrm{i}\partial^\mu \bar{c}^a D_\mu c^a, \tag{2.1}$$

where $F^a_{\mu\nu}$ is the field strength of gluons, A^a_μ is the gluon fields, ψ_i is the quark fields, B^a is Nakanishi-Lautorap fields [64, 65], c^a and $\bar{c}^a$ is the Faddeev-Popov ghost fields and anti-ghost fields [66], ξ is a gauge fixing parameter [67], g is the coupling constant, f_{abc} is the structure constant. The field strength of gluon fields are defined as $F^a_{\mu\nu} = \partial_\mu A^a_\nu - \partial_\nu A^a_\mu + g f_{abc} A^b_\mu A^c_\nu$, and the covariant derivative of the quark fields and the ghost fields are $D_\mu \psi_i = \partial_\mu \psi_i - \mathrm{i}g(t^a)^j_i A^a_\mu \psi_j$ and $D_\mu c^a = \partial_\mu c^a + g f_{abc} A^b_\mu c^c$, where $(t^a)^j_i$ is the generator of SU(3) gauge group in the fundamental representation. Since Nakanishi-Lautorap fields B^a are auxiliary fields which do not have kinetic term, they can be easily integrated out and we obtain

$$\tilde{\mathcal{L}} = -\frac{1}{4}F^a_{\mu\nu}F^{a\mu\nu} + \bar{\psi}(\mathrm{i}\not{\partial} - m)\psi - \frac{1}{2\xi}(\partial^\mu A^a_\mu)(\partial^\nu A^a_\nu) - \mathrm{i}\partial^\mu \bar{c}^a D_\mu c^a. \tag{2.2}$$

We will use the Lagrangian (2.2) in §2.2 and §3.1, and use the Lagrangian (2.1) in the appendix A.

2.1 Baryon as a pole of three-quark Green's function

In the constituent quark model for baryon in §1.4.1, the baryon is treated as a bound state of three constituent quarks in the quantum mechanical way, namely, we first construct the quantum mechanical Hamiltonian of the system, and then solve eigenvalue equation. Most of the studies in the case of exotic hadrons in §1.4.2 are also essentially same.

In this section, we briefly review the way to consider hadrons based on QCD. The description of bound state in terms of quantum field theory was first proposed by Gell-Mann and Low [68], and by Bethe and Salpeter [69] independently in 1951 in the case of two-body system. Its extension to the three-body system was proposed by Faddeev in 1961 [70]. Since the beginning, the essential point is not changed, that is, the poles of Green's functions are regarded as indications of bound

states.

Consider the three-quark Green's function

$$G(x_1, x_2, x_3, y_1, y_2, y_3) = \langle \psi(x_1)\psi(x_2)\psi(x_3)\bar{\psi}(y_1)\bar{\psi}(y_2)\bar{\psi}(y_3)\rangle \,, \tag{2.3}$$

where we omit various indices for the sake of simplicity. Here and in the following we use a shorthand notation $\langle O\rangle \equiv \langle 0|\,\mathrm{T}O\,|0\rangle$. We assume $x_1^0 \simeq x_2^0 \simeq x_3^0 > y_1^0 \simeq y_2^0 \simeq y_3^0$, namely, the operators are clustered in the time direction. In principle, the three-quark Green's function (2.3) contains all information about the system including the scattering, but we are interested only in the bound states, so we extract the information of the bound states in the following. For this purpose, we insert the completeness relation

$$1 = \sum_{\Psi,\in\mathcal{H}^{\mathrm{asym.}}} \int \frac{\mathrm{d}^3\mathbf{P}}{(2\pi)^3} \frac{1}{2\sqrt{M_\Psi^2 + \mathbf{P}}} \;|\Psi,\mathbf{P}\rangle\,\langle\Psi,\mathbf{P}|\,, \tag{2.4}$$

into the left-hand-side of (2.3). One important property of the state $|\Psi,\mathbf{P}\rangle$ is that it is a momentum-eigenstate, whether it is a one-particle state or multi-particle state. Therefore we can define the total momentum $\mathbf{P}$ and the total energy of system $\sqrt{M_\Psi^2+\mathbf{P}^2}$ for every states. Note that M_Ψ needs not to be discrete in the multi-particle states. The insertion of the completeness relation (2.4) into the left-hand-side of (2.3) gives

$$G(x_1, x_2, x_3, y_1, y_2, y_3) = \sum_{\Psi\in\mathcal{H}^{\mathrm{asym.}}} \int \frac{\mathrm{d}^3\mathbf{P}}{(2\pi)^3} \frac{\chi_{\Psi,P}(x_1,x_2,x_3)\;\bar{\chi}_{\Psi,P}(y_1,y_2,y_3)}{2\sqrt{M_\Psi^2+\mathbf{P}}} \tag{2.5}$$

$$\sim \sum_{\text{bound states}} \int \frac{\mathrm{d}^4P}{(2\pi)^4} \frac{\mathrm{i}\chi_{\Psi,P}(x_1,x_2,x_3)\bar{\chi}_{\Psi,P}(y_1,y_2,y_3)}{P^2 - M_\Psi^2 + \mathrm{i}0^+}, \tag{2.6}$$

where $\chi_{\Psi,P} \equiv \langle 0|\,\mathrm{T}\psi\psi\psi\,|\Psi,\mathbf{P}\rangle$, $\bar{\chi}_{\Psi,P} \equiv \langle\Psi,\mathbf{P}|\,\mathrm{T}\bar{\psi}\bar{\psi}\bar{\psi}\,|0\rangle$ and the sign "$\sim$" in Eq.(2.6) means the left-hand-side is equal to the right-hand-side near the pole. In deriving Eq.(2.6), the existence of isolated poles with respect to P^0 is assumed. In other words, only baryons are supposed to be extracted. Diagrammatically, Eq.(2.5) and Eq.(2.6) are expressed as

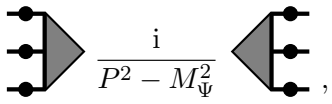

(2.7)

where the black bullets stand for the exact quark propagator.

In the momentum representation, the three-quark Green's function becomes

$$G(P, p_1, p_2, \bar{p}_1, \bar{p}_2) \sim \frac{\mathrm{i}\chi_{\Psi,P}(p_1,p_2)\bar{\chi}_{\Psi,P}(\bar{p}_1,\bar{p}_2)}{P^2 - M^2} \tag{2.8}$$

near the bound state pole if there is a bound state. Conversely, if there is no such pole, it means there is no bound state in that channel. It is known that such poles do not appear within the perturbative calculation of the Green's function with respect to the coupling expansion. What Faddeev proposed was the self-consistent equation which is expressed diagrammatically as [70]

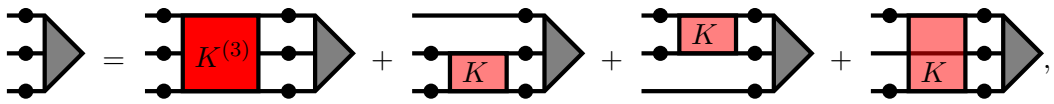

(2.9)

where $K^{(3)}$ is the three-particle irreducible interaction kernel, and K is the two-particle irreducible interaction kernel.

The generalization to tetraquark state and pentaquark state (and more) is straightforward.

Reduction to a two-body problem

Solving the Faddeev equation is difficult, and only recently the investigations incorporating the dressed quark propagator are becoming available [19, 20, 21], but still restricted to the low-lying states. When we look into the baryon spectra including excited states, some additional approximation to reduce the complexity is needed. One such treatment is to consider the diquark correlation.

Suppose that the following two-quark Green's function has a pole with respect to the center of mass momentum of the two-quark scattering channel P:

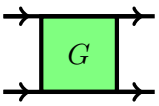

$$\sim \frac{\mathrm{i}\chi_{\Psi,P}(p)\bar{\chi}_{\Psi,P}(\bar{p})}{P^2 - M^2}. \tag{2.10}$$

This is a pure assumption. The two-quark Green's function satisfies the Bethe-Salpeter equation [68, 69]

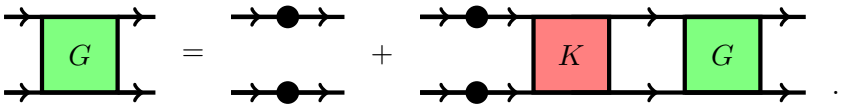

(2.11)

From Eqs.(2.10), (2.11), the pole can be regarded as a consequence of a resummation of the two-particle-irreducible kernel. In this situation, it can be a good approximation of the Faddeev equation to resum one of the two-particle-irreducible kernel first, and reduce the three-body problem to the two-body problem. A consistent treatment of this kind is seen only recently [22].

The resummation of the two-quark interaction is possible even without the pole, but in that case the four-point Green's function depends on both the center of mass momentum and the relative momentum of diquark system, so the calculation will not be simplified compared to the case with pole.

The Bethe-Salpeter equation in the diquark channel (2.11) is the main subject of this thesis. We investigate especially the problem of whether or not the diquark Bethe-Salpeter equation (2.11) has poles. We will review some attempts to study the diquark Bethe-Salpeter equation in §2.3, but before that, let us first look at the studies of the dressed (exact) quark propagator. It enters in the diquark Bethe-Salpeter equation as the black bullets in Eq.(2.11).

2.2 Dyson-Schwinger equation and quark propagator

In the previous section, we show that the bound states are described as poles of the Green's functions. More generally, most of the problems in quantum filed theory reduce to a problem of how to obtain the Green's functions of various systems.

In this section, we briefly review the functional method, which is one of the most powerful way to analyze the Green's function systematically. In this framework, relations between various Green's functions are utilized. This kind of relations were derived originally with the operator formalism by Dyson [71] and Schwinger [72, 73], and called Dyson-Schwinger equation. In a modern point of view, it is more transparent to derive them in the path integral formalism, so we follow that way in this thesis.

Consider the generating functional using the action $\tilde{\mathcal{S}} = \int d^4x \tilde{\mathcal{L}}$ with the Lagrangian (2.2),

$$Z[\bar{\eta}, \eta, J] \equiv \mathrm{e}^{\mathrm{i}W[\bar{\eta},\eta J]} \equiv \int \mathscr{D}(\psi, A)\mathrm{e}^{\mathrm{i}\mathcal{S}}, \qquad \mathcal{S} = \tilde{\mathcal{S}} + \int \mathrm{d}^4x(\bar{\eta}\psi + \bar{\psi}\eta + J^{a\mu}A^a_\mu), \tag{2.12}$$

where $\bar{\eta}, \eta, J^{a\mu}$ are the source terms. The exact propagators of quark and gluon are derived as

$$S(x-y) = \mathrm{i}\left.\frac{\delta^2 W}{\delta\bar{\eta}(x)\delta\eta(y)}\right|_{J_X=0}, \qquad D(x-y)^{ab}_{\mu\nu} = -\mathrm{i}\left.\frac{\delta^2 W}{\delta J^{a\mu}(x)\delta J^{b\nu}(y)}\right|_{J_X=0}. \tag{2.13}$$

Here and in the following we denote ϕ_X to represent any of $\psi, \bar{\psi}A$ and J_X accordingly. The functional integral (2.12) is unchanged under a redefinition of the fields, so with an infinitesimal change of field preserving the integral measure leads

$$0 = \int \mathscr{D}(\psi, A)\mathrm{e}^{\mathrm{i}\mathcal{S}}\frac{\delta\mathcal{S}}{\delta\phi_X} = \left(\left.\frac{\delta\mathcal{S}}{\delta\phi_X}\right|_{\phi_X=\frac{\delta}{\delta J_X}} + J_X\right) Z[\bar{\eta}, \eta, J]. \tag{2.14}$$

This is the general form of the Dyson-Schwinger equation. An infinite tower of self-consistency equations among various Green's functions is generated by operating the functional derivative $\delta/\delta J_X$ to Eq.(2.14). The most simple one in QCD is obtained by choosing $\phi_X = \psi$ in Eq.(2.14) and operation of $\delta/\delta\bar{\eta}$, resulting in

$$S(p) = S_0(p) + S(p)\int_q \mathrm{i}g\gamma_\mu t^a S(p+q)\Gamma^a_\nu(q,p)D_{\mu\nu}(q^2)S_0(p), \tag{2.15}$$

where $\Gamma^a_\nu(q,p)$ is the exact one-particle-irreducible (1PI) quark-gluon vertex, and various functions are transformed into the momentum space. The equation (2.15) is expressed diagrammatically as

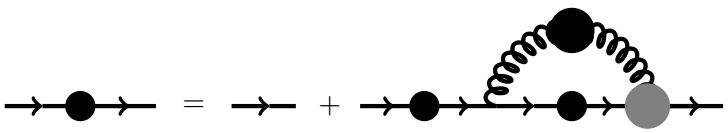

(2.16)

where the black bullets stand for the exact propagators of quark and gluon, and the gray bullet stands for the exact 1PI quark-gluon vertex.

Approximation of the dressed gluon propagator and quark-gluon vertex

It is known that the Dyson-Schwinger equations are not closed set of integral equation, so we have to truncate them at some level and approximate remaining parts with some models to perform practical calculation. As one such approximation, we first reduce the structure of the exact 1PI quark-gluon vertex to be

$$\Gamma^a_\mu(q,p) \to -\mathrm{i}gt^a\gamma_\mu\mathcal{G}(q^2). \tag{2.17}$$

In the following we adopt the Euclidian metric convention. The construction of Euclidian theory is studied [74], and the Wick rotation of the Lagrangian including fermions is studied [75, 76]. In this thesis, we simply perform the Wick rotation after all functional relations are derived. For the Wick rotation of the gamma-matrices, we follow the method displayed in Ref.[75, 76]. We write the dressed quark propagator and the dressed gluon propagator in the Landau gauge as

$$S(p) = -\mathrm{i}\not{p}\mathcal{A}(p^2) + \mathcal{B}(p^2), \quad D_{\mu\nu}(q) = \frac{\mathcal{Z}(q^2)}{q^2}\left(\delta_{\mu\nu} - \frac{q_\mu q_\nu}{q^2}\right), \tag{2.18}$$

and substituting Eqs.(2.17), (2.18) into Eq.(2.15), the Dyson-Schwinger equation becomes a coupled equation

$$\begin{aligned}
\frac{\mathcal{A}(p^2)}{p^2\mathcal{A}^2(p^2)+\mathcal{B}^2(p^2)} &= Z_2(\mu) + \frac{4}{3}\int_k \frac{\mathcal{G}(k^2)}{k^2}\mathcal{Z}(q^2)\mathcal{A}((p+k)^2)\left(1+3\frac{kp}{p^2}+2\frac{(kp)^2}{k^2p^2}\right) \\
\frac{\mathcal{B}(p^2)}{p^2\mathcal{A}^2(p^2)+\mathcal{B}^2(p^2)} &= m(\mu) + 4\int_k \frac{\mathcal{G}(k^2)}{k^2}\mathcal{Z}(q^2)\mathcal{B}((p+k)^2),
\end{aligned} \tag{2.19}$$

where we implicitly assuming some regularization and renormalization scheme but omitting counter terms for simplicity. The free quark propagator S_0 is expressed as renormalized parameters $Z_2(\mu), m(\mu)$ renormalized at some point μ.

Maris-Tandy model

One of the most extensively applied model in studying various hadron properties is the Maris-Tandy model, which was suggested in 1999 [77]. In this model, a product of the dressing functions $\mathcal{Z}$ and $\mathcal{G}$ in Eqs.(2.19) is parameterized as

$$\mathcal{G}(q^2)\frac{\mathcal{Z}(q^2)}{q^2} = \frac{4\pi^2 Dq^2}{\omega^6}\mathrm{e}^{-k^2/\omega^2} + \frac{4\pi^2\gamma_m\left(1-\mathrm{e}^{-k^2/4m_t^2}\right)}{\frac{1}{2}\ln\left(\tau+(1+q^2/\Lambda_{\mathrm{QCD}})^2\right)}. \tag{2.20}$$

The value of parameters slightly vary in various studies, and one example of the parameter set is $\gamma_m = 12/(33-2n_f), m_t = 0.5$ GeV, $\tau = \mathrm{e}^2-1, \Lambda_{\mathrm{QCD}} = 0.234$ GeV, $\omega = 0.4$ GeV, $D = 0.93$ GeV^2. The behavior of Eq.(2.20) is shown in Fig.2.1.

The Maris-Tandy model successfully reproduce meson masses [47, 46, 78, 79] as mentioned in §1.4.2. The electromagnetic form factor is also studied with this model in detail [80].

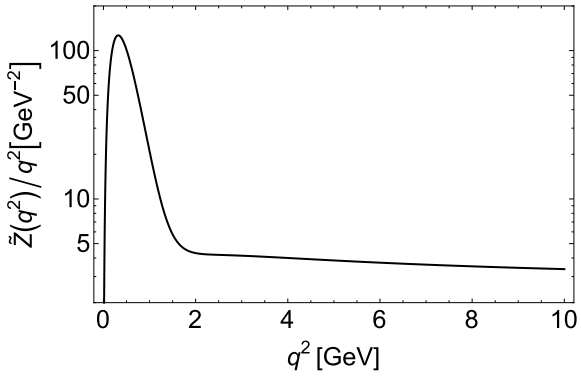

Figure 2.1: The momentum dependence of the dressed functions in the Maris-Tandy model (2.20). In the plot label, a redefinition $\tilde{Z}(q^2) = \mathcal{G}(q^2)\mathcal{Z}(q^2)$ is done.

Munczek-Nemirovsky model

In 1983, Munczek and Nemirovsky proposed a model to reproduce the ground state mass spectra of various flavored mesons [81]. In the model, the product of full vertex and dressing function is

$$\mathcal{G}(q^2)Z(q^2)/q^2 = G(2\pi)^4\delta^4(q), \qquad G \equiv \eta^2/4, \tag{2.21}$$

where η is a dimensionful parameter. The value of η fitted from the ground state mesons is $\eta \simeq 1$ GeV. This model is also used to reproduce the value of quark condensation [82]. In this model, the dressed functions show a blow up at the origin $q = 0$. On the other hand, based on extensive studies, at present there is a consensus that the gluon dressing function is strongly suppressed in the infrared region, like the Maris-Tandy model, [See Fig.2.1.] although the way to be suppressed is under controversial discussion. In this thesis, we treat the Munczek-Nemirovsky model as a simplification of the Maris-Tandy model, regarding the delta-function as an approximation of the enhancement near $q^2 \simeq 1$ GeV^2 in Fig.2.1. In this sense, the Munczek-Nemirovsky model may not be able to predict various quantities in the precision better than 1 GeV. Therefore we take the results from the Munczek-Nemirovsky model as quantitative indication in this thesis. As we will see later, the Munczek-Nemirovsky model reproduces qualitatively well the results from more realistic calculation, as long as the quark propagator in the space-like momentum region is concerned.

The marked feature of the Munczek-Nemirovsky model is, it removes all momentum integrations due to the delta function (2.21), and enable us to perform higher looped calculations. In the Munczek-Nemirovsky model, the quark Dyson-Schwinger equations (2.19) become

$$\frac{\mathcal{A}(p^2)}{p^2\mathcal{A}^2(p^2) + \mathcal{B}^2(p^2)} = 1 + \eta^2\frac{\mathcal{A}(p^2)}{2}, \qquad \frac{\mathcal{B}(p^2)}{p^2\mathcal{A}^2(p^2) + \mathcal{B}^2(p^2)} = m_0 + \eta^2\mathcal{B}(p^2), \tag{2.22}$$

which are just a pair of cubic equations, and can be solved analytically. Here we treat m_0 as an input parameter. This prescription is equivalent to specifying a certain renormalization scheme at certain point μ with $m(\mu)$ which may not identical to m_0. If we measure the dimensionful quantities in a unit of $\eta \simeq 1$ GeV, the dependence on η totally disappear from the calculation, and the model

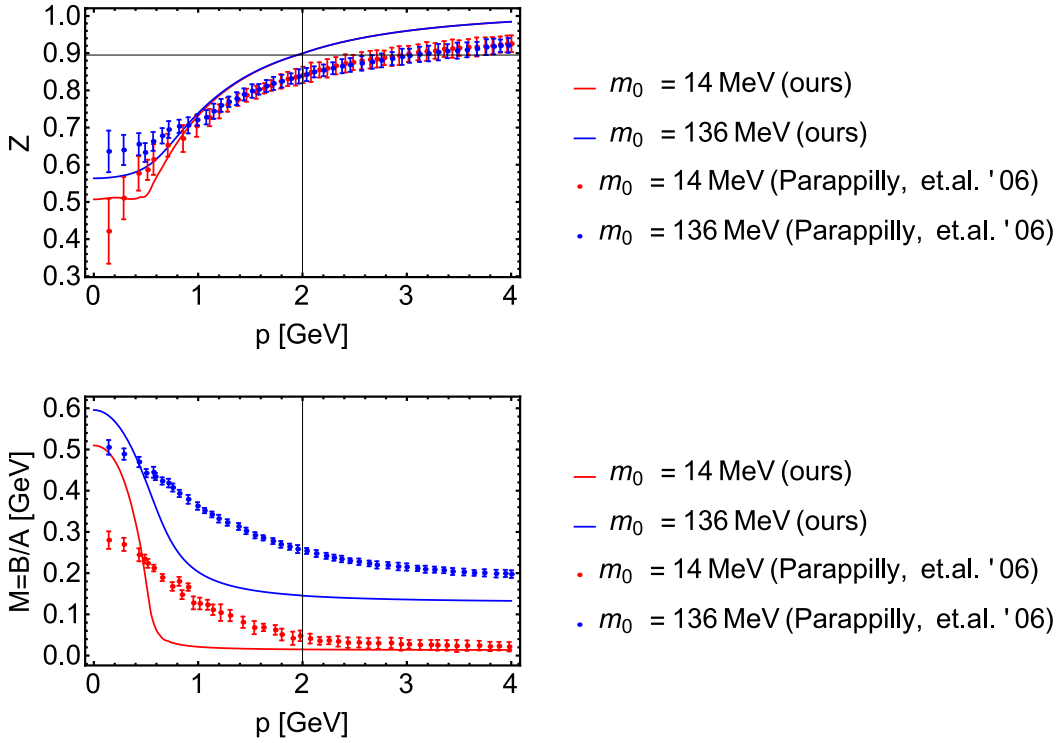

Figure 2.2: Comparison of the dressed quark wave function Z (upper plots) and dressed quark mass M (lower plots) between the lattice result [83] and those obtained with the Munczek-Nemirovsky model, namely, the solutions of Eqs.(2.22) with $\eta = 1$. The data points of lattice result are read from Fig.1 of the Ref.[83], in which the data points are much more and the cases of other mass values are also presented.

becomes essentially one-parameter-model, with a single parameter m_0. In this thesis, we use this mass unit to simplify the notation. The dependence on η is easily restored by the replacement $\mathcal{A} \to \eta^2\mathcal{A}, \mathcal{B} \to \eta\mathcal{B}, p^2 \to p^2/\eta^2, m_0 \to m_0/\eta$ at any stage of calculation.

In the rest of this section, we examine in what extent the Munczek-Nemirovsky model works.

Comparison of the dressed quark propagator with realistic results

One of the latest results of the lattice simulation of quark propagator is shown in Fig,2.2 with an another expression of the dressed quark propagator

$$S(p) = Z(p^2)/\left(i\not{p} + M(p^2)\right) \tag{2.23}$$

is used instead of $S = -i\not{p}\mathcal{A} + \mathcal{B}$. They are related as $Z = p^2\mathcal{A} + \mathcal{B}^2/\mathcal{A}$ and $M = \mathcal{B}/\mathcal{A}$.

The results of the lattice simulation and the analytic solutions of Eqs.(2.22) show qualitatively the same momentum dependences. The dressed quark functions Z, M calculated using the Munczek-Nemirovsky model show exaggerated suppression and enhancement, respectively. This is reasonable since the model overestimate the infrared dynamics.

We proceed the comparison with lattice results by another group [84]. They present a fitting

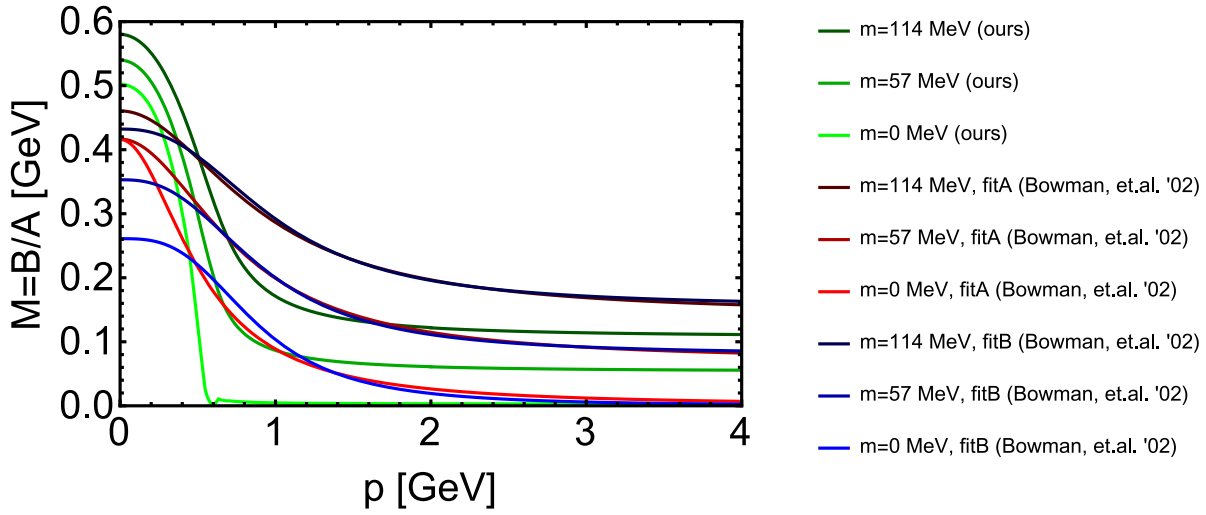

Figure 2.3: Comparison of the dressed quark mass M between the lattice result [84] (red- and blue-based lines) and those obtained with the Munczek-Nemirovsky model with $\eta = 1$ GeV (green-based lines). Here we use the fitting function (2.24) of the lattice result with parameters summarized in Eq.(2.25). In the legends, "fit A" stands for the parameter sets taken from the upper half (with fixed $\alpha = 1.0$) of Eq.(2.25), and "fit B" stands for the lower half (with fitted α).

function which describes the simulated results well:

$$M(q) = \frac{c\Lambda^{1+2\alpha}}{q^{2\alpha} + \Lambda^{2\alpha}} + m_0 \tag{2.24}$$

with parameters

m [MeV]	c	Λ [MeV]	m_0 [MeV]	α	$M(0)$ [MeV]	χ^2 [per d.o.f.]
114	0.35(1)	910(20)	142(7)	1.0	462(9)	0.38
57	0.45(4)	770(50)	70(7)	1.0	410(20)	0.51
0	0.80(20)	520(50)	0.0	1.0	400(40)	1.3
114	0.28(1)	990(30)	155(7)	1.25(4)	428(7)	0.38
57	0.30(2)	910(40)	80(6)	1.30(2)	354(9)	0.41
0	0.30(4)	870(60)	0.0	1.52(23)	260(20)	0.49

(2.25)

and we plot this fitting function in Fig.2.3 comparing with the dressed mass function obtained from the analytic solutions of Eqs.(2.22). For all the mass parameter, the tendency is the same as Fig.2.2.

Comparison with other lattice results [85, 86] give qualitatively the same insight.

Finally we compare the Munczek-Nemirovsky model with one of the latest results form the Maris-Tandy model [87]. We summarize the results in Fig.2.4. Note that here the compared functions are $\mathcal{A}, \mathcal{B}$, and the argument is changed from p to p^2, so the region considered is reduced. The difference of deep infrared behavior between these models vary with the value of input quark mass. In the case of light mass $m_0 = 5$ MeV, the blow up in the region $p^2 \leq 0.3\text{GeV}^2$ is much severe in the Maris-Tandy model compared to the Munczek-Nemirovsky model. On the other hand, in the case of heavier mass $m_0 = 1$ GeV, the Maris-Tandy model results are not so enhanced, although

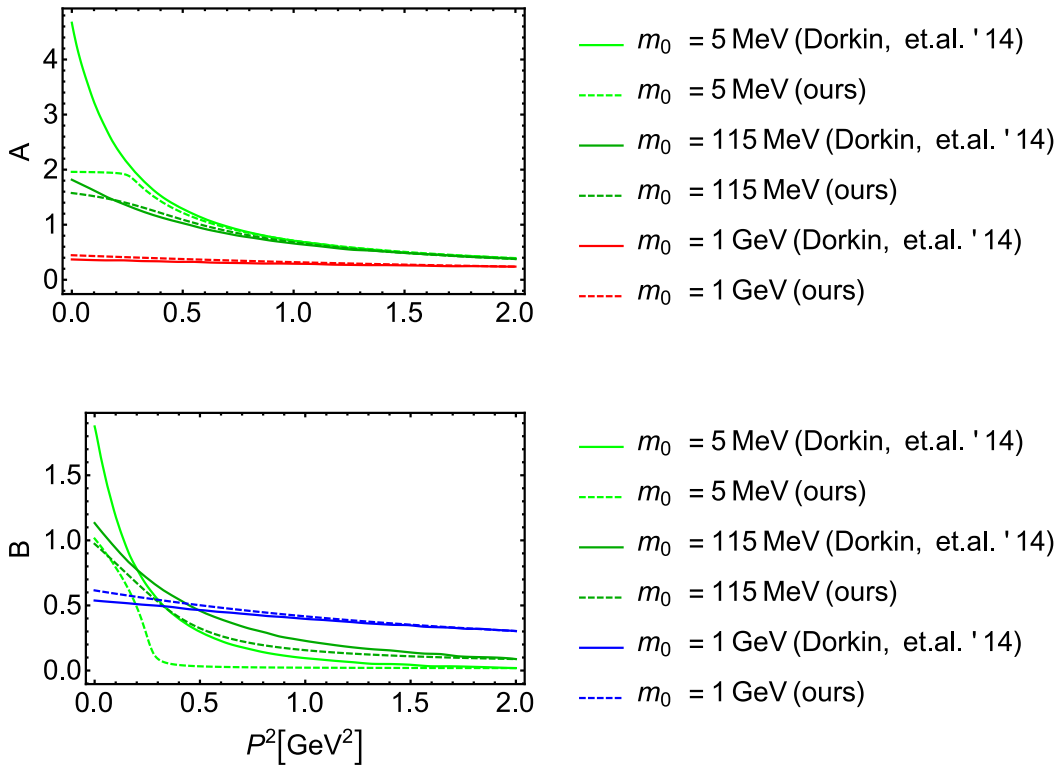

Figure 2.4: Comparison of the quark propagator $S = -i\not{p}\mathcal{A} + \mathcal{B}$ between the Maris-Tandy model [87] and the Munczek-Nemirovsky model. In these two plots, the solid lines stand for those read from figures of the Ref.[87] and the dashed lines stand for the solutions of Eqs.(2.22).

the difference is rather small.

To summarize this subsection, the Munczek-Nemirovsky model reproduces qualitatively well the energy dependence of dressed quark propagator calculated from the lattice simulation and the Maris-Tandy model, despite its seemingly oversimplified approximation.

2.3 Bethe-Salpeter equation and diquark

As we state at the end of §2.1, we focus on the two-quark Green's function, which is an ingredient of the baryon Green's function, or other hadronic Green's functions. It can be redefined as

$$G(x_1, x_2, y_1, y_2) = \langle \psi(x_1)\psi(x_2)\bar{\psi}(y_1)\bar{\psi}(y_2)\rangle \,, \tag{2.26}$$

in the coordinate space. The two-quark Green's function satisfies the following self-consistency equation called Bethe-Salpeter equation:

$$\begin{aligned} G(P, p_1, p_2) =& S\left(P + \tfrac{p_1}{2}\right) \otimes S\left(P - \tfrac{p_1}{2}\right) (2\pi)^4 \delta(p_1 - p_2) \\ &+ S\left(P + \tfrac{p_1}{2}\right) \otimes S\left(P - \tfrac{p_1}{2}\right) \int_k K(P, p_1, k) G(P, k, p_2), \end{aligned} \tag{2.27}$$

where K is a two-particle-irreducible (2PI) interaction kernel. The 2PI diagrams are those do not split into two clusters with any cuts of two quark propagators. We write down a diagrammatic expression of Eq.(2.27) here again:

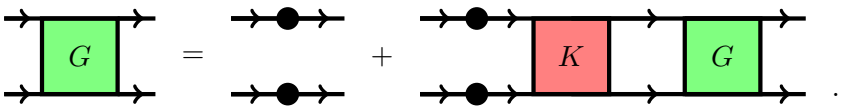

(2.28)

Note that the Green's function G is defined not by Eq.(2.27) but by Eq.(2.26), and 2PI-ness of K is a consequence of the quantum field theory. Intuitively, or diagrammatically, the 2PI-ness of K is reasonable once we notice that Eq.(2.28) shows G is obtained by the resummation of K. A proof of 2PI-ness of K based on the functional method was first given in the context of the statistical field theory in 1972 [88] and later given independently in the context of the quantum field theory in 1974 [89].

The Bethe-Salpeter equation (2.27) reduces to more simple form when we focus only on the behavior of the diquark Green's function near the pole. The diquark Green's functions can be classified according to their representation of color, spin and flavor, and the position of poles varies according with the representation in general. We can extract the channel under interest by inserting the corresponding operators (for example Eqs.(1.3)).

Suppose that the diquark Green's function in the scalar channel has a pole, then the amplitude

$$\epsilon_{ijk}\epsilon_{\mathfrak{abc}}\Phi^{qq0^+}(P,p)C = \int_{X,x} \langle \psi_{i\mathfrak{a}}(X + \tfrac{x}{2})\psi_{j\mathfrak{b}}(X - \tfrac{x}{2}) \left[\mathfrak{O}^\dagger_{qq0^+}(0)\right]_{k\mathfrak{c}} \rangle \, \mathrm{e}^{-\mathrm{i}(PX+px)} \tag{2.29}$$

satisfies the homogeneous Bethe-Salpeter equation

$$\epsilon_{ijk}[\Phi^{qq0^+}(P,p)C]_{\alpha\beta} = \int_{p'} [S(P + \tfrac{p}{2})S(P - \tfrac{p}{2})K(P,p,p')]^{i'j'\alpha'\beta'}_{ij\alpha\beta} \epsilon_{i'j'k}[\Phi^{qq0^+}(P,p')C]_{\alpha'\beta'}, \tag{2.30}$$

or diagrammatically

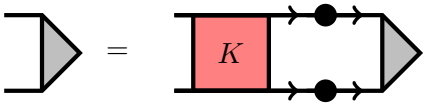

(2.31)

Note that the gray triangle stands for $S^{-1} \otimes S^{-1}\Phi^{qq0^+}$. This form of Bethe-Salpeter equation is called the homogeneous Bethe-Salpeter equation. The factorization of the charge conjugation operator C in the left-hand-side of Eq.(2.29) is for later convenience. [See the sentence below Eq.(3.36).]

The homogeneous Bethe-Salpeter equation is derived under the assumption that the diquark Green's function has a pole. Therefore, if there is no nontrivial solution to Eq.(2.30), it means that there is no pole in the diquark Green's function at that channel. In this thesis, we call the nontrivial solution of homogeneous Bethe-Salpeter equation as "a bound-state solution." This term is reasonable in the case of physical states like mesons, but we should be careful in the case of unphysical states like diquarks. Anyway, the question of whether or not the diquark Bethe-Salpeter equation has a bound-state solution is a calculable problem, and this is what we discuss in this thesis.

The first calculation of the diquark Bethe-Salpeter equation with the dressed quark propagator determined by the Dyson-Schwinger equation was done in 1987 [90]. Since then, many studies based on various models for the Green's function were done, and basically all the result shows that the diquark Bethe-Salpeter equation has a bound-state solution within the ladder truncation. This result is reasonable because in the one-gluon exchange approximation, the interaction kernel of diquark Bethe-Salpeter equation is just the half of meson's one and the meson Bethe-Salpeter equation has bound-state solutions in the ladder truncation.

However, in 1996, it was found that the bound-state solution of the diquark Green's function disappears when the crossed ladder contribution is included [91], namely,

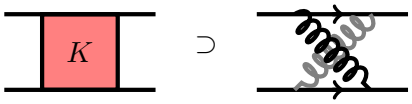

(2.32)

where we color one of the gluon lines gray to indicate there is no self-interaction vertex. The calculation was done with the Munczek-Nemirovsky model. Soon after, the same argument was reported with another model, the Nambu-Jona-Lasinio model with an infrared and an ultraviolet cutoff [92]. The disappearance was interpret as a realization of the confinement. There is an extension of this study introducing one more parameter in the Bethe-Salpeter equation [82], but the result is essentially the same as that of Ref.[91].

We will show in §3.2.1.c that the arguments based on these analyses are not conclusive, by exhibiting the break down of the truncation. It is shown that the presence and the absence of the bound-state solution alternate as we increase the number of ladders including the completely crossed ladder diagrams. [See Figs.3.6 and 3.7.]

Chapter 3

Crossed ladder diagrams in the diquark Bethe-Salpeter equation

The main subject of this chapter is "which kinds of diagrams should be considered in the diquark Bethe-Salpeter kernel?" and "whether or not there is a bound-state solution in the diquark Bethe-Salpeter equation?"

In §3.1.1, we find that all the completely crossed ladder diagrams like

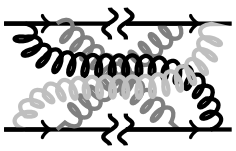

(3.1)

are the leading order in the 't Hooft limit. In other words, the color factors of these diagrams are enhanced. In §3.1.2, we discuss the validity of results obtained under the 't Hooft limit, and in §3.1.3, we see the color-factor enhancement actually occurs in the case of $N_{\rm c} = 3$.

In §3.2, we solve the diquark Bethe-Salpeter equation with the Munczek-Nemirovsky model, and investigate whether or not it has a bound-state solution. At present, this model is the only one which enables the analysis of n-gluon exchange effect done in this section. In §3.2.1, we examine truncation schemes in which the completely crossed n-gluon exchange diagrams are included in the Bethe-Salpeter kernel up to n. The existence and absence of bound-state solution in the diquark Bethe-Salpeter equation alternate repeatedly, and we conclude that the truncation schemes with finite n-gluon exchange are not sensible. In §3.2.2, we perform a resummation of the completely crossed ladder diagrams motivated by the result in §3.1 and §3.2.1. Then we find that there is a bound-state solution in the diquark Bethe-Salpeter equation. In §3.2.3, we give interpretations and discussions of our result.

This chapter is based on the work collaborated with R. Jinno and T. Kitahara [1].

3.1 Green's functions of two quarks in light of the 't Hooft limit

So far we consider the SU(3) gauge theory as a theory to describe the strong interaction. Of course there are a lot of evidences that the real world can be described by that theory, and no other gauge group matches the nature. However, in this section, let us try considering SU(N_c) gauge theory instead and investigate what kind of diagrams contribute dominantly to the Green's functions when we take $N_c \to \infty$ satisfying a scaling of the coupling constant $\alpha_S \propto 1/N_c$. The idea to treat $1/N_c$ as a expansion parameter in the SU(N_c) gauge theory was first proposed by 't Hooft in 1974 [93].

Consider the Lagrangian (2.2). Here we express the fields of adjoint representation as matrix-valued fields:

$$(A_\mu)_i^j \equiv A_\mu^a (t^a)_i^j, \quad C_i^j \equiv c^a (t^a)_i^j, \quad \bar{C}_i^j \equiv \bar{c}^a (t^a)_i^j. \tag{3.2}$$

Usually we use the strong coupling constant $\alpha_S \equiv g^2/4\pi$, but in the 't Hooft limit, a redefined coupling constant $\lambda_{\alpha_S} \equiv N_c \alpha_S$ is used. In other words, the scaling $\alpha_S \propto 1/N_c$ is assumed. With this scaling, the property of asymptotic freedom of QCD is preserved under the large-N_c limit since the renormalization group equation of the coupling λ_{α_S} at the leading order becomes

$$\mu^2 \frac{\mathrm{d}\lambda_{\alpha_S}}{\mathrm{d}\mu^2} = -\left(\frac{11}{3} - \frac{2}{3}\frac{n_f}{N_c}\right)\left(\frac{\lambda_{\alpha_S}}{4\pi}\right)^2 \tag{3.3}$$

where n_f is the number of active quarks.

Double line notation

Double line notation is a convenient way to grasp what kind of diagrams contribute to various Green's functions dominantly. Here we consider the gauge group to be U(N_c) instead of SU(N_c) in order to make discussion simple. For the leading order result, the case of U(N_c) and SU(N_c) are identical [93], so it is sufficient for our purpose.

The propagator of matrix-valued gluon defined in Eq.(3.2) becomes

$$\langle (A_\mu)_{i_1}^{j_1}(x)(A_\nu)_{i_2}^{j_2}(y)\rangle = \frac{1}{2}\delta_{i_1}^{j_2}\delta_{i_2}^{j_1} D_{\mu\nu}(x-y). \tag{3.4}$$

When we focus on the flow of color index i_1, i_2, etc., the matrix-valued gluon propagator can be viewed as a pair of quark and antiquark propagators. The notation to express this fact is the double line notation. In the double line notation, the quark propagator, the gluon propagator and the quark-gluon vertex are expressed as

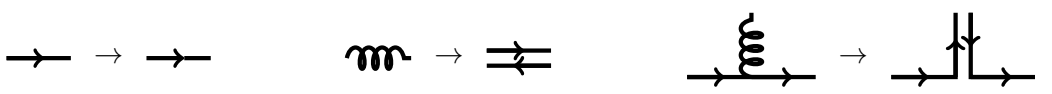

(3.5)

Similar notations for the gluon self-interaction vertex and the ghost fields can be constructed [93], but they are irrelevant in the discussion here. The inclusion of these vertices is straightforward. [See the paragraph below Eq.(3.20).]

One important example of the 't Hooft limit is the meson Green's function. Consider a two-

gluon-exchange diagram with a cross of gluons. In the double line notation, the diagram becomes

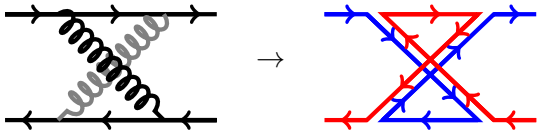

$$\propto \frac{\lambda_{\alpha_S}^2}{N_{\rm c}^2}, \tag{3.6}$$

where one of the gluon lines is colored gray in order to indicate there is no self-interaction vertex. We also color the double lined diagram to make its way of contraction clear. The rightest-hand-side of Eq.(3.6) stands for that this diagram behaves as $1/N_{\rm c}^2$ in the 't Hooft limit. In this example, the source of the factor $N_{\rm c}$ is only $\alpha_S = \lambda_{\alpha_S}/N_{\rm c}$, so the exponent of $1/N_{\rm c}$ increases as the number of loops increase.

Next we consider ladder diagrams, which has no crossing gluons, with n-gluon exchange in the double line notation:

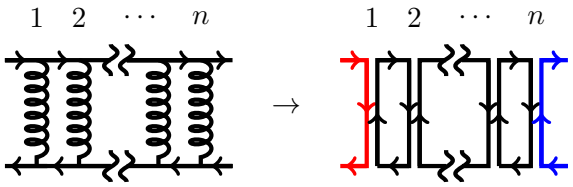

$$\propto \frac{\lambda_{\alpha_S}^n}{N_{\rm c}^n} N_{\rm c}^{n-1}, \tag{3.7}$$

where we color the internal closed loops black because it can have any colors. Contrary to the case of the internal closed lines, the colors of external lines are fixed. In the ladder diagrams, the suppression from the coupling constant is compensated by the extra factor $N_{\rm c}$ generated by the closed loop, since it indicates the contraction of the Kronecker delta:

$$= \delta_i^j \delta_j^i = N_{\rm c}. \tag{3.8}$$

As a result, all these ladder diagrams are the same order $\mathcal{O}(1/N_{\rm c})$, which is the leading in this Green's function. The crossed ladder diagrams like Eq.(3.6) is sub-leading due to the absence of extra $N_{\rm c}$-factors. Note that the number of closed loop (black line) is equal to the exponent of the additional $N_{\rm c}$-factor in the rightest-hand-side of Eq.(3.7). The discussion above can be generalized, and the generalization of the ladder diagrams above is "the planer diagrams" [93].

A glance at the completely crossed three-gluon-exchange diagram in the double line notation is useful in the later discussion in Eq.(3.17):

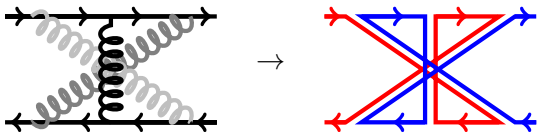

$$\propto \frac{\lambda_{\alpha_S}^3}{N_{\rm c}^3}. \tag{3.9}$$

In Eq.(3.9), the configuration of the color of external lines is different from that of Eq.(3.6). Meson is a gauge singlet state, so color of the lines should be assigned in a way to make the state gauge-singlet. In Eq.(3.9), this condition is automatically fulfilled in any combination of red line and blue line. On the other hand, in Eq.(3.6), color of the red line and the blue line must be the same. This constraint gives an additional $1/N_{\rm c}$ suppression to Eq.(3.6) when we extract the information

of meson from the Green's function.

To summarize the consideration of this subsubsection, the meson Green's function at the leading order in the 't Hooft limit is the sum of planer diagrams:

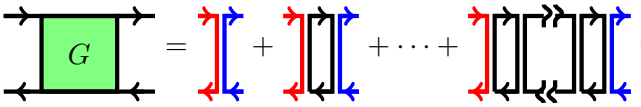

(3.10)

The crossed ladder diagrams, or in general the non-planar diagrams, are suppressed by the factor $1/N_{\rm c}$.

3.1.1 Double line notation in the diquark Green's function

Let us apply the double line notation to the diquark Green's function. The one-gluon exchange diagram becomes

$$\propto \frac{\lambda_{\alpha_S}}{N_{\rm c}}. \tag{3.11}$$

The rightest-hand-side is the same as the case of meson, but the flow of color-indices is different. The two-gluon exchange diagrams of ladder type becomes

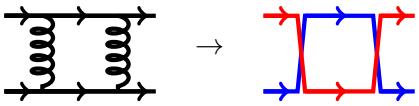

$$\propto \frac{\lambda_{\alpha_S}^2}{N_{\rm c}^2}, \tag{3.12}$$

and the n-gluon exchange diagram becomes

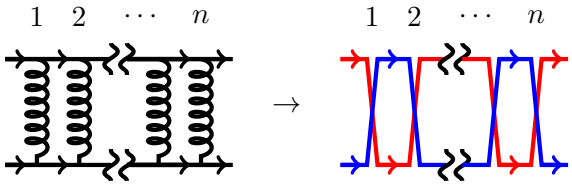

$$\propto \frac{\lambda_{\alpha_S}^n}{N_{\rm c}^n}. \tag{3.13}$$

Now the difference between the diquark and the meson is apparent. Contrary to Eq.(3.7), there is no closed loop in Eq.(3.13), so there is no additional $N_{\rm c}$-factor.

Actually, the closed loop of the double line notation in the diquark Green's function appears in crossed ladder diagrams. For example, the two-gluon exchange diagram with a cross becomes

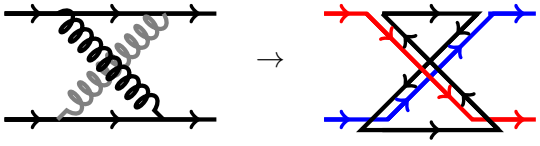

$$\propto \frac{\lambda_{\alpha_S}^2}{N_{\rm c}^2} N_{\rm c}, \tag{3.14}$$

and the completely crossed three-gluon exchange diagram becomes

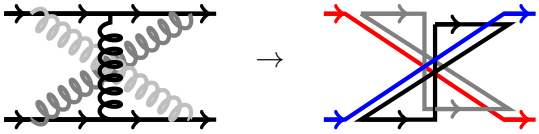

$$\propto \frac{\lambda_{\alpha_S}^3}{N_{\rm c}^3} N_{\rm c}^2, \tag{3.15}$$

where the black lines and the gray line are the closed loops and can have any color, resulting in the additional N_c-factors.

For definiteness, we write down the expression of color factors explicitly. In the meson channel, the ladder diagrams have a factor

$$t^{a_1}t^{a_2}\cdots t^{a_{n-1}}t^{a_n}t^{a_n}t^{a_{n-1}}\cdots t^{a_2}t^{a_1} = \frac{1}{2^n}\left(N_c - \frac{1}{N_c}\right)^n, \tag{3.16}$$

whereas the completely crossed ladder diagrams have

$$t^{a_1}t^{a_2}\cdots t^{a_n}t^{a_1}t^{a_2}\cdots t^{a_n} = \frac{1}{2^{n+1}}\left(N_c - \frac{1}{N_c}\right)\left[\left(-1 - \frac{1}{N_c}\right)^{n-1} + \left(1 - \frac{1}{N_c}\right)^{n-1}\right] \equiv \mathfrak{C}_n^{q\bar{q}}. \tag{3.17}$$

We defined $\mathfrak{C}_n^{q\bar{q}}$ for the later use. The large-N_c behavior of $\mathfrak{C}_n^{q\bar{q}}$ is $\mathcal{O}(N_c)$ for odd n and $\mathcal{O}(1)$ for even n, which reflects the extra suppression discussed in the below of Eq.(3.9).

The ladder diagrams in the diquark channel have a factor

$$t^{a_1}t^{a_2}\cdots t^{a_{n-1}}t^{a_n}\epsilon t^{Ta_n}t^{Ta_{n-1}}\cdots t^{Ta_2}t^{Ta_1} = \frac{1}{2^n}\left(-1 - \frac{1}{N_c}\right)^n \epsilon, \tag{3.18}$$

whereas the completely crossed ladder diagrams have

$$t^{a_1}t^{a_2}\cdots t^{a_n}\epsilon t^{Ta_1}t^{Ta_2}\cdots t^{Ta_n} = \frac{1}{2^n}\left[(-1)^n(N_c+1)\frac{1}{N_c^{n+1}} - \frac{1}{N_c}\left(N_c - \frac{1}{N_c}\right)^n\right]\epsilon \equiv \mathfrak{C}_n^{qq}\epsilon. \tag{3.19}$$

Again, we defined $\mathfrak{C}_n^{qq}$ for the later use.

The color flow of completely crossed ladder diagrams seems complicated at first sight, but it is actually as simple as that of ladder diagrams once we notice the relation

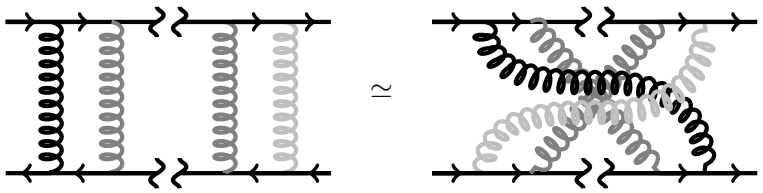

$$\simeq \quad = \quad \mathcal{O}(N_c^{-1}), \tag{3.20}$$

where the semi-equality means that the order of N_c is the same. Therefore, the completely crossed ladder diagrams are the leading order in the 't Hooft limit.

In general, any diagram of the diquark Green's function has its counterpart in the meson Green's function, and the counterpart is obtained by flipping one side of the quark line. The leading order diagrams of the meson Green's function in the 't Hooft limit are the planar diagram, therefore, the leading order contribution of the diquark Green's function is the diagrams made by flipping one side of the quark line of the planar diagrams.

The conclusion of this subsection is that the crossed ladder diagrams in the diquark Green's function are not suppressed in contrast to the meson case, and the leading order diagrams are the diagrams made by flipping one side of the quark line of the planar diagrams.

3.1.2 Comment on the application of t' Hooft limit to the diquark

Two points should be discussed before we go on to the next section, where we will work on the leading order approximation of the diquark Bethe-Salpeter kernel in terms of the 't Hooft limit. The first one is validity of $1/N_c$ expansion in the case of $N_c = 3$ (§3.1.2.a). The second one is a difficulty of treating diquarks in the 't Hooft limit (§3.1.2.b).

3.1.2.a How far can we trust the 't Hooft limit in the real world QCD?

In this and the next section, we consider only the leading order contribution of the 't Hooft limit, which is a certain kind of large-N_c limit. However, in the real world, $N_c = 3$, so the validity of the expansion with respect to $1/N_c = 1/3$ is not obvious. After all, we can not know a priori whether or not the $1/N_c$ expansion works, and should examine the validity after calculation.

In order to convince ourselves of the validity of 't Hooft limit, we briefly review phenomenological successes of it. First of all, as we saw in §3.1, the 't Hooft limit supports the ladder approximation in the meson Bethe-Salpeter equation, which is a successful truncation scheme. It is worth noting that any other argument can support this truncation in the case of light mesons so far. In 1979, Witten summarized phenomenology of the 't Hooft limit, namely, the suppression in hadronic physics of the $q\bar{q}$ sea, the realization of Zweig's rule, and the dominance of resonant two-body decay in unstable mesons [94]. Recently, Weinberg pointed out the existence of exotic mesons, which were thought to be absent in the 't Hooft limit [95]. This finding is also consistent with observation of the real world.

There is one thing which Witten could not do in his paper [94] – examining the coefficient of $1/N_c$ series using the exact result of QCD calculation. Even if $1/N_c$ is sufficiently small, the expansion with respect to $1/N_c$ can break down when each coefficients are considerably large. In fact, this kind of break down is considered to occur in the usual coupling expansion at very high order, as pointed out by Dyson in 1952 [96]. According to the paper, what the coupling expansion produces is not a convergence series, but an asymptotic series which diverges at a certain order as long as the coupling constant has a finite value. This property is generic in the gauge theory. Furthermore, in the case of QCD, the infrared renormalon makes the convergence of perturbative series worse [97]. For example, the relation between the pole mass and $\overline{\rm MS}$ mass $\bar{m}$ of the heavy quark is

$$m_{\rm pole} = \bar{m}\left(1 + 0.42\alpha_S + 1.4\alpha_S^2 + 6.1\alpha_S^3 + 36\alpha_S^4 + \mathcal{O}(\alpha_S^5)\right), \tag{3.21}$$

which shows a signal of the bad convergence behavior.

Here we try applying the $1/N_c$ expansion to the known analytic results calculated in the usual perturbation theory at a finite fixed orders. We consider the QCD potential and the Adler function because these two objects are calculated analytically at the highest order at present.

The static QCD potential is calculated in the next-to-next-to-next-to-leading order [98, 99]:

$$V_{\rm QCD}(q^2) = -\frac{1}{q^2}\left[\lambda_{\alpha_S}\left(6.3 - \frac{6.3}{N_{\rm c}^2}\right) + \lambda_{\alpha_S}^2\left(1.7 - \frac{1.7}{N_{\rm c}} - \frac{1.7}{N_{\rm c}^2} + \frac{1.7}{N_{\rm c}^3}\right)\right.$$
$$+ \lambda_{\alpha_S}^3\left(2. - \frac{2.6}{N_{\rm c}} - \frac{1.6}{N_{\rm c}^2} + \frac{2.6}{N_{\rm c}^3} - \frac{0.44}{N_{\rm c}^4} + \frac{0.027}{N_{\rm c}^5}\right)$$
$$\left. + \lambda_{\alpha_S}^4\left(1.6 - \frac{3.5}{N_{\rm c}} + \frac{0.13}{N_{\rm c}^2} + \frac{3.5}{N_{\rm c}^3} - \frac{1.7}{N_{\rm c}^4} - \frac{0.17}{N_{\rm c}^5} + \frac{0.022}{N_{\rm c}^6} + \frac{0.12}{N_{\rm c}^7}\right) + \mathcal{O}(\lambda_{\alpha_S}^5)\right], \qquad (3.22)$$

for the case with $n_f = 3$, as an example, and the renormalization scale is set to be $\mu = \alpha_S m_{\rm pole}$. Generally, the convergence is better when the number of active quark n_f is small because the quark loop corrections are always sub-leading order.

Adler function is calculated in the five loop order [100]:

$$A(Q^2) = \left[\lambda_{\alpha_S}\left(0.375 - \frac{0.375}{N_{\rm c}^2}\right) + \lambda_{\alpha_S}^2\left(0.25 - \frac{0.13}{N_{\rm c}} - \frac{0.22}{N_{\rm c}^2} + \frac{0.13}{N_{\rm c}^3} - \frac{0.023}{N_{\rm c}^4}\right)\right.$$
$$+ \lambda_{\alpha_S}^3\left(0.79 - \frac{1.6}{N_{\rm c}} - \frac{0.75}{N_{\rm c}^2} + \frac{1.6}{N_{\rm c}^3} - \frac{0.11}{N_{\rm c}^4} + \frac{0.027}{N_{\rm c}^5} + \frac{0.067}{N_{\rm c}^6}\right)$$
$$\left. + \lambda_{\alpha_S}^4\left(1.9 - \frac{4.3}{N_{\rm c}} - \frac{0.033}{N_{\rm c}^2} + \frac{4.2}{N_{\rm c}^3} - \frac{2.6}{N_{\rm c}^4} + \frac{0.5}{N_{\rm c}^5} + \frac{0.58}{N_{\rm c}^6} - \frac{0.4}{N_{\rm c}^7} + \frac{0.16}{N_{\rm c}^8}\right) + \mathcal{O}(\lambda_{\alpha_S}^5)\right], \qquad (3.23)$$

for the case of $n_f = 3$ as an example, and the renormalization scale is set to be $\mu^2 = Q^2$.

In Eqs.(3.22) and (3.23), the coefficients of $1/N_{\rm c}$ series are not growing. Therefore, within our present knowledge, the break down of $1/N_{\rm c}$ expansion itself does not seem to be occurring.

3.1.2.b Diquarks in the SU($N_{\rm c}$) gauge theory

Some of the properties of diquarks are peculiar to SU(3) QCD and not persist in the case of general SU($N_{\rm c}$) QCD. The most important one here is the color representation of diquarks. As mentioned in §1.4.1, the anti-fundamental nature of diquark is crucial for obtaining sensible results of baryons, but it is not the case in SU($N_{\rm c}$) QCD. The application of 't Hooft limit to baryon is first discussed in two dimension by Durgut in 1976 [101], and more general study was given by Witten in 1979 [94]. In these papers, the baryons are considered to be composed of $N_{\rm c}$ quarks to construct color-singlet states. Therefore relation between the diquark and the baryon is unclear once we consider SU($N_{\rm c}$) QCD naively. In order to make the relation clear, we can regard baryon as a bound state of "lark" [102] and diquark, instead of a bound state of quark and diquark in the SU(3) QCD. The lark has a color representation of $\overline{N_{\rm c}(N_{\rm c}-1)/2}$, so in the case of $N_{\rm c} = 3$ it coincides with the fundamental representation, and keep the baryon three-particle-object in any $N_{\rm c}$.

On the other hand, in the case of diquarks composing exotic mesons, specific representations of diquarks are not a crucial point. This situation is similar to the case of meson, whose quark content $(q\bar{q})$ does not change in any $N_{\rm c}$.

3.1.3 Color factors of various two-quark Green's functions in SU(3) QCD

What the 't Hooft limit takes into account is basically the coupling constant and the color factor, which is a certain trace of the generator $(t^a)^i_j$. In this subsection, we consider the color factors

of meson and diquark Green's functions explicitly in the case of $N_c = 3$, and examine whether or not the difference in the completely crossed ladder diagrams arises. A knowledge about two-particle-irreducible diagrams are sufficient since the color factors of two-particle-reducible diagrams are product of those of the two-particle-irreducible diagrams.

In the case of meson, all the diagrams generated by the prescription introduced in Eq.(3.40) such as

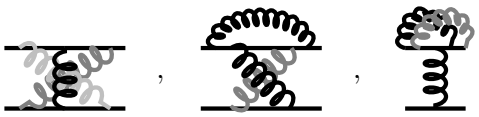

(3.24)

have the same color factors. This is because the meson Bethe-Salpeter amplitude is color-singlet and the flow of color indices are the same as that of the quark propagator. The values of color factors of n-gluon exchange diagrams are

$$\begin{aligned}\mathfrak{C}_r^{q\bar{q}} &= t^{a_1}t^{a_2}\cdots t^{a_n}t^{a_1}t^{a_2}\cdots t^{a_n} = \frac{2}{3}\left[\left(\frac{1}{3}\right)^{n-1} + \left(-\frac{2}{3}\right)^{n-1}\right] \\ &= \{1.3, -0.22, 0.37, -0.17, 0.14, -0.085, 0.059, -0.039, 0.026, -0.017, \dots\},\end{aligned} \tag{3.25}$$

which show a converging behavior. In the case of diquark, each of diagrams in Eq.(3.24) has different color factors and they are expressed as

$$\begin{aligned}&(t^{b_1}\cdots t^{b_{n_2}})(t^{a_1}\cdots t^{a_{n_1}})(t^{b_1}\cdots t^{b_{n_2}})\epsilon(t^{Ta_1}\cdots t^{Ta_{n_1}}) \\ &= \frac{1}{9}(-1)^{n_2-1}2^{-n_2-n_1+1}\left(\left(\frac{4}{3}\right)^{n_2-1}\left(4\left(-\frac{1}{3}\right)^{n_1} + \frac{2^{3n_1+1}}{3^{n_1}}\right) + \frac{(-2)^{n_2}(-1)^{n_1-1}}{3^{n_2+n_1-2}}\right)\end{aligned} \tag{3.26}$$

where n_1 is the number of gluons exchanged between two quarks and n_2 is the number of gluons going over the n_1-gluon exchange part. The values of the color factors (3.26) for fixed $n = n_1 + n_2$ with varying n_2 are

$$\begin{aligned}
n = 1 \quad &, \quad \{-0.67\} \\
n = 2 \quad &, \quad \{-0.56, 0.11\} \\
n = 3 \quad &, \quad \{-0.8, 0.43, -0.19\} \\
n = 4 \quad &, \quad \{-1.1, 0.52, -0.27, 0.086\} \\
n = 5 \quad &, \quad \{-1.4, 0.7, -0.35, 0.18, -0.07\} \\
n = 6 \quad &, \quad \{-1.9, 0.94, -0.47, 0.23, -0.12, 0.043\} \\
n = 7 \quad &, \quad \{-2.5, 1.2, -0.62, 0.31, -0.16, 0.081, -0.03\} \\
n = 8 \quad &, \quad \{-3.3, 1.7, -0.83, 0.42, -0.21, 0.1, -0.054, 0.019\}.
\end{aligned} \tag{3.27}$$

The case of $n = 3$ corresponds to the color factors of each diagrams of Eq.(3.24) respectively. From Eqs.(3.27), we see that the argument presented in §3.1.1 actually holds even in the case of $N_c = 3$, which are summarized in the following two points: the first point is that, for a fixed n, the largest color factor is that of the completely crossed one, namely, that of $n_2 = 0$. There are many other diagrams whose color factors does not have the expression (3.26), but we can confirm that most of

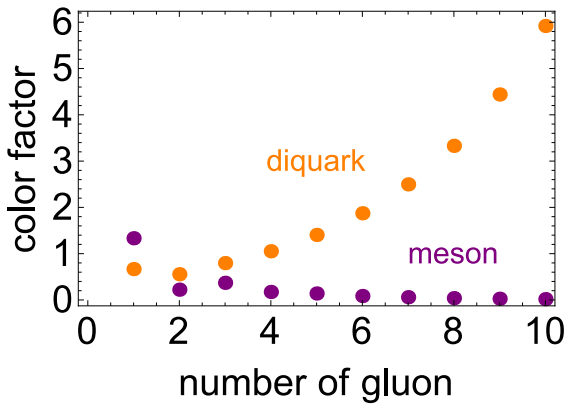

Figure 3.1: Comparison of the color factors of completely crossed ladder diagrams in the case of meson (3.25) and diquark (3.29).

them are smaller than the completely crossed diagrams. The second point is that, the color factors of completely crossed ladder diagrams grow as we increase n in contrast to the case of meson (3.25). We denote the color factor of completely crossed ladder diagrams as $\mathfrak{C}_n^{qq0^+}$:

$$\mathfrak{C}_n^{qq0^+} = -\frac{1}{9}2^{1-n}\left(\frac{3}{4}\left(4\left(-\frac{1}{3}\right)^n + 2^{3n+1}3^{-n}\right) + (-1)^{n-1}3^{2-n}\right), \tag{3.28}$$

$$= \{-0.67, -0.56, -0.8, -1.1, -1.4, -1.9, -2.5, -3.3, -4.4, -5.9, \dots\} \tag{3.29}$$

which is used in the later calculation (3.66). We compare the absolute values of color factors of completely crossed ladder diagrams in the case of meson (3.25) and diquark (3.29) in Fig.3.1, and we can clearly see the quite impressive difference.

Note that we do not relay on any specific models of the gluon dressing function and so on. The color-factor enhancement of the completely crossed ladder diagrams in the diquark channel holds generally in QCD.

3.2 Application to the Munczek-Nemirovsky model

In the previous subsection, we show that all of the completely crossed ladder diagrams are the leading order in the 't Hooft limit. Therefore, as long as we assume that the large-N_c approximation is valid, we have to take into account all of these contributions in the analysis of diquark Bethe-Salpeter equation. However, at present, it is well known that even the leading order contribution of t' Hooft limit can not be exactly calculated in the QCD of four dimension because of its complexity.

In this section we use the Munczek-Nemirovsky model introduced in Eq.(2.21) as a first attempt to reveal the qualitative behavior of the diquark Bethe-Salpeter equation under the 't Hooft limit. We know that the Munczek-Nemirovsky model is not so accurate in a modern point of view, but still it is considered to possess many important properties to grasp the infrared behavior of QCD. The marked feature of the Munczek-Nemirovsky model is its simplicity and it enables us to evaluate an infinitely-crossing ladder diagram. As far as we currently know, the use of Munczek-Nemirovsky model is the only way to perform an evaluation of multi-gluon exchanged diagrams.

Calculations presented in this section are performed by using `FORM` [103, 104] and `Mathematica`.

3.2.1 Finite fixed order truncations

3.2.1.a The rainbow-ladder truncation

First let us consider by far the most extensively used truncation scheme, the rainbow-ladder truncation. Diagrammatically this truncation scheme is expressed as

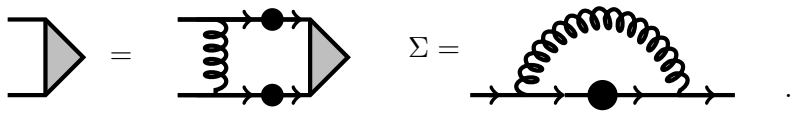

(3.30)

In the algebraic expression, the Bethe-Salpeter equation becomes

$$\Phi^{qq0^+}C = \frac{1}{2}G\gamma_\mu S(P/2)\Phi^{qq0^+}CS(P/2)^{\mathrm{T}}{\gamma_\mu}^{\mathrm{T}}. \tag{3.31}$$

In the Munczek-Nemirovsky model, the Bethe-Salpeter amplitude $\Phi(P,p)$ introduced in Eq.(2.29) has no relative momentum dependence because gluon does not transfer the momentum. Therefore here and in the following we express the amplitude as $\Phi(P)$. The algebraic expression of quark Dyson-Schwinger equation is

$$S(p) = S_0(p) - S(p)\Sigma[S(p)]S_0(p), \quad \Sigma[S(p)] = G\gamma_\mu S(p)\gamma_\mu, \tag{3.32}$$

where we introduce the quark self-energy function $\Sigma[S]$ for the sake of convenience. The product of the color factor $t^a t^a = \frac{4}{3}$ and the effective coupling $\frac{3}{4}G$ results in G.

Using the relation

$$CC^{-1} = 1, \quad C{\gamma_\mu}^{\mathrm{T}}C^{-1} = -\gamma_\mu, \quad CS(P/2)^{\mathrm{T}}C^{-1} = S(-P/2), \tag{3.33}$$

the Bethe-Salpeter equation (3.31) becomes

$$\Phi^{qq0^+} = -\frac{1}{2} G\gamma_\mu S_+ \Phi^{qq0^+} S_- \gamma_\mu, \tag{3.34}$$

where we define $S_+ = S(P/2), S_- = S(-P/2)$. In the following, we assume that the light quarks are degenerate, so that the flavor SU(3) symmetry is exact. Under this approximation, the difference of the representation of the flavor symmetry (the scalar diquarks are flavor anti-triplet whereas the axial vector diquarks are flavor sextet) is not apparent.

For comparison, we also write down the case of the pseudo-scalar meson

$$\Phi^{q\bar{q}0^-} = -G\gamma_\mu S_+ \Phi^{q\bar{q}0^-} S_- \gamma_\mu. \tag{3.35}$$

Note that the difference of the coefficient comes from the color factor.

The Bethe-Salpeter amplitude has a spinor structure, and in this case,

$$\Phi^\Psi(P) = \gamma_5 [f_1^\Psi(P^2) + \mathrm{i}\not{P} f_2^\Psi(P^2)], \quad \Psi = qq0^+, q\bar{q}0^-. \tag{3.36}$$

We recall that the states with opposite parities can be expressed in the same form (3.36) because we factor out the charge conjugation operator C of the diquark in Eq.(2.29).

Substituting Eq.(3.36) into Eq.(3.34), it becomes an eigenvalue equation of an two-component vector

$$\begin{pmatrix} f_1^{qq0^+} \\ f_2^{qq0^+} \end{pmatrix} = \mathcal{M}^{qq0^+} \begin{pmatrix} f_1^{qq0^+} \\ f_2^{qq0^+} \end{pmatrix}, \qquad \mathcal{M}^{qq0^+} = \begin{pmatrix} \mathcal{A}^2 s - 4\mathcal{B}^2 & -4\mathcal{A}\mathcal{B} \\ -2\mathcal{A}\mathcal{B}s & 2\mathcal{B}^2 - \frac{\mathcal{A}^2 s}{2} \end{pmatrix}, \tag{3.37}$$

where $\mathcal{A}$ and $\mathcal{B}$ are introduced in Eq.(2.18). If Eq.(3.37) have a nontrivial solution, the eigenvalue condition

$$\mathcal{D}^{qq0^+}(P^2) \equiv \det[1 - \mathcal{M}^{qq0^+}(P^2)] = 0 \tag{3.38}$$

is satisfied at some point. In order to investigate whether or not Eq.(3.38) has a solution, we plot the $\mathcal{D}^{qq0^+}$ as a function of P^2 in Fig.3.2 varying the input mass. They indeed have intersection points with x-axis, which indicate that the eigenvalue condition is satisfied at the point. The parallel procedure is possible for the case of meson, and we also plot them in Fig.3.2.

3.2.1.b Effect of the two-gluon exchange diagram with a cross

Next we include the contribution of the two-gluon exchange with a cross, namely,

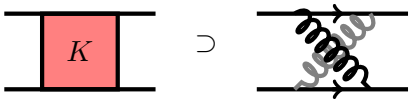

(3.39)

In the case of the meson Bethe-Salpeter equation, the preservation of chiral symmetry is essential. A truncation scheme to preserve the chiral symmetry was first proposed in a massive gluon model in 1974 [105], and the general one was discussed in 1993 [106]. Later, in 1996, that was proposed

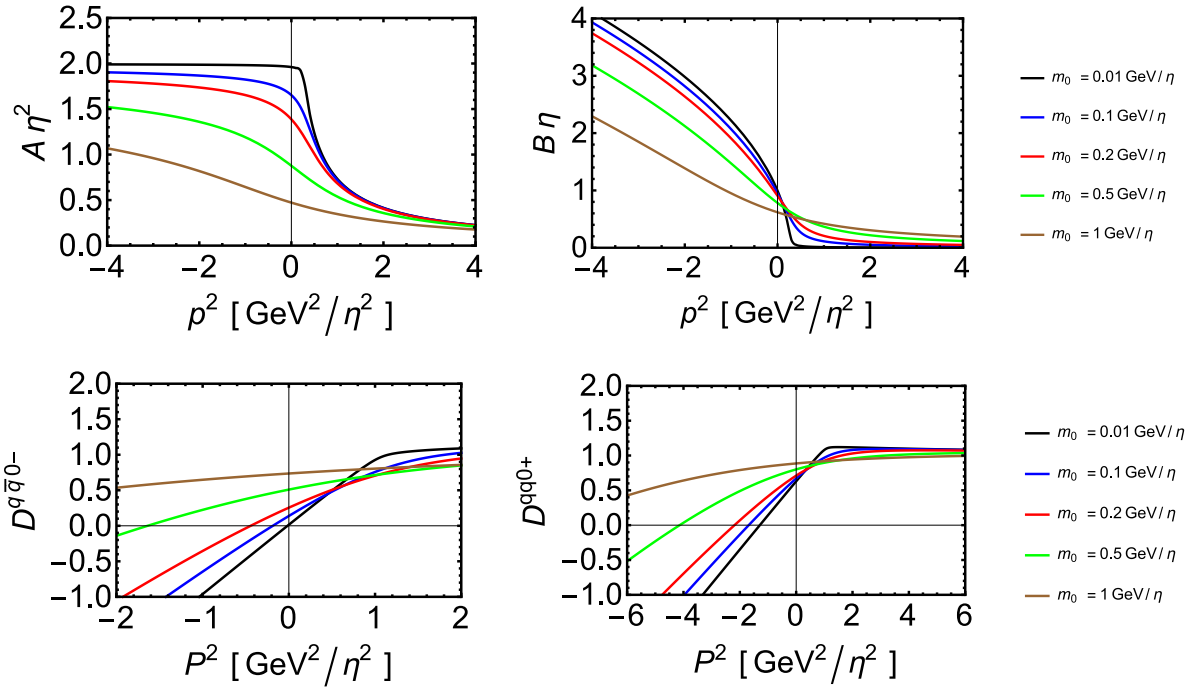

Figure 3.2: Behavior of the quark propagator $S = -\mathrm{i}\mathcal{A} + \mathcal{B}$ (upper panels) which is the solution of Eq.(3.32) and the eigenvalue equation $\mathcal{D}^{qq0^+}$, $\mathcal{D}^{q\bar{q}0^-}$ (lower panels) defined in Eq.(3.38) with the input quark mass $m_0/\eta = 0.01, 0.1, 0.2, 0.5, 1$.

independently [91]. In this chiral symmetry preserving scheme, the homogeneous Bethe-Salpeter equation is determined by a replacement of the quark self-energy function $\Sigma[S(p)]$ by

$$S(p) \to S_+ \Phi^{q\bar{q}0^-}(P) S_- . \tag{3.40}$$

The quark self-energy function up to two-gluon exchange is

$$\Sigma = G\gamma_\mu S \gamma_\mu + \frac{1}{8} G^2 \gamma_\mu S \gamma_\nu S \gamma_\mu S \gamma_\nu , \tag{3.41}$$

and applying the prescription (3.40), the resultant meson Bethe-Salpeter equation becomes

$$\begin{aligned} \Phi^{q\bar{q}0^-} =& -G\gamma_\mu S_+ \Phi^{q\bar{q}0^-} S_- \gamma_\mu \\ & - \frac{1}{8} G^2 \gamma_\mu S_+ \left[\Phi^{q\bar{q}0^-} S_- \gamma_\nu S_- \gamma_\mu + \gamma_\nu S_+ \Phi^{q\bar{q}0^-} S_- \gamma_\mu + \gamma_\nu S_+ \gamma_\mu S_+ \Phi^{q\bar{q}0^-} \right] S_- \gamma_\nu , \end{aligned} \tag{3.42}$$

and its diagrammatic expression is

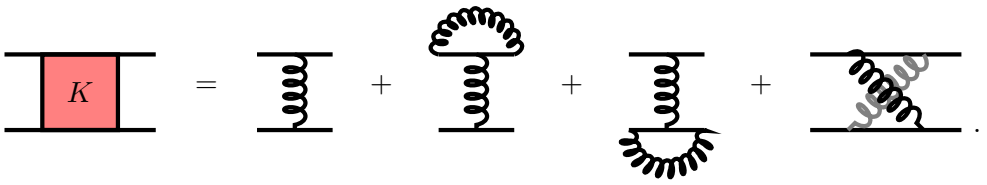

(3.43)

In Ref.[91], the same diagrams are considered for the diquark Bethe-Salpeter equation, resulting

$$\begin{aligned}\Phi^{qq0^+} =& -\frac{1}{2}G\gamma_\mu S_+\Phi^{qq0^+}S_-\gamma_\mu \\ & -\frac{1}{16}G^2\gamma_\mu S_+\left[\Phi^{qq0^+}S_-\gamma_\nu S_-\gamma_\mu + 5\gamma_\nu S_+\Phi^{qq0^+}S_-\gamma_\mu + \gamma_\nu S_+\gamma_\mu S_+\Phi^{qq0^+}\right]S_-\gamma_\nu. \end{aligned} \tag{3.44}$$

However, the diquark system is not related to the chiral symmetry at all. This means that the quark self-energy and the Bethe-Salpeter kernel is not necessarily related. Therefore we try combinations of the self-energy (3.32) and (3.41) and the diquark Bethe-Salpeter equation (3.44) and the following:

$$\Phi^{qq0^+} = -\frac{1}{2}G\gamma_\mu S_+\Phi^{qq0^+}S_-\gamma_\mu - \frac{5}{16}G^2\gamma_\mu S_+\gamma_\nu S_+\Phi^{qq0^+}S_-\gamma_\mu S_-\gamma_\nu, \tag{3.45}$$

which is expressed diagrammatically as

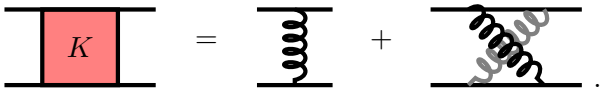

(3.46)

With this truncation, we focus only on the effect of the crossed ladder diagram. The resultant plot of eigenvalue equation is shown in Fig.3.3.

As we can see from the Fig.3.3, the intersections with x-axis disappear in the case of diquark Bethe-Salpeter equation for all three choices of the truncation schemes explained above, in contrast to the case of meson.

It is worth emphasizing that, at each terms of the meson Bethe-Salpeter equation (3.42) and the diquark Bethe-Salpeter equation (3.44), the structures of the gamma matrices and the quark propagators are exactly the same, and the differences are the coefficients of them, originating from the different way to contract the color indices. In the case of the two-gluon exchange diagrams with a cross, the color factors of the meson and diquark are respectively,

$$(t^a t^b)_i^j (t^a t^b)_j^k = -\frac{2}{9}\delta_i^k, \quad (t^a t^b)_i^j \epsilon_{jkl}(t^{a\mathrm{T}} t^{b\mathrm{T}})_m^k = -\frac{5}{9}\epsilon_{ilm}, \tag{3.47}$$

which shows the relative enhancement in the diquark channel.

What we see here are, the behavior of diquark Bethe-Salpeter equation changes drastically when we include the two-gluon exchange interaction into the interaction kernel, and this seems to be a consequence of the relatively large color factor in the diquark channel. These understanding was obtained in Ref.[91, 92].

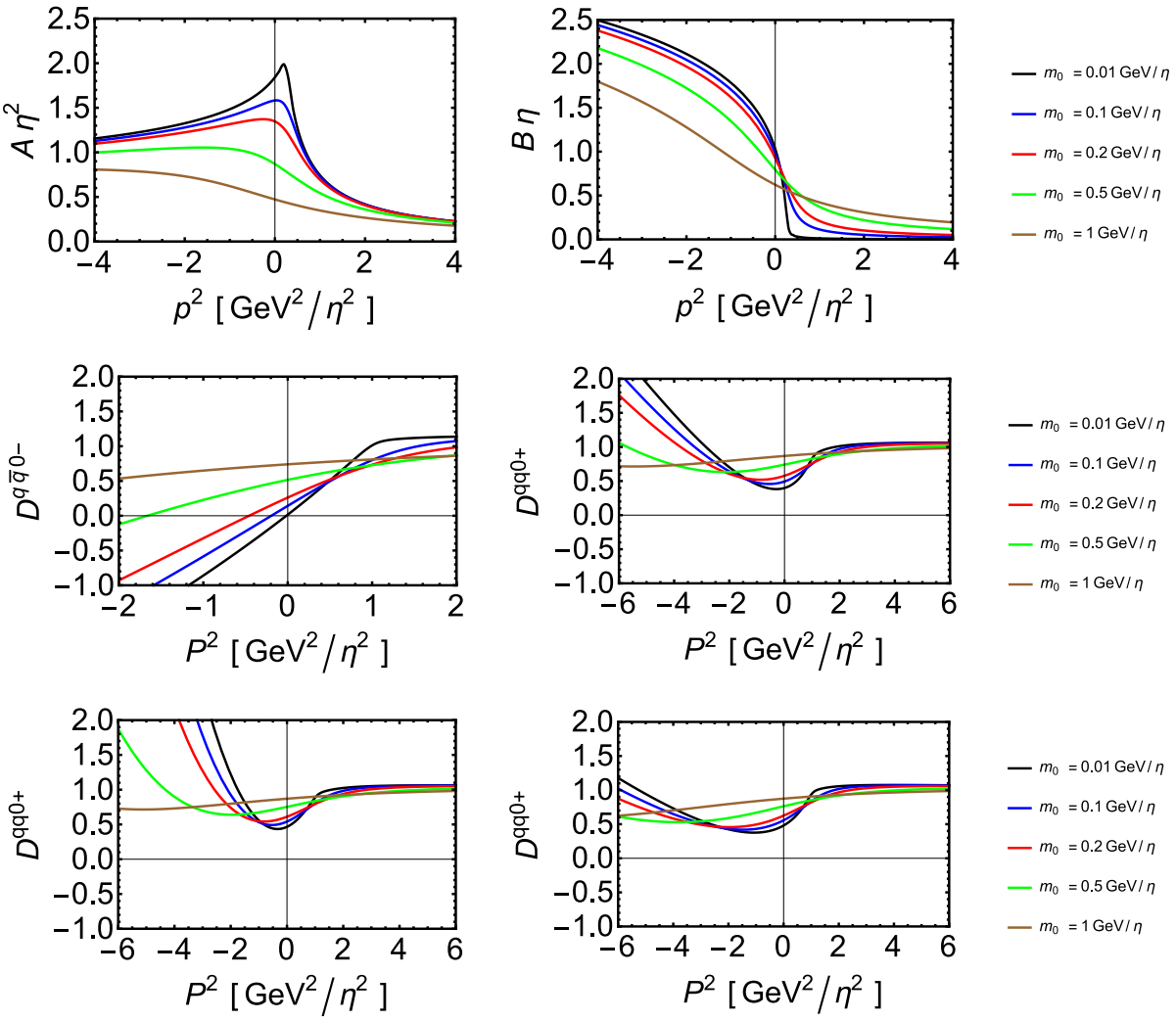

Figure 3.3: Behavior of the quark propagator $S = -\mathrm{i}\mathcal{A} + \mathcal{B}$ (top panels) which is the solution of Eq.(3.41) and the eigenvalue equation $\mathcal{D}^{qq0^+}$, $\mathcal{D}^{q\bar{q}0^-}$ (lower panels) defined in Eq.(3.38) with the input quark mass $m_0/\eta = 0.01, 0.1, 0.2, 0.5, 1$. The middle-left plot is obtained from Eq.(3.42) with Eq.(3.41). The middle-right plot is obtained from Eq.(3.44) with Eq.(3.41). The bottom-left plot is obtained from Eq.(3.44) with Eq.(3.32). The bottom-right plot is obtained from Eq.(3.45) with Eq.(3.41).

3.2.1.c Effect of the n-gluon exchange diagram with the complete crossing

Inspired by the enhancement of the completely crossed ladder diagrams in the diquark Bethe-Salpeter kernel shown in §3.1, we try including further crossed ladder contributions, namely,

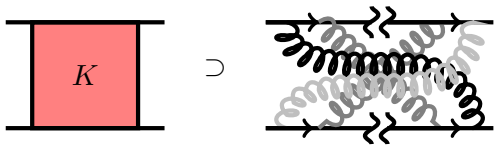

(3.48)

The minimal way to achieve Eq.(3.48) is to include the completely crossed ladder diagrams only. In this case, the number of diagrams in the kernel up to n-gluon exchange diagrams is n. For the sake of comparison, we also try "the apparently same truncation scheme as meson," in which the kernel is determined by the replacement (3.40) of the self-energy function with the completely crossing gluons:

$$\Sigma = -\sum_{r=1}^{n}(-G)^r \left(\frac{3}{4}\right)^r \mathfrak{C}_r^{q\bar{q}} \gamma_{\mu_1} S \gamma_{\mu_2} S \cdots S \gamma_{\mu_r} S \gamma_{\mu_1} S \cdots S \gamma_{\mu_r}. \tag{3.49}$$

For example, at $n = 3$,

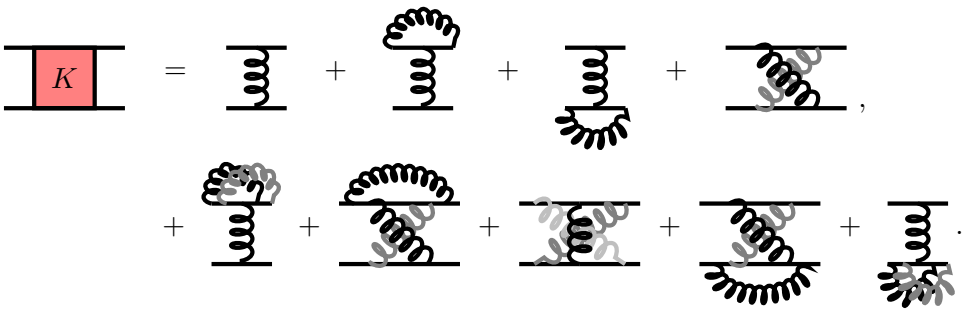

(3.50)

In this case, the kernel includes $2n-1$ diagrams for each n-gluon exchanges, and the number of diagrams in the kernel up to n-gluon exchange is n^2. Note that, in contrast to the case of the meson Bethe-Salpeter equation, this prescription is used only to determine the diagrams to include. If we apply this prescription literally, each diagrams with the same number of exchanging gluons have the same color factor, which not case with the diquark Bethe-Salpeter equation as we show in §3.1.3.

We also vary the truncation scheme for the quark Dyson-Schwinger. The self-energy function we consider up to n-gluon exchange is Eq.(3.49). The corresponding Dyson-Schwinger equation in terms of $\mathcal{A}(p^2)$ and $\mathcal{B}(p^2)$ defined in Eq.(2.18) becomes a pair of self-consistency equations

$$\begin{aligned}
\frac{\mathcal{A}}{p^2\mathcal{A}^2+\mathcal{B}^2} &= 1 - \sum_{r=1}^{n}(-G)^r \left(\tfrac{3}{4}\right)^r \mathfrak{C}_r^{q\bar{q}} \sum_{j=1}^{r} \mathfrak{a}_j^{(r)} \mathcal{A}(\mathcal{A}^2p^2)^{j-1}(\mathcal{B}^2)^{r-j} \\
\frac{\mathcal{B}}{p^2\mathcal{A}^2+\mathcal{B}^2} &= m_0 - \sum_{r=1}^{n}(-G)^r \left(\tfrac{3}{4}\right)^r \mathfrak{C}_r^{q\bar{q}} \sum_{j=1}^{r} \mathfrak{b}_j^{(r)} \mathcal{B}(\mathcal{A}^2p^2)^{r-j}(\mathcal{B}^2)^{j-1},
\end{aligned} \tag{3.51}$$

where the coefficients $\mathfrak{a}_j^{(n)}, \mathfrak{b}_j^{(n)}$ are summarized in Tab.3.1.

The solutions of Eqs.(3.51) are displayed in Fig.3.4 up to $n = 6$, with the input quark mass

Table 3.1: Coefficients $\mathfrak{a}_j^{(n)}$ and $\mathfrak{b}_j^{(n)}$ in Eqs.(3.51).

	$\mathfrak{a}_j^{(n)}$						$\mathfrak{b}_j^{(n)}$					
n	j						j					
	1	2	3	4	5	6	1	2	3	4	5	6
1	2						4					
2	-8	-12					-12	-8				
3	32	64	16				32	32	16			
4	-128	-336	-256		-112		-112	-256	-336	-128		
5	512	1536	1728	1152	192		384	1152	1728	768	64	
6	-2048	-7360	-12288	-12672	-6144	-1472	-1472	-6144	-12672	-12288	-7360	-2048

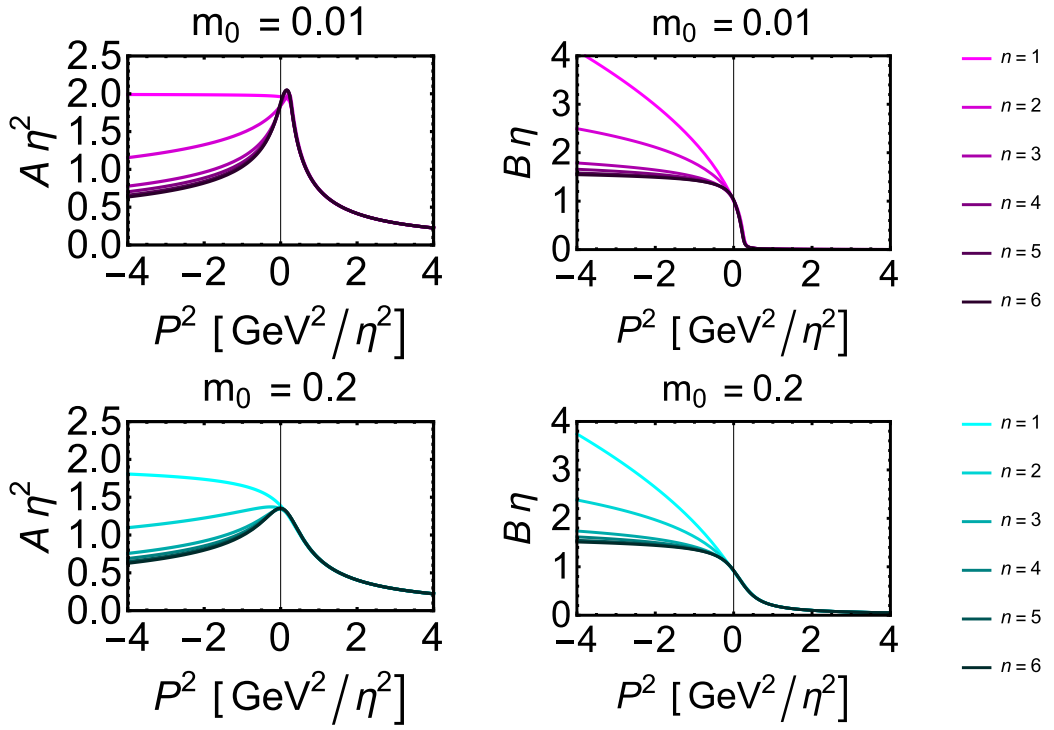

Figure 3.4: The behavior of the quark propagator $S(p) = -i\not{p}\mathcal{A}(p^2) + \mathcal{B}(p^2)$ as the solutions of the Dyson-Schwinger equation (3.51), with the input mass parameter $m_0/\eta = 0.01$ (upper panels) and $m_0/\eta = 0.2$ (lower panels).

$m_0/\eta = 0.01$ and $m_0/\eta = 0.2$. The equations (3.51) are $(2n+1)$-th order equations, which have multi solutions in general. Here we choose the solution which is the most close to the rainbow-ladder solution at $p^2/\eta^2 = 4$, where the convergence of the perturbative expansion is considered to be good.

Now we go on to the Bethe-Salpeter equation. First we consider the case of meson in order to compare with diquark later. The meson Bethe-Salpeter equation is obtained by the prescription (3.40), resulting

$$\mathcal{M}_n^{q\bar{q}0^-}(P^2) = \sum_{r=1}^{n}(-G)^r \left(\tfrac{3}{4}\right)^r \mathfrak{C}_r^{q\bar{q}0^-} h_r^{q\bar{q}0^-}(P^2) \tag{3.52}$$

$$h_n^{q\bar{q}0^-} = \begin{pmatrix} h_{n,(1,1)}^{q\bar{q}0^-} & h_{n,(1,2)}^{q\bar{q}0^-} \\ h_{n,(2,1)}^{q\bar{q}0^-} & h_{n,(2,2)}^{q\bar{q}0^-} \end{pmatrix} = \sum_{k=0}^{n} \begin{pmatrix} h_{n,(1,1),k}^{q\bar{q}0^-} & h_{n,(1,2),k}^{q\bar{q}0^-}(\mathcal{B}/\mathcal{A}) \\ h_{n,(2,1),k}^{q\bar{q}0^-}(\mathcal{A}/\mathcal{B}) & h_{n,(2,2),k}^{q\bar{q}0^-} \end{pmatrix} (\mathcal{A}^2P^2)^{n-k}(\mathcal{B}^2)^k, \tag{3.53}$$

Table 3.2: Coefficients in Eqs.(3.53), (3.56)

	$h^{q\bar{q}0^-}_{n,(i,j),k}$							$h^{qq0^+}_{n,(i,j),k}$						
$n,(i,j)$	j							j						
	0	1	2	3	4	5	6	0	1	2	3	4	5	6
1,(1, 1)	1	-4						-1	4					
1,(1, 2)	4	0						-4	0					
1,(2, 1)	0	2						0	-2					
1,(2, 2)	−1/2	2						1/2	-2					
2,(1, 1)	−1/4	3	8					−1/4	3	8				
2,(1, 2)	-2	-4	0					-2	-4	0				
2,(2, 1)	0	-1	-8					0	-1	-8				
2,(2, 2)	1/2	3	-4					1/2	3	-4				
3,(1, 1)	1	6	12	-16				−1/4	0	0	16			
3,(1, 2)	3	20	48	0				−3/2	-8	-24	0			
3,(2, 1)	0	3	28	48				0	−3/2	-16	-24			
3,(2, 2)	−1/2	0	36	80				1/2	3	-12	-32			
4,(1, 1)	−13/16	−23/4	-19	28	128			−1/16	1/4	5	76	128		
4,(1, 2)	−5/2	-23	-112	-176	0			-1	-11	-64	-80	0		
4,(2, 1)	0	−11/4	-28	-92	-160			0	−5/4	-16	-44	-64		
4,(2, 2)	1/2	7/4	-19	-92	-208			1/2	19/4	5	4	-16		
5,(1, 1)	1	33/2	99	204	144	-64		−1/16	−3/2	-9	36	96	64	
5,(1, 2)	11/4	45	288	720	704	0		−7/8	-15	-108	-240	-224	0	
5,(2, 1)	0	13/4	51	288	816	832		0	−11/8	-21	-108	-336	-352	
5,(2, 2)	−1/2	−3/2	51	396	1296	1472		1/2	21/4	9	-36	-336	-512	
6,(1, 1)	−61/64	−159/16	−93/2	-78	-36	720	2048	−1/64	−27/16	−21/2	66	492	1680	2048
6,(1, 2)	−21/8	−139/4	-240	-936	-2528	-3264	0	−3/4	−73/4	-168	-648	-1472	-1344	0
6,(2, 1)	0	−51/16	−79/2	-234	-960	-2224	-2688	0	−21/16	-23	-162	-672	-1168	-768
6,(2, 2)	1/2	45/16	−9/4	-78	-744	-2544	-3904	1/2	105/16	123/4	66	-168	-432	-64

where $\mathcal{A} = \mathcal{A}(P^2/4)$ and $\mathcal{B} = \mathcal{B}(P^2/4)$, and the coefficients $h^{q\bar{q}0^-}_{n,(i,j),k}$ are summarized in Tab.3.2.

We plot the left-hand-side of the eigenvalue equation (3.38) in Fig.3.5 with the input mass parameter $m_0/\eta = 0.01$ and $m_0/\eta = 0.2$ for each n of Eq.(3.52). We see from these plots that the solution of the meson Bethe-Salpeter equation is stable against the change of truncation scheme once the interaction kernel is determined by the chiral symmetry preserving prescription. Note that the correct choice of the quark self-energy function is only one for each plots, but even so, the deviations of incorrect plots form the correct one are quite small. The reason is considered to be the following: the difference of darkness of the curves of Fig.3.5 corresponds to the difference of the quark self-energy function. However from Fig.3.4, we can see that the quark propagator is almost unchanged against the change of the quark self-energy function around $p^2 \simeq 0$, and this region is where the meson Bethe-Salpeter equation has a solution. This is why the dependence of the solution of the meson Bethe-Salpeter equation on the quark self-energy function is small.

Next we consider the diquark Bethe-Salpeter equation. In the minimal inclusion of the completely crossed ladder diagrams, the diquark Bethe-Salpeter equation becomes

$$\Phi^{qq0^+} = -\sum_{r=1}^{n}(-G)^r \left(\frac{3}{4}\right)^r \mathfrak{C}_r^{qq0^+} \gamma_{\mu_1} S_+ \cdots S_+ \gamma_{\mu_r} S_+ \Phi^{qq0^+} S_+ \gamma_{\mu_1} S_- \cdots S_- \gamma_{\mu_r}. \tag{3.54}$$

The matrix appearing in the eigenvalue equation (3.38) becomes

$$\mathcal{M}_n^{qq0^+}(P^2) = \sum_{r=1}^{n}(-G)^r \left(\tfrac{3}{4}\right)^r \mathfrak{C}_r^{qq0^+} h_r^{qq0^+}(P^2), \tag{3.55}$$

$$h_n^{qq0^+} = \begin{pmatrix} h^{qq0^+}_{n,(1,1)} & h^{qq0^+}_{n,(1,2)} \\ h^{qq0^+}_{n,(2,1)} & h^{qq0^+}_{n,(2,2)} \end{pmatrix} = \sum_{k=0}^{n} \begin{pmatrix} h^{qq0^+}_{n,(1,1),k} & h^{qq0^+}_{n,(1,2),k}(\mathcal{B}/\mathcal{A}) \\ h^{qq0^+}_{n,(2,1),k}(\mathcal{A}/\mathcal{B}) & h^{qq0^+}_{n,(2,2),k} \end{pmatrix} (\mathcal{A}^2 P^2)^{n-k} (\mathcal{B}^2)^k, \tag{3.56}$$

and the coefficients $h^{qq0^+}_{n,(i,j),k}$ are summarized in Tab.3.2.

The behavior of the resultant eigenvalue equation $\mathcal{D}^{qq0^+}(P^2) \equiv \det[1 - \mathcal{M}^{qq0^+}(P^2)]$ are plotted

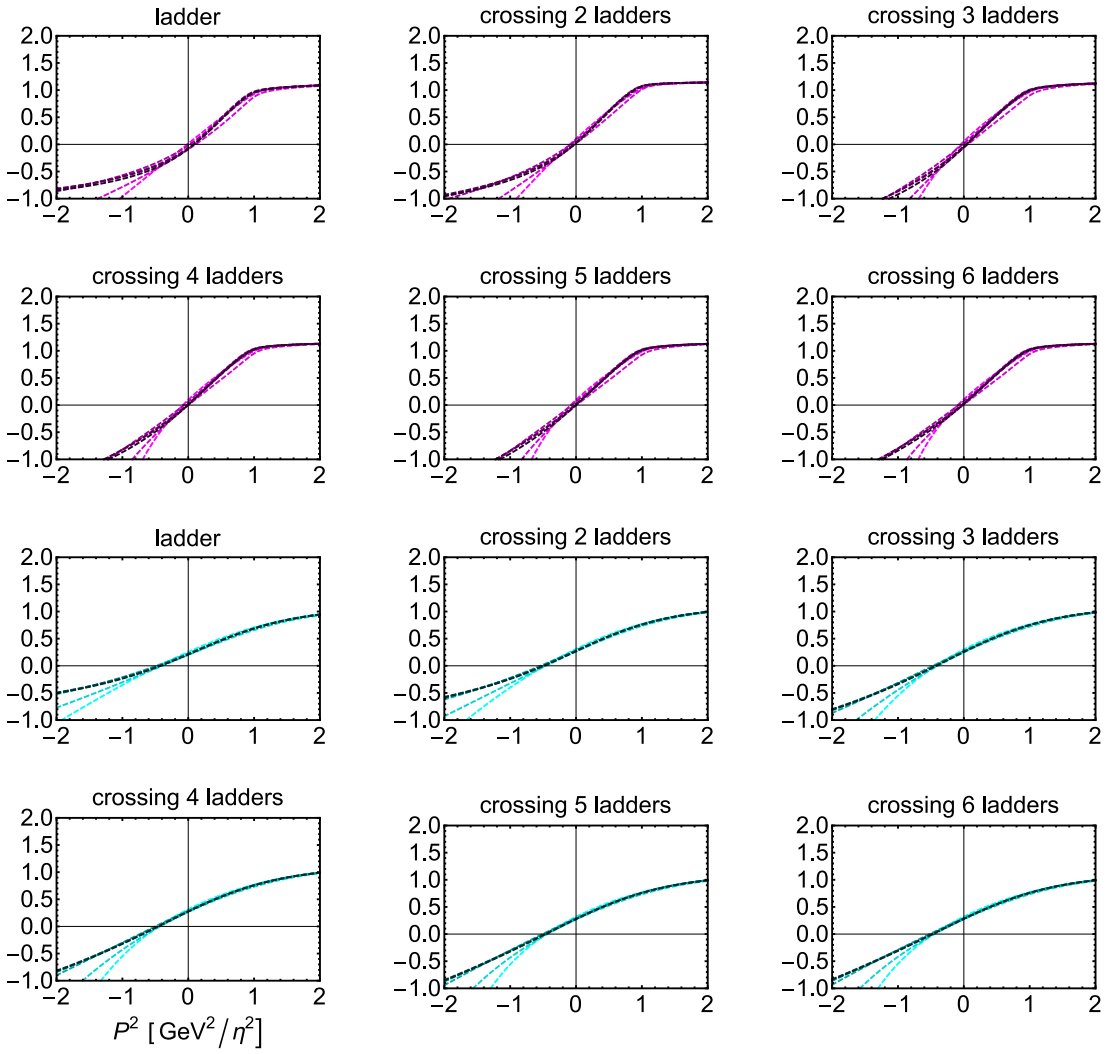

Figure 3.5: The behavior of the eigenvalue equation $\mathcal{D}^{q\bar{q}0^-}(P^2) \equiv \det[1 - \mathcal{M}^{q\bar{q}0^-}(P^2)]$ with $\mathcal{M}^{q\bar{q}0^-}$ determined in Eq.(3.52). The input mass parameter is $m_0/\eta = 0.01$ (upper six panels) and $m_0/\eta = 0.2$ (lower six panels), and the color of lines are the same as that of Fig.3.4. The plot label "ladder" corresponds to $\mathcal{M}_1^{q\bar{q}0^-}$ and "crossing n ladders" corresponds to $\mathcal{M}_n^{q\bar{q}0^-}$ for $n \geq 2$. These plots show that the solution of the meson Bethe-Salpeter equation is stable against the change of truncation scheme once the interaction kernel is determined by the chiral symmetry preserving prescription. Not that the correct choice of the quark self-energy function is only one for each plots. Even so, the deviations of incorrect plots form the correct one are quite small.

in Fig.3.6 with the input mass parameter $m_0/\eta = 0.01$ and $m_0/\eta = 0.2$. The one-gluon exchange approximation results in the existence of the intersection with x-axis, and it disappears in the two-gluon exchange approximation, as we already see in §3.2.1.a and §3.2.1.b respectively. This tendency is basically independent of the choice of the self-energy function of the quark Dyson-Schwinger equation within our consideration. In the three-gluon exchange approximation, the intersection turns out to revive. As far as we see Fig.3.6, every time the number of gluons exchanged increases, the behavior of the diquark Bethe-Salpeter equation changes drastically.

Finally we consider the diquark Bethe-Salpeter equation whose interaction kernel is determined by the analogy of the meson Bethe-Salpeter equation. The resultant behavior of $\mathcal{D}^{qq0^+}(P^2)$ is shown in Fig.3.7. The qualitative tendency is similar to the case of Fig.3.6, although the Bethe-Salpeter kernel of Fig.3.6 includes only n out of n^2 diagrams in that of Fig.3.7. This fact supports the idea that the completely crossed ladder diagrams give the dominant contribution at each orders.

We would like to emphasize once again that, the only difference between the Bethe-Salpeter equation of Fig.3.5 (meson) and Fig.3.7 (diquark) is the color factor, which results in a considerable differences in the behavior of the eigenvalue equation.

With the observation of this subsection, we conclude that the truncation of the diquark Bethe-Salpeter kernel at certain finite number of gluons exchanged does not work.

3.2.2 Resummation of the completely crossed ladder diagrams

Let us recall the homogeneous Bethe-Salpeter equation derived in §2.3,

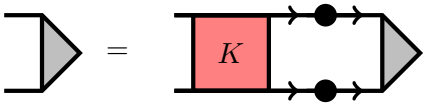

(3.57)

In this subsection, we will include all the completely crossed ladder diagrams into the interaction kernel K, and denote the resultant one as $K^\sharp$. Then $K^\sharp$ is expressed as

$$K^\sharp = -\tfrac{3}{4}G\left[\gamma^\mu t^a\right]\otimes\left[\gamma^\mu t^a\right]^{\mathrm{T}} + \left(\tfrac{3}{4}\right)^2 G^2\left[\gamma^\mu t^a S(p)\gamma^\nu t^b\right]\otimes\left[\gamma^\mu t^a S(p)\gamma^\nu t^b\right]^{\mathrm{T}} + \cdots \tag{3.58}$$

$$= \quad + \quad + \cdots . \tag{3.59}$$

Formally this kernel satisfies the self-consistency relation

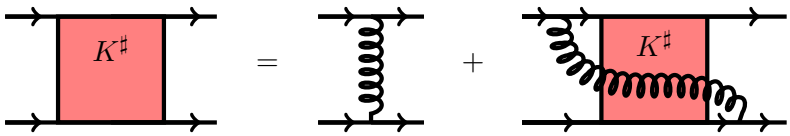

(3.60)

in a diagrammatic expression and

$$K^\sharp = -\tfrac{3}{4}G\left[\gamma^\mu t^a\right]\otimes\left[\gamma^\mu t^a\right]^{\mathrm{T}} - \tfrac{3}{4}G\left[\gamma^\mu t^a\right]\otimes\left[\gamma^\mu t^a\right]^{\mathrm{T}} K^\sharp \tag{3.61}$$

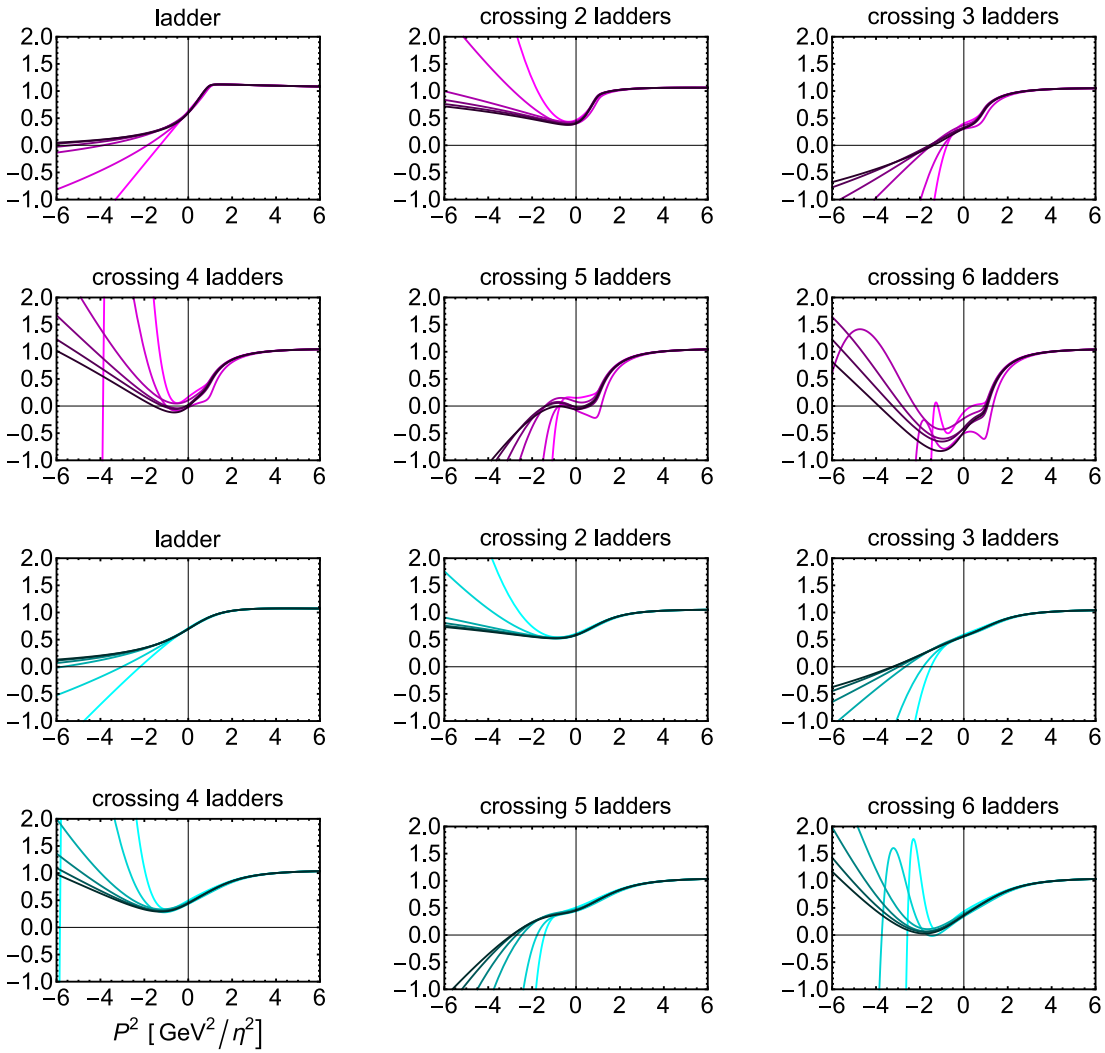

Figure 3.6: The behavior of the eigenvalue equation $\mathcal{D}^{qq0^+}(P^2) \equiv \det[1 - \mathcal{M}^{qq0^+}(P^2)]$ with $\mathcal{M}^{qq0^+}$ determined in Eq.(3.55). The input mass parameter is $m_0/\eta = 0.01$ (upper six panels) and $m_0/\eta = 0.2$ (lower six panels), and the color of lines are the same as that of Fig.3.4. The plot label "ladder" corresponds to $\mathcal{M}_1^{qq0^+}$ and "crossing n ladders" corresponds to $\mathcal{M}_n^{qq0^+}$ for $n \geq 2$.

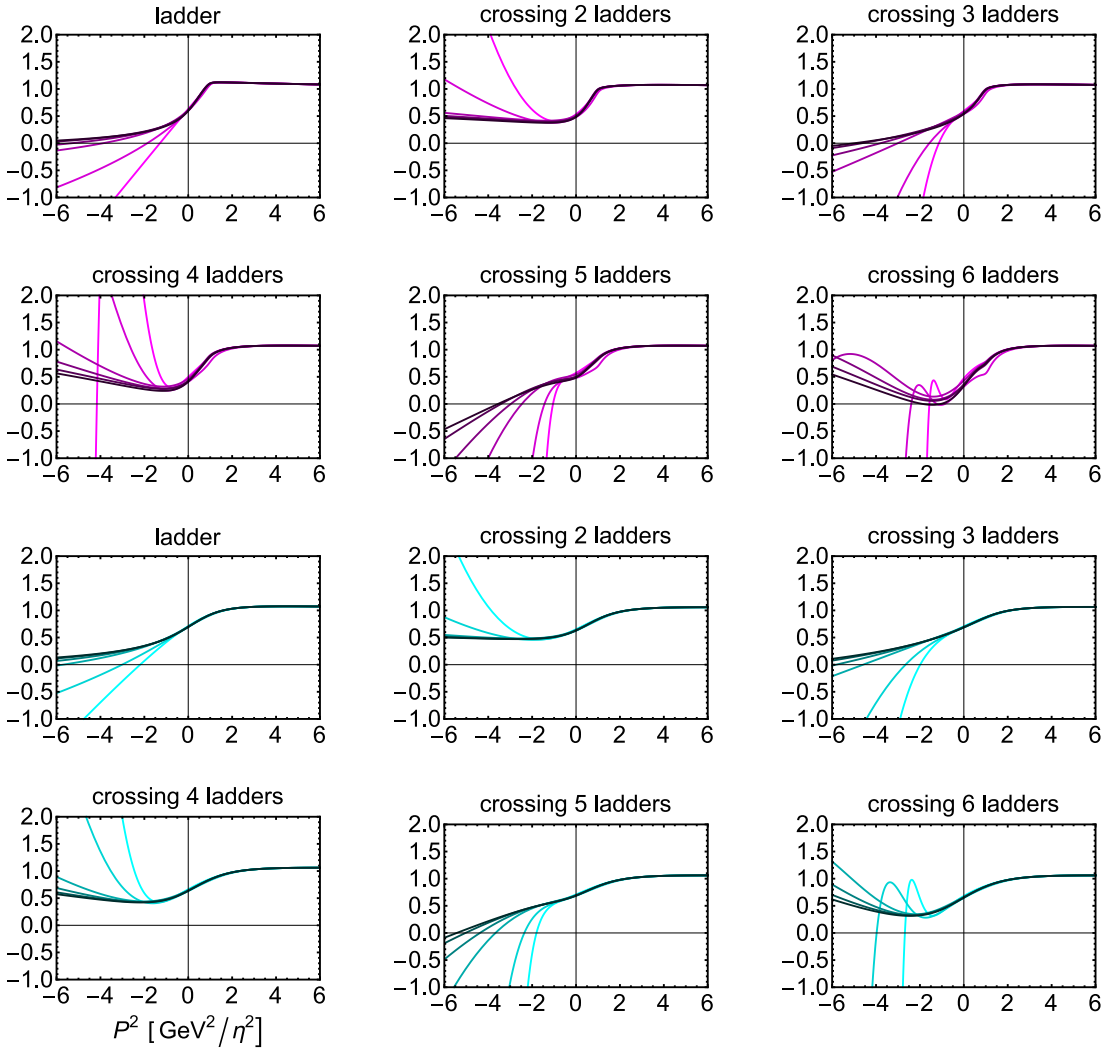

Figure 3.7: The behavior of the eigenvalue equation $\mathcal{D}^{qq0^+}(P^2) \equiv \det[1 - \mathcal{M}^{qq0^+}(P^2)]$ with $\mathcal{M}^{qq0^+}$ determined by the prescription of analogy with meson. [See the below Eq.(3.48).] The input mass parameter is $m_0/\eta = 0.01$ (upper six panels) and $m_0/\eta = 0.2$ (lower six panels), and the color of lines are the same as that of Fig.3.4. The plot label "ladder" corresponds to $\mathcal{M}_1^{qq0^+}$ and "crossing n ladders" corresponds to $\mathcal{M}_n^{qq0^+}$ for $n \geq 2$.

in an algebraic expression. We expand $K^\sharp$ in terms of the effective coupling G:

$$K^\sharp = \sum_{n=1}^{\infty} G^n K_n, \tag{3.62}$$

where

$$K_1 = -\tfrac{3}{4}\left[\gamma^\mu t^a\right] \otimes \left[\gamma^\mu t^a\right]^{\mathrm{T}}, \quad K_2 = \left(\tfrac{3}{4}\right)^2 \left[\gamma^\mu t^a S(p) \gamma^\nu t^b\right] \otimes \left[\gamma^\mu t^a S(p) \gamma^\nu t^b\right]^{\mathrm{T}}, \ldots \tag{3.63}$$

and Eq.(3.61) becomes a recurrence relation

$$K_{n+1} = -\tfrac{3}{4} G \left[\gamma^\mu S(p) t^a\right] \otimes \left[\gamma^\mu S(p) t^a\right]^{\mathrm{T}} K_n \qquad (n \geq 1). \tag{3.64}$$

Substituting $K^\sharp$ into the diquark Bethe-Salpeter equation, we obtain

$$\Phi^{qq0^+}(P)_{\alpha\beta} = \tilde{K}_{\alpha\beta\alpha'\beta'} [S_+ \Phi^{qq0^+}(P) S_-]_{\alpha'\beta'}. \tag{3.65}$$

The expansion of $\tilde{K}$ can be factorized into the color factor times Dirac matrices, and we can further expand $\tilde{K}_n$ with respect to the basis of Dirac matrices:

$$\tilde{K} = \sum_{n=1}^{\infty} \mathfrak{C}_n^{qq0^+} \left(-\tfrac{3}{4} G\right)^n \tilde{K}_n, \qquad \tilde{K}_n = \mathbf{a}_n \cdot \mathbf{b} = \sum_{I=1}^{12} a_{n,I} b_I, \tag{3.66}$$

where the color factor is defined in Eq.(3.28) and b_I's are

$$\begin{array}{lll}
b_1 = \gamma_\mu \otimes \gamma_\mu, & b_5 = \gamma_\mu\gamma_\nu \otimes \gamma_\mu\gamma_\nu, & b_9 = \gamma_\mu\gamma_\nu\gamma_\rho \otimes \gamma_\mu\gamma_\nu\gamma_\rho, \\
b_2 = \mathrm{i}\gamma_\mu \otimes \not{P}\gamma_\mu, & b_6 = \mathrm{i}\gamma_\mu\gamma_\nu \otimes \not{P}\gamma_\mu\gamma_\nu, & b_{10} = \mathrm{i}\gamma_\mu\gamma_\nu\gamma_\rho \otimes \not{P}\gamma_\mu\gamma_\nu\gamma_\rho, \\
b_3 = \mathrm{i}\not{P}\gamma_\mu \otimes \gamma_\mu, & b_7 = \mathrm{i}\not{P}\gamma_\mu\gamma_\nu \otimes \gamma_\mu\gamma_\nu, & b_{11} = \mathrm{i}\not{P}\gamma_\mu\gamma_\nu\gamma_\rho \otimes \gamma_\mu\gamma_\nu\gamma_\rho, \\
b_4 = -\not{P}\gamma_\mu \otimes \not{P}\gamma_\mu/P^2, & b_8 = -\not{P}\gamma_\mu\gamma_\nu \otimes \not{P}\gamma_\mu\gamma_\nu/P^2, & b_{12} = -\not{P}\gamma_\mu\gamma_\nu\gamma_\rho \otimes \not{P}\gamma_\mu\gamma_\nu\gamma_\rho/P^2.
\end{array} \tag{3.67}$$

An apparently independent element $\gamma_\mu\gamma_\nu\gamma_\rho\gamma_\sigma \otimes \gamma_\mu\gamma_\nu\gamma_\rho\gamma_\sigma$ is in fact expressed as

$$\gamma_\mu\gamma_\nu\gamma_\rho\gamma_\sigma \otimes \gamma_\mu\gamma_\nu\gamma_\rho\gamma_\sigma = \left(4P^2\gamma_\mu\gamma_\nu \otimes \gamma_\mu\gamma_\nu + 4\not{P}\gamma_\mu\gamma_\nu\gamma_\rho \otimes \not{P}\gamma_\mu\gamma_\nu\gamma_\rho - 16\not{P}\gamma_\mu \otimes \not{P}\gamma_\mu\right)/P^2. \tag{3.68}$$

The elements such as $\mathbf{1} \otimes \mathbf{1}$ and $\mathbf{1} \otimes \not{P}$ are linearly independent with the basis (3.67), but never appear in the recurrence relation (3.64). The proof is the following: The recurrence relation (3.64) adds either γ^μ or $\mathrm{i}\gamma^\mu\not{P}$ to each elements of basis (3.67) form left. Then we move $\not{P}$ to the left if it exists. During this procedure, the number of $\gamma_\mu \otimes \gamma_\mu$ pairs does not decrease. When the number of gamma matrix pairs becomes more than four, the identity (3.68) is applicable, but this procedure does not completely vanish the pair $\gamma_\mu \otimes \gamma_\mu$, leaving at least one gamma matrix pair. Therefore the elements like $\mathbf{1} \otimes \mathbf{1}$ do not appear in our calculation. From above consideration, the basis (3.67) is sufficient for our purpose even though it is not the complete set of the Dirac bi-matrices.

We can construct a 12×12 operator defined as

$$\mathcal{R}_I{}^J b_J = [[\gamma S] \otimes [\gamma S]]\, b_I, \tag{3.69}$$

and the explicit expression of $\mathcal{R}_I{}^J$ is

$$\begin{pmatrix}
0 & 0 & 0 & 0 & 0 & 0 & 0 & 0 & 4\mathcal{A}^2 s & -4\mathcal{A}\mathcal{B}s & -4\mathcal{A}\mathcal{B}s & 16\mathcal{B}^2 \\
-2\mathcal{A}\mathcal{B} & -\frac{\mathcal{A}^2 s}{2} & 2\mathcal{B}^2 & 2\mathcal{A}\mathcal{B} & 0 & 0 & 0 & 0 & -16\mathcal{A}\mathcal{B} & -4\mathcal{A}^2 s & 16\mathcal{B}^2 & 16\mathcal{A}\mathcal{B} \\
-2\mathcal{A}\mathcal{B} & 2\mathcal{B}^2 & -\frac{\mathcal{A}^2 s}{2} & 2\mathcal{A}\mathcal{B} & 0 & 0 & 0 & 0 & -16\mathcal{A}\mathcal{B} & 16\mathcal{B}^2 & -4\mathcal{A}^2 s & 16\mathcal{A}\mathcal{B} \\
0 & 0 & 0 & 0 & 0 & 0 & 0 & 0 & 16\mathcal{B}^2 & 4\mathcal{A}\mathcal{B}s & 4\mathcal{A}\mathcal{B}s & 4\mathcal{A}^2 s \\
\mathcal{B}^2 & \frac{\mathcal{A}\mathcal{B}s}{4} & \frac{\mathcal{A}\mathcal{B}s}{4} & \frac{\mathcal{A}^2 s}{4} & 0 & 0 & 0 & 0 & 4\mathcal{B}^2 & \mathcal{A}\mathcal{B}s & \mathcal{A}\mathcal{B}s & \mathcal{A}^2 s \\
\mathcal{A}\mathcal{B} & -\mathcal{B}^2 & \frac{\mathcal{A}^2 s}{4} & -\mathcal{A}\mathcal{B} & -2\mathcal{A}\mathcal{B} & -\frac{\mathcal{A}^2 s}{2} & 2\mathcal{B}^2 & 2\mathcal{A}\mathcal{B} & 4\mathcal{A}\mathcal{B} & -4\mathcal{B}^2 & \mathcal{A}^2 s & -4\mathcal{A}\mathcal{B} \\
\mathcal{A}\mathcal{B} & \frac{\mathcal{A}^2 s}{4} & -\mathcal{B}^2 & -\mathcal{A}\mathcal{B} & -2\mathcal{A}\mathcal{B} & 2\mathcal{B}^2 & -\frac{\mathcal{A}^2 s}{2} & 2\mathcal{A}\mathcal{B} & 4\mathcal{A}\mathcal{B} & \mathcal{A}^2 s & -4\mathcal{B}^2 & -4\mathcal{A}\mathcal{B} \\
\frac{\mathcal{A}^2 s}{4} & -\frac{1}{4}\mathcal{A}\mathcal{B}s & -\frac{1}{4}\mathcal{A}\mathcal{B}s & \mathcal{B}^2 & 0 & 0 & 0 & 0 & \mathcal{A}^2 s & -\mathcal{A}\mathcal{B}s & -\mathcal{A}\mathcal{B}s & 4\mathcal{B}^2 \\
0 & 0 & 0 & 0 & \mathcal{B}^2 & \frac{\mathcal{A}\mathcal{B}s}{4} & \frac{\mathcal{A}\mathcal{B}s}{4} & \frac{\mathcal{A}^2 s}{4} & -\mathcal{A}^2 s & \mathcal{A}\mathcal{B}s & \mathcal{A}\mathcal{B}s & -4\mathcal{B}^2 \\
0 & 0 & 0 & 0 & \mathcal{A}\mathcal{B} & -\mathcal{B}^2 & \frac{\mathcal{A}^2 s}{4} & -\mathcal{A}\mathcal{B} & 2\mathcal{A}\mathcal{B} & \frac{\mathcal{A}^2 s}{2} & -2\mathcal{B}^2 & -2\mathcal{A}\mathcal{B} \\
0 & 0 & 0 & 0 & \mathcal{A}\mathcal{B} & \frac{\mathcal{A}^2 s}{4} & -\mathcal{B}^2 & -\mathcal{A}\mathcal{B} & 2\mathcal{A}\mathcal{B} & -2\mathcal{B}^2 & \frac{\mathcal{A}^2 s}{2} & -2\mathcal{A}\mathcal{B} \\
0 & 0 & 0 & 0 & \frac{\mathcal{A}^2 s}{4} & -\frac{1}{4}\mathcal{A}\mathcal{B}s & -\frac{1}{4}\mathcal{A}\mathcal{B}s & \mathcal{B}^2 & -4\mathcal{B}^2 & -\mathcal{A}\mathcal{B}s & -\mathcal{A}\mathcal{B}s & -\mathcal{A}^2 s
\end{pmatrix}. \tag{3.70}$$

This matrix is used to evaluate each coefficients $a_{n+1,I}$:

$$a_{n+1,I} = a_{n,J}\mathcal{R}_I{}^J = a_{1,J}(\mathcal{R}^n)_I{}^J = \delta_{1,J}(\mathcal{R}^n)_I{}^J, \tag{3.71}$$

where the Kronecker delta $\delta_{1,J}$ appears because $\tilde{K}_1 = -\gamma_\mu \otimes \gamma_\mu$. Now the kernel (3.62) can be expressed as

$$\tilde{K} = \sum_{n=1}^{\infty} \left(-\tfrac{3}{4}G\right)^n \mathfrak{C}_n^{qq0^+} \delta_{1,J}(\mathcal{R}^{n-1})_I{}^J b_I = G[(-\tfrac{3}{4}GR + 6)^{-1} - (-\tfrac{3}{4}G4R - 3)^{-1}]_I{}^J b_I \delta_{1.J}. \tag{3.72}$$

Next we consider the eigenvalue equation (3.37) for each elements of the basis (3.67), and express them as

$$\begin{pmatrix} f_1^{qq0^+} \\ f_2^{qq0^+} \end{pmatrix} = \mathfrak{P}^{qq0^+}[b_I] \begin{pmatrix} f_1^{qq0^+} \\ f_2^{qq0^+} \end{pmatrix}. \tag{3.73}$$

The 2×2 matrices becomes

$$\begin{aligned}
&\mathfrak{P}^{qq0^+}[b_I] = \\
&\left\{ \begin{pmatrix} \mathcal{A}^2 s - 4\mathcal{B}^2 & -4\mathcal{A}\mathcal{B} \\ -2\mathcal{A}\mathcal{B}s & 2\mathcal{B}^2 - \frac{\mathcal{A}^2 s}{2} \end{pmatrix}, \begin{pmatrix} 2\mathcal{A}\mathcal{B}s & \frac{\mathcal{A}^2 s}{2} - 2\mathcal{B}^2 \\ \frac{\mathcal{A}^2 s^2}{4} - \mathcal{B}^2 s & -\mathcal{A}\mathcal{B}s \end{pmatrix}, \begin{pmatrix} \mathcal{A}\mathcal{B}s & \frac{\mathcal{A}^2 s}{4} - \mathcal{B}^2 \\ \frac{\mathcal{A}^2 s^2}{2} - 2\mathcal{B}^2 s & -2\mathcal{A}\mathcal{B}s \end{pmatrix}, \right. \\
&\begin{pmatrix} 2\mathcal{B}^2 - \frac{\mathcal{A}^2 s}{2} & 2\mathcal{A}\mathcal{B} \\ 4\mathcal{A}\mathcal{B}s & \mathcal{A}^2 s - 4\mathcal{B}^2 \end{pmatrix}, \begin{pmatrix} 2\mathcal{A}^2 s - 8\mathcal{B}^2 & -8\mathcal{A}\mathcal{B} \\ -4\mathcal{A}\mathcal{B}s & 4\mathcal{B}^2 - \mathcal{A}^2 s \end{pmatrix}, \begin{pmatrix} 4\mathcal{A}\mathcal{B}s & \mathcal{A}^2 s - 4\mathcal{B}^2 \\ \frac{\mathcal{A}^2 s^2}{2} - 2\mathcal{B}^2 s & -2\mathcal{A}\mathcal{B}s \end{pmatrix}, \\
&\begin{pmatrix} 2\mathcal{A}\mathcal{B}s & \frac{\mathcal{A}^2 s}{2} - 2\mathcal{B}^2 \\ \mathcal{A}^2 s^2 - 4\mathcal{B}^2 s & -4\mathcal{A}\mathcal{B}s \end{pmatrix}, \begin{pmatrix} 4\mathcal{B}^2 - \mathcal{A}^2 s & 4\mathcal{A}\mathcal{B} \\ 8\mathcal{A}\mathcal{B}s & 2\mathcal{A}^2 s - 8\mathcal{B}^2 \end{pmatrix}, \begin{pmatrix} 4\mathcal{A}^2 s - 16\mathcal{B}^2 & -16\mathcal{A}\mathcal{B} \\ -32\mathcal{A}\mathcal{B}s & 32\mathcal{B}^2 - 8\mathcal{A}^2 s \end{pmatrix}, \\
&\left. \begin{pmatrix} 8\mathcal{A}\mathcal{B}s & 2\mathcal{A}^2 s - 8\mathcal{B}^2 \\ 4\mathcal{A}^2 s^2 - 16\mathcal{B}^2 s & -16\mathcal{A}\mathcal{B}s \end{pmatrix}, \begin{pmatrix} 16\mathcal{A}\mathcal{B}s & 4\mathcal{A}^2 s - 16\mathcal{B}^2 \\ 2\mathcal{A}^2 s^2 - 8\mathcal{B}^2 s & -8\mathcal{A}\mathcal{B}s \end{pmatrix}, \begin{pmatrix} 32\mathcal{B}^2 - 8\mathcal{A}^2 s & 32\mathcal{A}\mathcal{B} \\ 16\mathcal{A}\mathcal{B}s & 4\mathcal{A}^2 s - 16\mathcal{B}^2 \end{pmatrix} \right\}.
\end{aligned} \tag{3.74}$$

Then the Bethe-Salpeter equation becomes

$$\begin{pmatrix} f_1^{qq0^+} \\ f_2^{qq0^+} \end{pmatrix} = \mathcal{M}_\sharp^{qq0^+} \begin{pmatrix} f_1^{qq0^+} \\ f_2^{qq0^+} \end{pmatrix} \tag{3.75}$$

$$\mathcal{M}_\sharp^{qq0^+} = G[(-\tfrac{3}{4}GR+6)^{-1} - (-\tfrac{3}{4}G4R-3)^{-1}]_I{}^1 \ \mathfrak{P}^{qq0^+}[b_I]. \tag{3.76}$$

Now that we are ready to consider the problem whether or not the diquark Bethe-Salpeter equation has a bound-state solution in our truncation scheme. In the same way as §3.2.1, we plot $\mathcal{D}_\sharp^{qq0^+}$ as a function of P^2 in Fig.3.8, varying the input quark mass $m_0/\eta = 0.01, 0.1, 0.2, 0.5, 1$. As we can see from Fig.3.8, each curves has an intersection with x-axis. This means the eigenvalue condition is satisfied at that point.

We can perform parallel calculation in the case of the pseudo-scalar diquark and the axial-vector diquark. Note that the kernel (3.72) is the same but its projection into the Bethe-Salpeter kernel changes. Let us see the case of axial-vector diquark as an example. We express the Bethe-Salpeter amplitude as

$$[\Phi^{qq1^+}(P)]^\lambda = \epsilon_\mu^\lambda[\gamma_\mu f_1^{qq1^+}(p^2) + \mathrm{i}\sigma_{\mu\nu}\not{P} f_2^{qq1^+}(P^2)], \tag{3.77}$$

where $\epsilon_\mu^\lambda(\lambda = -1, 0, +1)$ is the polarization four-vector, and $\sigma_{\mu\nu} = [\gamma_\mu, \gamma_\nu]/2$, and in this case Eq.(3.74) becomes

$$\begin{aligned} &\mathfrak{P}^{qq1^+}[b_I] = \\ &\left\{ \begin{pmatrix} \frac{\mathcal{A}^2 s}{2} - 2\mathcal{B}^2 & \mathcal{A}\mathcal{B} \\ 0 & 0 \end{pmatrix}, \begin{pmatrix} \mathcal{A}\mathcal{B}s & \frac{\mathcal{B}^2}{2} - \frac{\mathcal{A}^2 s}{8} \\ 0 & 0 \end{pmatrix}, \begin{pmatrix} 0 & 0 \\ 2\mathcal{B}^2 s - \frac{\mathcal{A}^2 s^2}{2} & -\mathcal{A}\mathcal{B}s \end{pmatrix}, \right. \\ &\begin{pmatrix} 0 & 0 \\ -4\mathcal{A}\mathcal{B}s & \frac{\mathcal{A}^2 s}{2} - 2\mathcal{B}^2 \end{pmatrix}, \begin{pmatrix} 4\mathcal{B}^2 - \mathcal{A}^2 s & -2\mathcal{A}\mathcal{B} \\ 16\mathcal{A}\mathcal{B}s & 8\mathcal{B}^2 - 2\mathcal{A}^2 s \end{pmatrix}, \begin{pmatrix} -2\mathcal{A}\mathcal{B}s & \frac{\mathcal{A}^2 s}{4} - \mathcal{B}^2 \\ 8\mathcal{B}^2 s - 2\mathcal{A}^2 s^2 & -4\mathcal{A}\mathcal{B}s \end{pmatrix}, \\ &\begin{pmatrix} 4\mathcal{A}\mathcal{B}s & 2\mathcal{B}^2 - \frac{\mathcal{A}^2 s}{2} \\ \mathcal{A}^2 s^2 - 4\mathcal{B}^2 s & 2\mathcal{A}\mathcal{B}s \end{pmatrix}, \begin{pmatrix} 8\mathcal{B}^2 - 2\mathcal{A}^2 s & -4\mathcal{A}\mathcal{B} \\ 8\mathcal{A}\mathcal{B}s & 4\mathcal{B}^2 - \mathcal{A}^2 s \end{pmatrix}, \begin{pmatrix} 8\mathcal{A}^2 s - 32\mathcal{B}^2 & 16\mathcal{A}\mathcal{B} \\ 0 & 0 \end{pmatrix}, \\ &\left. \begin{pmatrix} 16\mathcal{A}\mathcal{B}s & 8\mathcal{B}^2 - 2\mathcal{A}^2 s \\ 0 & 0 \end{pmatrix}, \begin{pmatrix} 0 & 0 \\ 32\mathcal{B}^2 s - 8\mathcal{A}^2 s^2 & -16\mathcal{A}\mathcal{B}s \end{pmatrix}, \begin{pmatrix} 0 & 0 \\ -64\mathcal{A}\mathcal{B}s & 8\mathcal{A}^2 s - 32\mathcal{B}^2 \end{pmatrix} \right\}. \end{aligned} \tag{3.78}$$

The resultant eigenvalue equation is

$$\begin{pmatrix} f_1^{qq1^+} \\ f_2^{qq1^+} \end{pmatrix} = \mathcal{M}_\sharp^{qq1^+} \begin{pmatrix} f_1^{qq1^+} \\ f_2^{qq1^+} \end{pmatrix} \tag{3.79}$$

$$\mathcal{M}_\sharp^{qq1^+} = G[(-\tfrac{3}{4}GR+6)^{-1} - (-\tfrac{3}{4}G4R-3)^{-1}]_I{}^1 \ \mathfrak{P}^{qq1^+}[b_I], \tag{3.80}$$

and the behavior of $\mathcal{D}_\sharp^{qq1^+} = \det[1 - \mathcal{M}_\sharp^{qq1^+}]$ is plotted in Fig.3.8. We also plot the case of pseudo-scalar diquark in Fig.3.8.

In each plots of Fig.3.8, we use the dressed quark propagator of Fig.3.2, namely, the lowest order quark Dyson-Schwinger equation is used. In order to investigate the truncation-scheme dependence on the quark Dyson-Schwinger equation, we vary the quark self-energy function (3.49) up to $n = 6$ order, whose results of quark propagator are shown in Fig.3.4. The truncation-scheme dependence of $\mathcal{D}_\sharp^{qq0^+}$ is shown in Fig.3.9 with the input mass $m_0/\eta = 0.2$, as a reference point. From Fig.3.9,

we can see that the behavior of $\mathcal{D}_{\sharp}^{qq0^+}$ is qualitatively unchanged against the change of the quark self-energy function.

To summarize this subsection, we find, as a result of a resummation of all the completely crossed ladder diagrams, that the diquark Bethe-Salpeter equation has a bound-state solution. The solution is present in the scalar, pseudo-scalar, and axial vector diquark channel, with every input mass parameter we consider. The results are rather stable against the change of the truncation scheme of the quark Dyson-Schwinger equation.

3.2.3 Interpretation of the results and discussion

First of all, we should discuss the uncertainty of result in the previous subsection. We have essentially done two approximation: the leading order approximation of 't Hooft limit and the use of Munczek-Nemirovsky model. The uncertainty from the 't Hooft limit is discussed in §3.1.2, and we expect that the leading order approximation of 't Hooft limit gives qualitatively correct results. In a quantitative sense, the uncertainty is hard to estimate, so we postpone this issue until the uncertainty from the Munczek-Nemirovsky model is considered.

The uncertainty from the Munczek-Nemirovsky model is also hard to estimate. As mentioned in §2.2, the Munczek-Nemirovsky model is considered to be an approximation of more realistic models like the Maris-Tandy model, with a coarse graining of the infrared dynamics below about 2 GeV^2 in the momentum space. In this sense, the Munczek-Nemirovsky model can not give prediction in the precision better than 2 GeV^2. Besides, the Maris-Tandy itself is an approximation of the real dressed gluon propagator and so on. We did compare the results from Munczek-Nemirovsky model with those from lattice simulation in §2.2, and find qualitative agreement. However, these are restricted to the quark propagator at the space-like region, so an extrapolation to more complicated diagrams seems not to be sensible. Furthermore, based on an analysis of quark propagator, it is known that a naive higher order calculation with the Munczek-Nemirovsky model does not converge [107]. This means an uncertainty estimation from the next-order contribution is not reliable.

There is an extension of the Munczek-Nemirovsky model [82] which possesses one additional parameter. In general, the more adjustable parameters a model possesses, the better prediction becomes. Therefore it may be interesting to investigate the completely crossed ladder diagrams in these models.

The following discussions and interpretations are based on the results in the previous subsection. We should keep in mind they are yet tentative results.

3.2.3.a Role of the diquark pole in the baryon Green's function

As mentioned in §2.3, the diquark Green's function has a pole within the rainbow-ladder truncation. This property holds in quite generic models since the Bethe-Salpeter equation is the same as that of mesons except for the factor 1/2. Functional analysis of excited baryons utilizing the diquark pole is performed recently [22], within the rainbow-ladder truncation. In Ref. [22], first the dressed quark propagator is obtained by the use of Dyson-Schwinger equation, just as same as this thesis. Next, the diquark Bethe-Salpeter equation is analyzed in the rainbow-ladder truncation, obtaining the bound-state mass of diquark. Finally, various baryons are investigated as bound states of the

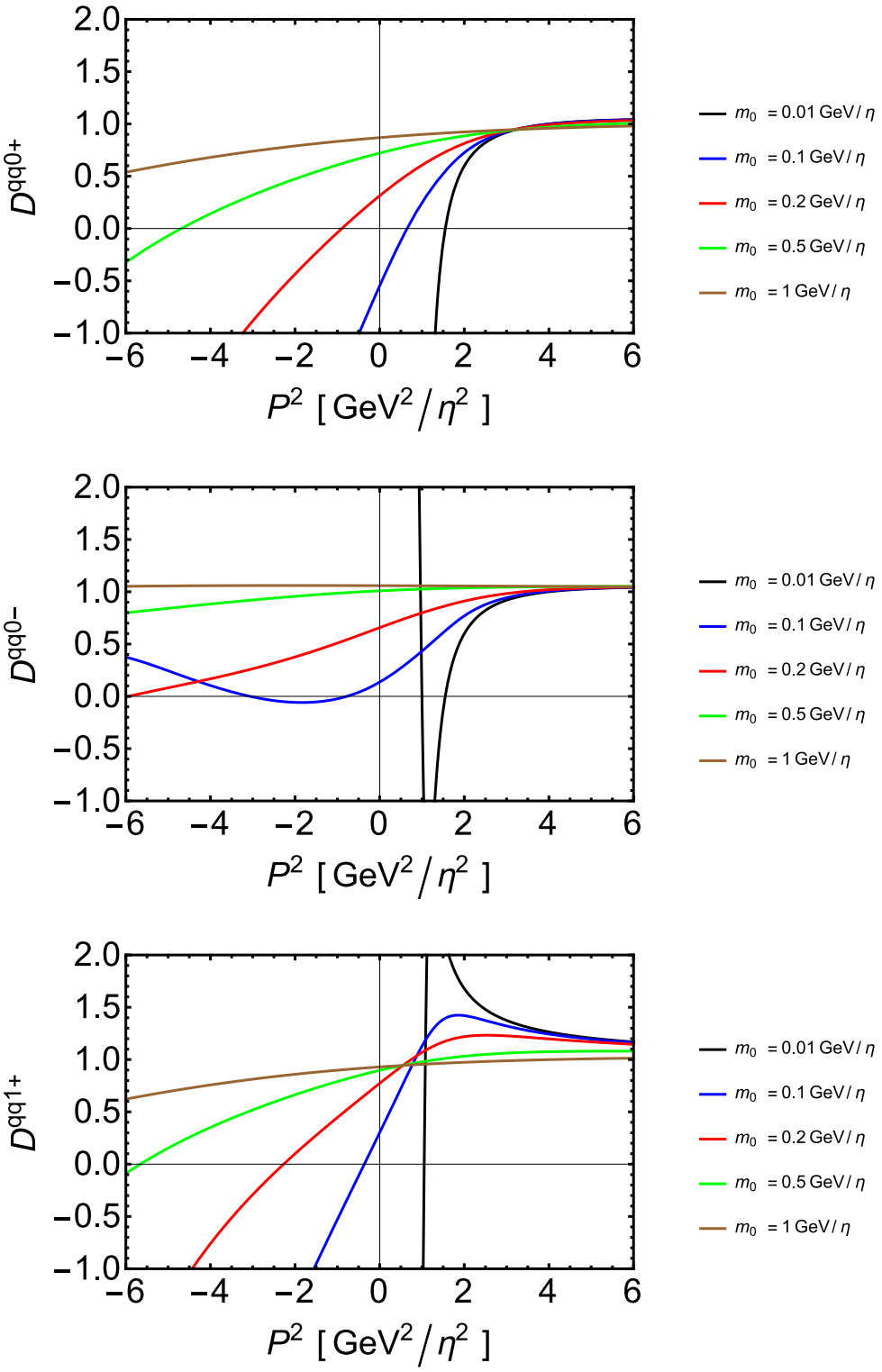

Figure 3.8: Behavior of $\mathcal{D}^{\Psi} = \det[1 - \mathcal{M}^{\Psi}_{\sharp}]$ for $\Psi = qq0^+$ and $\Psi = qq1^+$ with the input quark mass $m_0/\eta = 0.01, 0.1, 0.2, 0.5, 1$. The dressed quark propagators are those of upper two plots in Fig.3.2, with the same color-labeling.

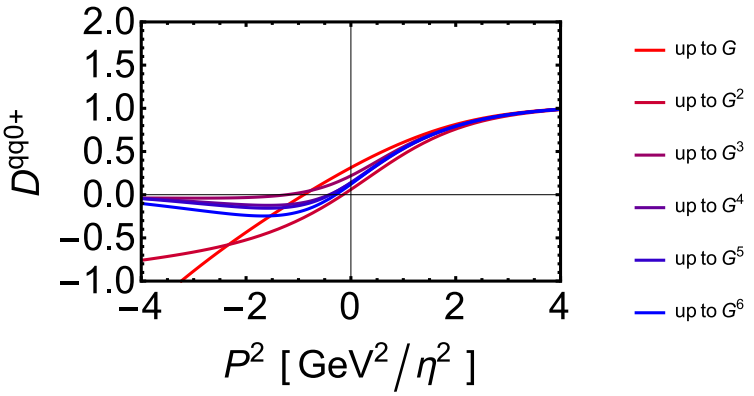

Figure 3.9: Behavior of $\mathcal{D}^{qq0^+} = \det[1 - \mathcal{M}_{\sharp}^{qq0^+}]$ with $\mathcal{M}_{\sharp}^{qq0^+}$ defined in Eq.(3.80) with the input quark mass $m_0/\eta = 0.2$ varying the truncation scheme of quark Dyson-Schwinger equation. The color of plots corresponds to that of Fig.3.4. This plot shows that the existence of the intersection with x-axis is rather stable against the truncation scheme of the quark Dyson-Schwinger equation.

dressed quark and the diquark. With adjusted two parameters in addition to the current quark mass of 7 MeV, the masses of diquark turn out to be 0.78 GeV in the scalar channel and 1.06 GeV in the axial-vector channel. Then the masses of baryons are roughly a sum of the diquark mass and a constituent quark mass. Thus the diquark masses contribute to the baryon masses in their calculation in a similar way as conventional constituent quark-diquark models. Note that the interaction between the quark and diquark is not an exchange of gluon but an exchange of quark.

What we calculate in this section, namely the pole-position of diquark Green's function, is the same as one in Ref. [22] in principle, so we expect our diquark masses enter in baryon masses in the same way.

3.2.3.b Role of the diquark pole in the tetraquark Green's function

As mentioned in §1.4.2, the existence of pole in charmed diquark Green's function is vital for the non-relativistic potential description of charmonium-like exotic mesons as bound states of diquark and anti-diquark. In this picture, the pole-position of diquark Green's function behaves as a pole mass of the diquark, and the tetraquark mass is a sum of diquark pole masses and potential energy, just like the ordinary charmonium and bottomonium.

The existence of pole in the diquark Green's function is also indispensable for the use of QCD sum rule mentioned in §1.4.2, so our result is satisfactory for the sum rule.

In §3.2.2, we consider only the diquarks composed of two quarks with equal masses, but we can perform the parallel procedure in the case of heavy-light diquarks simply by changing one of the quark mass. As a result, an intersection with x-axis is also confirmed in this case. This fact is reasonable since the intersection point persists in existing when we varying the input mass. [See Fig.3.8.]

However, as we will discuss in §3.2.3.e, the energy scale of charmed diquark may be too high to validate our calculation. Furthermore, there are some studies in which a naive extension of equal-mass system analysis to unequal-mass system analysis is not so effective [108].

Considering above two fact, we conclude that the case of heavy-light diquark needs more careful study, although our tentative result is preferred one.

3.2.3.c Relation between confinement and existence of the pole in the diquark Green's functions

The conclusion of §3.2.2 is that there is a pole in the diquark Green's functions, which contradicts to the previous works [91, 92, 109, 82]. Our calculation of §3.2.1.c shows that the analyses of Refs.[91, 92, 109, 82] are not conclusive because they did not include the effect of the completely crossed ladder diagrams correctly, so unstable against higher order corrections. Note that we adopt exactly the same model as that of Refs.[91, 109], the Munczek-Nemirovsky model. The model used in Ref.[82] is slightly different form ours but essentially the same discussion will hold, because the difference is minor. The model used in Ref.[92] is rather different from ours, but similar discussion is expected to hold because the enhancement of completely crossed ladder diagrams due to their color factor itself is universal among any models of QCD Green's function.

The absence of pole in the diquark Green's functions is regarded as a realization of the confinement in the previous works. In their scenario, diquarks drop out of the asymptotic Hilbert space because in the construction of the asymptotic Hilbert space from the total (interacting) Hilbert space, only the pole contributions survive. However, there is another confinement scenario based on the BRST formalism, that is so-called Kugo-Ojima confinement scenario [110]. In this scenario, the diquarks are confined in the same way as quarks. Therefore if we assume the Kugo-Ojima confinement mechanism to confine quarks, diquarks are automatically confined and we do not need additional confinement mechanism. In this thesis, we implicitly assume this scenario. For definiteness, we briefly review the Kugo-Ojima confinement mechanism in the appendix A.

3.2.3.d Space-like poles at small current quark masses

In Fig.3.8, there are space-like poles ($P^2 > 0$), which are not consistent with the usual bound state picture. We regard this behavior as a model artifact because of the uncertainty discussed in the beginning of this subsection.

3.2.3.e Crossed ladder diagrams in non-relativistic bound states

It is very well known that the ladder truncation is a good approximation in the case of hydrogen-like atoms and heavy quarkonium states. What happens to the crossed ladder diagrams in these system?

First of all, there is no color-factor enhancement explained in §3.1 in the case of the hydrogen-like atom and the heavy quarkonium. Furthermore, for example in the case of the hydrogen, the proton and the electron composing the hydrogen are nearly on-shell, and the crossed ladder diagrams are suppressed by the off-shell-ness in this situation.

It is known from the analysis of usual charmonium states like J/ψ, that the quark with mass around 1 GeV can be treated as a non-relativistic object. Therefore, the analysis of diquarks with

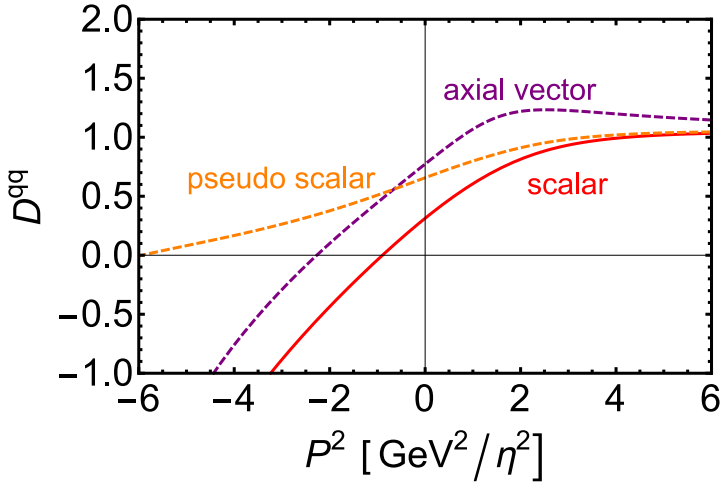

Figure 3.10: Comparison of the $\mathcal{D}^{qq0^+}$(scalar), $\mathcal{D}^{qq0^-}$(pseudo scalar) and $\mathcal{D}^{qq1^+}$(axial vector) obtained by the resummation of all the completely crossed ladder diagrams with the input mass $m_0/\eta = 0.2$ as a reference point. In each plots, the quark Dyson-Schwinger equation (3.32) is used in calculating the dressed quark propagator.

$m_0 = 1$ GeV in this chapter will not be conclusive since we neglect these kinds of kinematical suppression factors.

3.2.3.f Origin of the large excitation energy to solve the missing resonance problem

As stated in §1.4.1, the original motivation to introducing the diquark degrees of freedom is to reduce the number of states predicted in the quark model (a partial solution of the missing resonance problem). For this end, relatively large excitation energies between $\ell = 0$ diquarks and $\ell = 1$ diquarks are assumed. We think the many-gluon-exchange interaction considered in this thesis supports this assumption. Indeed, from Fig.3.10, we can read that the pseudo-scalar diquark mass turns out to be much heavier than that of scalar diquark and vector diquark.

3.2.3.g Origin of the abnormally strong force to form compact bound state

The vital assumption of the diquark models is that its size is small enough to separate the dynamics inside and outside hadron, so some abnormally strong force between the two quarks to form the compact bound state is needed. However, it is very hard for the one-gluon exchange potential to fulfill such a situation because the interaction strength of two quarks is half of that of quark and anti-quark, which is independent of the dynamics. The interaction between two quarks with many-gluon exchange considered in this thesis is a candidate of this force. Indeed, from Fig.3.11, we can read that the mass obtained with the completely crossed ladder resummation is lighter than that with the ladder truncation, indicating the strong binding force.

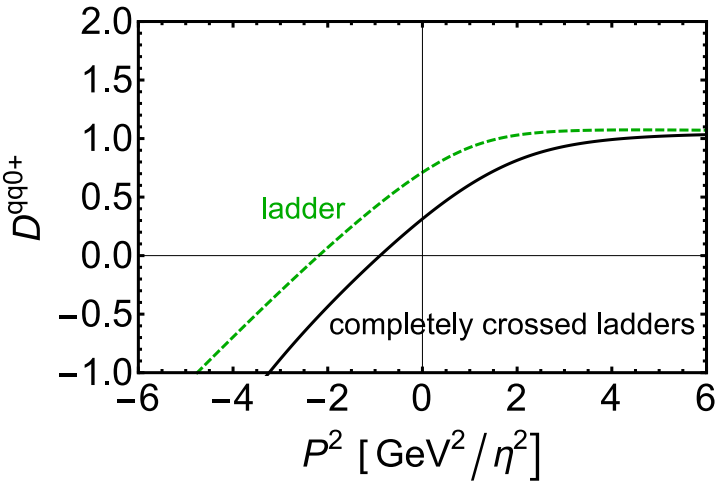

Figure 3.11: Comparison of the $\mathcal{D}^{qq0^+}$ with ladder truncation (3.37) and one obtained by the resummation of all the completely crossed ladder diagrams (3.76) with the input mass $m_0/\eta = 0.2$ as a reference point. In both plots, the quark Dyson-Schwinger equation (3.32) is used in calculating the dressed quark propagator.

Chapter 4

Summary

Diquarks are important ingredients for the studies of hadron spectra especially excited baryons and exotic mesons, but their properties are not yet understood well. One standard way to investigate such two-particle system is the use of Bethe-Salpeter equation. However, in contrast to the case of mesons, there is very little knowledge about which kinds of diagrams to be included in the diquark Bethe-Salpeter kernel. In fact, it is controversial issue whether or not the diquark Bethe-Salpeter equation has a bound-state solution.

In this thesis, we point out the importance of hitherto neglected completely crossed ladder diagrams, which are enhanced due to their color factors in the diquark Green's function. First we showed this fact under the 't Hooft limit because the 't Hooft limit makes the essence clear. Based on this finding, we performed a resummation of the completely crossed ladder diagrams with an arbitrary number of gluon-exchange, incorporating a simple model of dressed gluon propagator and dressed quark-gluon vertex, the Munczek-Nemirovsky model. As a result of our analysis, we found that there is a bound-state solution in the diquark Bethe-Salpeter equation.

Although the model artifact of Munczek-Nemirovsky model is thought to be quite large and what we obtained are tentative results, our results seem to be consistent with phenomenologically favored properties of diquarks. For example, it is found that the completely crossed ladder diagrams gives the large excitation energy of diquarks, which is one of the vital assumptions in the diquark models for baryons as a partial solution of the missing resonance problem. In the case of charmed diquarks, which are considered to be effective degrees of freedom in some models for exotic mesons, the existence of pole in the diquark Green's function supports the frequently used non-relativistic potential picture.

We anticipate that the completely crossed ladder diagrams in the diquark Green's function will play a key role in the study of the infrared QCD.

Acknowledgement

The author is grateful to his supervisor K. Hamaguchi for kind advises and stimulative discussions throughout the Ph.D. course, and reading this manuscript and giving comments.

The author thanks R. Jinno and T. Kitahara for the fruitful collaboration. The main results of this thesis are the fruits of the work with them.

The author wishes to express his sincere gratitude to K. Fukusima, the main referee of this thesis, for many valuable comments. The author is also grateful to T. Hatsuda, R. Hayano, Y. Kikukawa, and S. Matsumoto, the co-referees of this thesis, for various useful comments.

The author thanks T. Nishi for letting him notice the observation of the exotic meson in LHCb, which eventually leads him to the subject of this thesis.

Finally, the author thanks all the members of particle physics theory group at University of Tokyo for their hospitality.

Appendix A

Kugo-Ojima confinement of diquarks

We briefly review the BRST quantization of QCD and the Kugo-Ojima confinement mechanism, which is mentioned in §3.2.3.

In the expression (2.1), the BRST (Becchi-Rouet-Stora-Tyutin) symmetry [111, 112] is manifest:

$$\begin{aligned} &\{\mathrm{i}Q_B, \psi_i\} = \mathrm{i}g(t^a)_i^j c^a \psi_j, \quad [\mathrm{i}Q_B, A_\mu^a] = D_\mu c^a, \\ &\{\mathrm{i}Q_B, c^a\} = -\tfrac{g}{2} f_{abc} c^b c^c, \quad \{\mathrm{i}Q_B, \bar{c}^a\} = \mathrm{i}B^a, \quad [\mathrm{i}Q_B, B^a] = 0, \end{aligned} \tag{A.1}$$

where Q_B is the generator of BRST transformation, $(t^a)_i^j$ is the generator of the SU(3) transformation, and we show the color indices of quark fields explicitly.

Then we introduce two Hilbert spaces. The first one $\mathcal{H}^{\text{asym.}}$ is the asymptotic Hilbert space of total theory (2.1). The asymptotic state is defined to satisfy the free-particle equation of motion. This space consists of free-particle gluons, quarks, ghosts, and various bound states, and is indefinite norm space. We introduce two subspace of $\mathcal{H}^{\text{asym.}}$ as follows:

$$\mathscr{V}_{\text{phys}} : \quad \{|f\rangle \,|\, |f\rangle \in \mathcal{H}^{\text{asym.}}, Q_B |f\rangle = 0\} \tag{A.2}$$

$$\mathscr{V}_0 \quad : \quad \{|\chi\rangle \,|\, |\chi\rangle \in \mathscr{V}_{\text{phys}}, \langle\chi|\chi\rangle = 0\}\,. \tag{A.3}$$

The second one $\mathcal{H}^{\text{phys.}}$ is the physical Hilbert space defined as a quotient space $\mathcal{H}^{\text{phys.}} = \mathscr{V}_{\text{phys}}/\mathscr{V}_0$, namely,

$$\mathcal{H}^{\text{phys.}} : \quad |\hat{f}\rangle = \left\{|f'\rangle \,|\, |f'\rangle - |f\rangle \in \mathscr{V}_0, |f'\rangle \in \mathscr{V}_{\text{phys}}\right\}. \tag{A.4}$$

Since the BRST charge commute with the energy-momentum operator and other conserved charges, the asymptotic states in $\mathcal{H}^{\text{asym.}}$ are the irreducible representation of the BRST algebra. One can find $Q_B^2 = 0$ form Eqs.(A.1), so the asymptotic states in $\mathcal{H}^{\text{asym.}}$ are either singlet or doublet representation of BRST algebra. The definition of the BRST singlet and the BRST doublet are as follows: Suppose $|\varphi_{\text{d}}\rangle \equiv Q_B |\varphi_{\text{p}}\rangle \neq 0$. In this situation, it is called that $|\varphi_{\text{p}}\rangle$ and $|\varphi_{\text{d}}\rangle$ form the BRST doublet, and $|\varphi_{\text{p}}\rangle$ is called the BRST parent whereas $|\varphi_{\text{d}}\rangle$ is called the BRST daughter. Note that $Q_B |\varphi_{\text{d}}\rangle = 0$ because $Q_B^2 = 0$. The BRST singlet state is the state which satisfies $Q_B |\varphi_{\text{s}}\rangle = 0$ but can not written as $|\varphi_{\text{s}}\rangle = Q_B |\text{any states}\rangle$. It is proven that all BRST doublet states in $\mathscr{V}_{\text{phys}}$ are zero norm states [110].

Table A.1: Examples of the BRST doublets. The second column stands for the doublet of longitudinal gluon and ghost. The third and fourth columns stand for the doublet of transverse gluon and a bound state of transverse gluon-ghost, and the doublet of quark and a bound state of quark-ghost, respectively. We need a non-perturbative treatment to construct the BRST daughters of these doublet because they are bound states. The fifth column stands for the doublet of diquark and a bound state of diquark-ghost.

condition to form the BRST doublet	generic	Kugo-Ojima confinement scenario		
BRST parents	$A_{\text{longi.}}$ (longitudinal gluon)	$A_{\text{trans.}}$ (transverse gluon)	ψ (quark)	$\psi\psi$ (diquark)
BRST daughters	c	$cA_{\text{trans.}}$	$c\psi$	$c\psi\psi$

Kugo-Ojima confinement mechanism

Furthermore, if certain condition is satisfied, any colored state is BRST doublet state and disappears from the physical spectrum of $\mathcal{H}^{\text{phys}}$. In order words, the physical state is gauge singlet state. We show examples of the BRST doublet states in Tab.A.1.

In this scenario, quarks in $\mathcal{H}^{\text{asym.}}$do not appear as a finite norm state in $\mathscr{V}_{\text{phys}}$. This property is considered to be one realization of confinement, and nowadays called "Kugo-Ojima comfinement scenario." In exactly the same way as quarks, diquarks can be the elements of $\mathcal{H}^{\text{asym.}}$even if they are invisible in $\mathscr{V}_{\text{phys}}$.

In this thesis, we treat the diquarks as an element of $\mathcal{H}^{\text{asym.}}$. It is worth emphasizing that the diquarks in $\mathcal{H}^{\text{asym.}}$are automatically confined once the Kugo-Ojima confinement scenario is confirmed. There are some arguments for the evidence of diquark confinement showing a disappearance of bound state solution to the diquark Bethe-Salpeter equation [91, 92, 109] or showing an infrared divergence of the mass of diquark bound state [113], but there are not necessary as long as the Kugo-Ojima confinement scenario is assumed for the confinement of gluons or quarks (either heavy or light).

The BRST formalism explained above is summarized as the following schematic figure:

$$\begin{array}{ccccc} \mathcal{H}^{\text{tot.}} & = & \mathcal{H}^{\text{asym.}} & \supset & \mathscr{V}_{\text{phys}} \supset \mathscr{V}_0 \\ & & \cup & & \\ & & \text{gluon, quark diquark, hadron,...} & & \end{array} \qquad \begin{array}{c} \mathcal{H}^{\text{phys}} = \mathscr{V}_{\text{phys}}/\mathscr{V}_0 \\ \cup \\ \text{hadron} \end{array} \tag{A.5}$$

and what we discuss in this thesis is the diquarks in the $\mathcal{H}^{\text{asym.}}$.

Does the Kugo-Ojima confinement occur in the real world?

It is not proven that the criterion of the Kugo-Ojima confinement scenario is satisfied, but some indirect evidences are reported and the quest for proof is carried on. One direct approach is to investigate the bound states of gluon-ghost or quark-ghost (see Tab.A.1), and examine whether or not they have degenerate masses and indefinite metric. However, this kind of study is difficult because we have to know the behavior of exact ghost propagator and the exact gluon-ghost vertex. The current status of this approach is that it just started [114].

A useful sufficient condition for the Kugo-Ojima criterion in the Landau gauge is discovered in 1995 [115], which is certain divergent behavior of the ghost propagator in an infrared limit. Note that some resent lattice studies report an indication that the condition is not realized [116], but still the situation is unclear.

Bibliography

[1] G. Mishima, R. Jinno, and T. Kitahara, "Diquark Bound States with a Completely Crossed Ladder Truncation," *Phys. Rev.* **D91** no. 7, (2015) 076011, arXiv:1502.05415 [nucl-th].

[2] M. Gell-Mann, "A Schematic Model of Baryons and Mesons," *Phys. Lett.* **8** (1964) 214–215.

[3] G. Zweig, "An $SU(3)$ Model for Strong Interaction Symmetry and Its Breaking. Version 1,".

[4] M. Y. Han and Y. Nambu, "Three Triplet Model with Double $SU(3)$ Symmetry," *Phys. Rev.* **139** (1965) B1006–B1010.

[5] H. D. Politzer, "Reliable Perturbative Results for Strong Interactions?," *Phys. Rev. Lett.* **30** (1973) 1346–1349.

[6] D. J. Gross and F. Wilczek, "Ultraviolet Behavior of Nonabelian Gauge Theories," *Phys. Rev. Lett.* **30** (1973) 1343–1346.

[7] H. Fritzsch, M. Gell-Mann, and H. Leutwyler, "Advantages of the Color Octet Gluon Picture," *Phys. Lett.* **B47** (1973) 365–368.

[8] M. Ida and R. Kobayashi, "Baryon Resonances in a Quark Model," *Prog. Theor. Phys.* **36** (1966) 846.

[9] D. B. Lichtenberg and L. J. Tassie, "Baryon Mass Splitting in a Boson-Fermion Model," *Phys. Rev.* **155** (1967) 1601–1606.

[10] M. Anselmino and E. Predazzi, eds., *Diquarks 3. Proceedings, 3Rd Workshop, Torino, Italy, October 28-30, 1996.* 1998.

[11] C. J. Burden, L. Qian, C. D. Roberts, P. C. Tandy, and M. J. Thomson, "Ground State Spectrum of Light Quark Mesons," *Phys. Rev.* **C55** (1997) 2649–2664, arXiv:nucl-th/9605027 [nucl-th].

[12] M. B. Hecht, M. Oettel, C. D. Roberts, S. M. Schmidt, P. C. Tandy, and A. W. Thomas, "Nucleon Mass and Pion Loops," *Phys. Rev.* **C65** (2002) 055204, arXiv:nucl-th/0201084 [nucl-th].

[13] C. D. Roberts, I. C. Cloet, L. Chang, and H. L. L. Roberts, "Dressed-Quarks and the Roper Resonance," *AIP Conf. Proc.* **1432** (2012) 309–312, arXiv:1108.1327 [nucl-th].

[14] **PACS-CS** Collaboration, S. Aoki *et al.*, "2+1 Flavor Lattice QCD Toward the Physical Point," *Phys. Rev.* **D79** (2009) 034503, arXiv:0807.1661 [hep-lat].

[15] T. Ishikawa, T. Blum, M. Hayakawa, T. Izubuchi, C. Jung, and R. Zhou, "Full Qed+QCD Low-Energy Constants Through Reweighting," *Phys. Rev. Lett.* **109** (2012) 072002, arXiv:1202.6018 [hep-lat].

[16] S. Aoki *et al.*, "1+1+1 Flavor QCD + Qed Simulation at the Physical Point," *Phys. Rev.* **D86** (2012) 034507, arXiv:1205.2961 [hep-lat].

[17] **Budapest-Marseille-Wuppertal** Collaboration, S. Borsanyi *et al.*, "Isospin Splittings in the Light Baryon Octet from Lattice QCD and Qed," *Phys. Rev. Lett.* **111** no. 25, (2013) 252001, arXiv:1306.2287 [hep-lat].

[18] S. Borsanyi *et al.*, "Ab Initio Calculation of the Neutron-Proton Mass Difference," *Science* **347** (2015) 1452–1455, arXiv:1406.4088 [hep-lat].

[19] G. Eichmann, R. Alkofer, A. Krassnigg, and D. Nicmorus, "Nucleon Mass from a Covariant Three-Quark Faddeev Equation," *Phys. Rev. Lett.* **104** (2010) 201601, arXiv:0912.2246 [hep-ph].

[20] H. Sanchis-Alepuz, G. Eichmann, S. Villalba-Chavez, and R. Alkofer, "Delta and Omega Masses in a Three-Quark Covariant Faddeev Approach," *Phys. Rev.* **D84** (2011) 096003, arXiv:1109.0199 [hep-ph].

[21] H. Sanchis-Alepuz and C. S. Fischer, "Octet and Decuplet Masses: a Covariant Three-Body Faddeev Calculation," *Phys. Rev.* **D90** no. 9, (2014) 096001, arXiv:1408.5577 [hep-ph].

[22] H. L. L. Roberts, L. Chang, I. C. Cloet, and C. D. Roberts, "Masses of Ground and Excited-State Hadrons," *Few Body Syst.* **51** (2011) 1–25, arXiv:1101.4244 [nucl-th].

[23] **Particle Data Group** Collaboration, K. A. Olive *et al.*, "Review of Particle Physics," *Chin. Phys.* **C38** (2014) 090001.

[24] E. Santopinto and J. Ferretti, "Strange and nonstrange baryon spectra in the relativistic interacting quark-diquark model with a Gursey and Radicati-inspired exchange interaction," *Phys. Rev.* **C92** no. 2, (2015) 025202, arXiv:1412.7571 [nucl-th].

[25] J. Ferretti, A. Vassallo, and E. Santopinto, "Relativistic Quark-Diquark Model of Baryons," *Phys. Rev.* **C83** (2011) 065204.

[26] **Particle Data Group** Collaboration, J. Beringer *et al.*, "Review of Particle Physics (Rpp)," *Phys. Rev.* **D86** (2012) 010001.

[27] R. Bijker, F. Iachello, and A. Leviatan, "Algebraic Models of Hadron Structure. 1. Nonstrange Baryons," *Annals Phys.* **236** (1994) 69–116, arXiv:nucl-th/9402012 [nucl-th].

[28] R. Bijker, F. Iachello, and A. Leviatan, "Algebraic Models of Hadron Structure. 2. Strange Baryons," *Annals Phys.* **284** (2000) 89–133, arXiv:nucl-th/0004034 [nucl-th].

[29] **LHCb** Collaboration, R. Aaij *et al.*, "Observation of J/ψ p Resonances Consistent with Pentaquark States in $\Lambda_b^0 \to J/\psi\, K^- p$ Decays," *Phys. Rev. Lett.* **115** (2015) 072001, arXiv:1507.03414 [hep-ex].

[30] L. Maiani, A. D. Polosa, and V. Riquer, "The New Pentaquarks in the Diquark Model," *Phys. Lett.* **B749** (2015) 289–291, arXiv:1507.04980 [hep-ph].

[31] R. F. Lebed, "The Pentaquark Candidates in the Dynamical Diquark Picture," *Phys. Lett.* **B749** (2015) 454–457, arXiv:1507.05867 [hep-ph].

[32] V. V. Anisovich, M. A. Matveev, J. Nyiri, A. V. Sarantsev, and A. N. Semenova, "Pentaquarks and Resonances in the pJ/ψ Spectrum," arXiv:1507.07652 [hep-ph].

[33] G.-N. Li, M. He, and X.-G. He, "Some Predictions of Diquark Model for Hidden Charm Pentaquark Discovered at the Lhcb," arXiv:1507.08252 [hep-ph].

[34] R. F. Lebed, "A New Dynamical Picture for the Production and Decay of the XYZ Mesons," 2015. arXiv:1508.03320 [hep-ph]. http://inspirehep.net/record/1387768/files/arXiv:1508.03320.pdf.

[35] V. V. Anisovich, M. A. Matveev, J. Nyiri, A. V. Sarantsev, and A. N. Semenova, "Non-Strange and Strange Pentaquarks with Hidden Charm," *Int. J. Mod. Phys.* **A30** (2015) 1550190, arXiv:1509.04898 [hep-ph].

[36] L. Maiani, A. D. Polosa, and V. Riquer, "From Pentaquarks to Dibaryons in Lambda$_b$(5620) Decays," *Phys. Lett.* **B750** (2015) 37–38, arXiv:1508.04459 [hep-ph].

[37] R. Zhu and C.-F. Qiao, "Novel Pentaquarks from Diquark-Triquark Model," arXiv:1510.08693 [hep-ph].

[38] **LEPS** Collaboration, T. Nakano *et al.*, "Evidence for a Narrow S = +1 Baryon Resonance in Photoproduction from the Neutron," *Phys. Rev. Lett.* **91** (2003) 012002, arXiv:hep-ex/0301020 [hep-ex].

[39] **LEPS** Collaboration, T. Nakano *et al.*, "Evidence of the Theta+ in the Gamma D —≫ K+ K- Pn Reaction," *Phys. Rev.* **C79** (2009) 025210, arXiv:0812.1035 [nucl-ex].

[40] R. L. Jaffe, "Exotica," *Phys. Rept.* **409** (2005) 1–45, arXiv:hep-ph/0409065 [hep-ph].

[41] Y. Kato, "New Result on Θ^+ from Leps," *Few Body Syst.* **54** (2013) 1245–1249.

[42] T. Liu, Y. Mao, and B.-Q. Ma, "Present Status on Experimental Search for Pentaquarks," *Int. J. Mod. Phys.* **A29** no. 13, (2014) 1430020, arXiv:1403.4455 [hep-ex].

[43] Y. Kiyo and Y. Sumino, "Perturbative Heavy Quarkonium Spectrum at Next-To-Next-To-Next-To-Leading Order," *Phys. Lett.* **B730** (2014) 76–80, arXiv:1309.6571 [hep-ph].

[44] S. Recksiegel and Y. Sumino, "Fine and Hyperfine Splittings of Charmonium and Bottomonium: an Improved Perturbative QCD Approach," *Phys. Lett.* **B578** (2004) 369–375, arXiv:hep-ph/0305178 [hep-ph].

[45] T. Barnes, S. Godfrey, and E. S. Swanson, "Higher Charmonia," *Phys. Rev.* **D72** (2005) 054026, arXiv:hep-ph/0505002 [hep-ph].

[46] C. S. Fischer, S. Kubrak, and R. Williams, "Mass Spectra and Regge Trajectories of Light Mesons in the Bethe-Salpeter Approach," *Eur. Phys. J.* **A50** (2014) 126, arXiv:1406.4370 [hep-ph].

[47] N. SouCHLas, "Bethe-Salpeter Dynamics and the Constituent Mass Concept for Heavy Quark Mesons," *Phys. Rev.* **D81** (2010) 114019.

[48] C. B. Lang, L. Leskovec, D. Mohler, and S. Prelovsek, "Vector and Scalar Charmonium Resonances with Lattice QCD," *JHEP* **09** (2015) 089, arXiv:1503.05363 [hep-lat].

[49] **Belle** Collaboration, S. K. Choi *et al.*, "Observation of a Narrow Charmonium - Like State in Exclusive $B_\pm \to K_\pm \pi^+ \pi^- J/\Psi$ Decays," *Phys. Rev. Lett.* **91** (2003) 262001, arXiv:hep-ex/0309032 [hep-ex].

[50] **CDF** Collaboration, D. Acosta *et al.*, "Observation of the Narrow State $X(3872) \to J/\Psi\pi^+\pi^-$ in $\bar{p}p$ Collisions at $\sqrt{s} = 1.96$ TeV," *Phys. Rev. Lett.* **93** (2004) 072001, arXiv:hep-ex/0312021 [hep-ex].

[51] **BaBar** Collaboration, B. Aubert *et al.*, "Observation of the Decay $B \to J/\Psi\eta K$ and Search for $X(3872) \to J/\Psi\eta$," *Phys. Rev. Lett.* **93** (2004) 041801, arXiv:hep-ex/0402025 [hep-ex].

[52] **D0** Collaboration, V. M. Abazov *et al.*, "Observation and Properties of the $X(3872)$ Decaying to $J/\psi\pi^+\pi^-$ in $p\bar{p}$ Collisions at $\sqrt{s} = 1.96$ TeV," *Phys. Rev. Lett.* **93** (2004) 162002, arXiv:hep-ex/0405004 [hep-ex].

[53] **LHCb** Collaboration, R. Aaij *et al.*, "Observation of $X(3872)$ Production in pp Collisions at $\sqrt{s} = 7$ TeV," *Eur. Phys. J.* **C72** (2012) 1972, arXiv:1112.5310 [hep-ex].

[54] L. Maiani, F. Piccinini, A. D. Polosa, and V. Riquer, "Diquark-Antidiquarks with Hidden Or Open Charm and the Nature of X(3872)," *Phys. Rev.* **D71** (2005) 014028, arXiv:hep-ph/0412098 [hep-ph].

[55] **Belle** Collaboration, R. Mizuk *et al.*, "Dalitz Analysis of $B \to K\pi + \psi$-prime Decays and the Z(4430)+," *Phys. Rev.* **D80** (2009) 031104, arXiv:0905.2869 [hep-ex].

[56] **LHCb** Collaboration, R. Aaij *et al.*, "Observation of the Resonant Character of the $Z(4430)^-$ State," *Phys. Rev. Lett.* **112** no. 22, (2014) 222002, arXiv:1404.1903 [hep-ex].

[57] S. J. Brodsky, D. S. Hwang, and R. F. Lebed, "Dynamical Picture for the Formation and Decay of the Exotic Xyz Mesons," *Phys. Rev. Lett.* **113** no. 11, (2014) 112001, arXiv:1406.7281 [hep-ph].

[58] Z.-G. Wang, "Analysis of the Scalar and Axial-Vector Heavy Diquark States with QCD Sum Rules," *Eur. Phys. J.* **C71** (2011) 1524, arXiv:1008.4449 [hep-ph].

[59] R. T. Kleiv, T. G. Steele, A. Zhang, and I. Blokland, "Heavy-Light Diquark Masses from QCD Sum Rules and Constituent Diquark Models of Tetraquarks," *Phys. Rev.* **D87** no. 12, (2013) 125018, arXiv:1304.7816 [hep-ph].

[60] M. A. Shifman, A. I. Vainshtein, and V. I. Zakharov, "QCD and Resonance Physics. Theoretical Foundations," *Nucl. Phys.* **B147** (1979) 385–447.

[61] M. A. Shifman, A. I. Vainshtein, and V. I. Zakharov, "QCD and Resonance Physics: Applications," *Nucl. Phys.* **B147** (1979) 448–518.

[62] H. G. Dosch, M. Jamin, and B. Stech, "Diquarks, QCD Sum Rules and Weak Decays," *Z. Phys.* **C42** (1989) 167.

[63] M. Jamin and M. Neubert, "Diquark Decay Constants from QCD Sum Rules," *Phys. Lett.* **B238** (1990) 387.

[64] N. Nakanishi, "Covariant Quantization of the Electromagnetic Field in the Landau Gauge," *Prog. Theor. Phys.* **35** (1966) 1111–1116.

[65] B. Lautrup, "Canonical Quantum Electrodynamics in Covariant Gauges," *Kong. Dan. Vid. Sel. Mat. Fys. Med.* **35** no. 11, (1967) .

[66] L. D. Faddeev and V. N. Popov, "Feynman Diagrams for the Yang-Mills Field," *Phys. Lett.* **B25** (1967) 29–30.

[67] K. Fujikawa, B. W. Lee, and A. I. Sanda, "Generalized Renormalizable Gauge Formulation of Spontaneously Broken Gauge Theories," *Phys. Rev.* **D6** (1972) 2923–2943.

[68] M. Gell-Mann and F. Low, "Bound States in Quantum Field Theory," *Phys. Rev.* **84** (1951) 350–354.

[69] E. E. Salpeter and H. A. Bethe, "A Relativistic Equation for Bound State Problems," *Phys. Rev.* **84** (1951) 1232–1242.

[70] L. D. Faddeev, "Scattering Theory for a Three Particle System," *Sov. Phys. JETP* **12** (1961) 1014–1019. [Zh. Eksp. Teor. Fiz.39,1459(1960)].

[71] F. J. Dyson, "The S Matrix in Quantum Electrodynamics," *Phys. Rev.* **75** (1949) 1736–1755.

[72] J. S. Schwinger, "On the Green's Functions of Quantized Fields. 1.," *Proc. Nat. Acad. Sci.* **37** (1951) 452–455.

[73] J. S. Schwinger, "On the Green's Functions of Quantized Fields. 2.," *Proc. Nat. Acad. Sci.* **37** (1951) 455–459.

[74] R. Alkofer and L. von Smekal, "The Infrared Behavior of QCD Green's Functions: Confinement Dynamical Symmetry Breaking, and Hadrons as Relativistic Bound States," *Phys. Rept.* **353** (2001) 281, arXiv:hep-ph/0007355 [hep-ph].

[75] P. van Nieuwenhuizen and A. Waldron, "A Continuous Wick Rotation for Spinor Fields and Supersymmetry in Euclidean Space," in *Gauge Theories, Applied Supersymmetry and Quantum Gravity. Proceedings, 2Nd Conference, London, Uk, July 5-10, 1996*, pp. 394–403. 1996. arXiv:hep-th/9611043 [hep-th].

[76] P. van Nieuwenhuizen and A. Waldron, "On Euclidean Spinors and Wick Rotations," *Phys. Lett.* **B389** (1996) 29–36, arXiv:hep-th/9608174 [hep-th].

[77] P. Maris and P. C. Tandy, "Bethe-Salpeter Study of Vector Meson Masses and Decay Constants," *Phys. Rev.* **C60** (1999) 055214, arXiv:nucl-th/9905056 [nucl-th].

[78] T. Hilger, M. Gomez-Rocha, and A. Krassnigg, "Masses of $J^{PC} = 1^{-+}$ Exotic Quarkonia in a Bethe-Salpeter-Equation Approach," *Phys. Rev.* **D91** no. 11, (2015) 114004, arXiv:1503.08697 [hep-ph].

[79] T. Hilger, M. Gomez-Rocha, and A. Krassnigg, "Investigating Light-Quarkonium Spectra in a Bethe-Salpeter-Equation Approach," arXiv:1508.07183 [hep-ph].

[80] H. Sanchis-Alepuz and C. S. Fischer, "Hyperon Elastic Electromagnetic Form Factors in the Space-Like Momentum Region," arXiv:1512.00833 [hep-ph].

[81] H. J. Munczek and A. M. Nemirovsky, "The Ground State Q Anti-Q Mass Spectrum in QCD," *Phys. Rev.* **D28** (1983) 181.

[82] M. S. Bhagwat, A. Holl, A. Krassnigg, C. D. Roberts, and P. C. Tandy, "Aspects and Consequences of a Dressed Quark Gluon Vertex," *Phys. Rev.* **C70** (2004) 035205, arXiv:nucl-th/0403012 [nucl-th].

[83] M. B. Parappilly, P. O. Bowman, U. M. Heller, D. B. Leinweber, A. G. Williams, and J. B. Zhang, "Scaling Behavior of Quark Propagator in Full QCD," *Phys. Rev.* **D73** (2006) 054504, arXiv:hep-lat/0511007 [hep-lat].

[84] P. O. Bowman, U. M. Heller, and A. G. Williams, "Lattice Quark Propagator with Staggered Quarks in Landau and Laplacian Gauges," *Phys. Rev.* **D66** (2002) 014505, arXiv:hep-lat/0203001 [hep-lat].

[85] M. S. Bhagwat, M. A. Pichowsky, C. D. Roberts, and P. C. Tandy, "Analysis of a Quenched Lattice QCD Dressed Quark Propagator," *Phys. Rev.* **C68** (2003) 015203, arXiv:nucl-th/0304003 [nucl-th].

[86] S. Furui and H. Nakajima, "Unquenched Kogut-Susskind Quark Propagator in Lattice Landau Gauge QCD," *Phys. Rev.* **D73** (2006) 074503.

[87] S. M. Dorkin, L. P. Kaptari, T. Hilger, and B. Kampfer, "Analytical Properties of the Quark Propagator from a Truncated Dyson-Schwinger Equation in Complex Euclidean Space," *Phys. Rev.* **C89** (2014) 034005, arXiv:1312.2721 [hep-ph].

[88] A. K. Kazanskii and A. N. Vasilev, "Legendre Transformations for Generating Functionals in Quantum Field Theory," *Teor. Mat. Fiz.* **12** (1972) 352–369.

[89] J. M. Cornwall, R. Jackiw, and E. Tomboulis, "Effective Action for Composite Operators," *Phys. Rev.* **D10** (1974) 2428–2445.

[90] R. T. Cahill, C. D. Roberts, and J. Praschifka, "Calculation of Diquark Masses in QCD," *Phys. Rev.* **D36** (1987) 2804.

[91] A. Bender, C. D. Roberts, and L. Von Smekal, "Goldstone Theorem and Diquark Confinement Beyond Rainbow Ladder Approximation," *Phys. Lett.* **B380** (1996) 7–12, arXiv:nucl-th/9602012 [nucl-th].

[92] G. Hellstern, R. Alkofer, and H. Reinhardt, "Diquark Confinement in an Extended Njl Model," *Nucl. Phys.* **A625** (1997) 697–712, arXiv:hep-ph/9706551 [hep-ph].

[93] G. 't Hooft, "A Planar Diagram Theory for Strong Interactions," *Nucl. Phys.* **B72** (1974) 461.

[94] E. Witten, "Baryons in the 1/N Expansion," *Nucl. Phys.* **B160** (1979) 57.

[95] S. Weinberg, "Tetraquark Mesons in Large N Quantum Chromodynamics," *Phys. Rev. Lett.* **110** (2013) 261601, arXiv:1303.0342 [hep-ph].

[96] F. J. Dyson, "Divergence of Perturbation Theory in Quantum Electrodynamics," *Phys. Rev.* **85** (1952) 631–632.

[97] M. Beneke, "Renormalons," *Phys. Rept.* **317** (1999) 1–142, arXiv:hep-ph/9807443 [hep-ph].

[98] C. Anzai, Y. Kiyo, and Y. Sumino, "Static QCD Potential at Three-Loop Order," *Phys. Rev. Lett.* **104** (2010) 112003, arXiv:0911.4335 [hep-ph].

[99] A. V. Smirnov, V. A. Smirnov, and M. Steinhauser, "Three-Loop Static Potential," *Phys. Rev. Lett.* **104** (2010) 112002, arXiv:0911.4742 [hep-ph].

[100] P. A. Baikov, K. G. Chetyrkin, J. H. Kuhn, and J. Rittinger, "Adler Function, Sum Rules and Crewther Relation of Order O(α_S^4): the Singlet Case," *Phys. Lett.* **B714** (2012) 62–65, arXiv:1206.1288 [hep-ph].

[101] M. Durgut, "Baryon Bound State in Two-Dimensional $SU(N)$ Gauge Theory," *Nucl. Phys.* **B116** (1976) 233.

[102] E. Corrigan and P. Ramond, "A Note on the Quark Content of Large Color Groups," *Phys. Lett.* **B87** (1979) 73.

[103] J. A. M. Vermaseren, "New Features of Form," arXiv:math-ph/0010025 [math-ph].

[104] J. Kuipers, T. Ueda, J. A. M. Vermaseren, and J. Vollinga, "Form Version 4.0," *Comput. Phys. Commun.* **184** (2013) 1453–1467, arXiv:1203.6543 [cs.SC].

[105] T. Maskawa and H. Nakajima, "Spontaneous Symmetry Breaking in Vector-Gluon Model," *Prog. Theor. Phys.* **52** (1974) 1326–1354.

[106] M. Bando, M. Harada, and T. Kugo, "External Gauge Invariance and Anomaly in Bs Vertices and Bound States," *Prog. Theor. Phys.* **91** (1994) 927–948, arXiv:hep-ph/9312343 [hep-ph].

[107] H. H. Matevosyan, A. W. Thomas, and P. C. Tandy, "Consequences of Fully Dressing Quark-Gluon Vertex Function with Two-Point Gluon Lines," *J. Phys.* **G34** (2007) 2153–2164, arXiv:0706.2393 [nucl-th].

[108] E. Rojas, B. El-Bennich, and J. P. B. C. de Melo, "Exciting Flavored Bound States," *Phys. Rev.* **D90** (2014) 074025, arXiv:1407.3598 [nucl-th].

[109] A. Bender, W. Detmold, C. D. Roberts, and A. W. Thomas, "Bethe-Salpeter Equation and a Nonperturbative Quark Gluon Vertex," *Phys. Rev.* **C65** (2002) 065203, arXiv:nucl-th/0202082 [nucl-th].

[110] T. Kugo and I. Ojima, "Local Covariant Operator Formalism of Nonabelian Gauge Theories and Quark Confinement Problem," *Prog. Theor. Phys. Suppl.* **66** (1979) 1–130.

[111] C. Becchi, A. Rouet, and R. Stora, "Renormalization of Gauge Theories," *Annals Phys.* **98** (1976) 287–321.

[112] I. V. Tyutin, "Gauge Invariance in Field Theory and Statistical Physics in Operator Formalism," arXiv:0812.0580 [hep-th].

[113] R. Alkofer, "QCD Green Functions and Their Application to Hadron Physics," *Braz. J. Phys.* **37** (2007) 144–164, arXiv:hep-ph/0611090 [hep-ph].

[114] N. Alkofer and R. Alkofer, "Features of Ghost-Gluon and Ghost-Quark Bound States Related to BRST Quartets," *Phys. Lett.* **B702** (2011) 158–163, arXiv:1102.2753 [hep-th].

[115] T. Kugo, "The Universal Renormalization Factors Z(1) / Z(3) and Color Confinement Condition in Nonabelian Gauge Theory," in *Brs Symmetry. Proceedings, International Symposium on the Occasion of Its 20Th Anniversary, Kyoto, Japan, September 18-22, 1995*, pp. 107–119. 1995. arXiv:hep-th/9511033 [hep-th].

[116] A. Sternbeck, M. Schaden, and V. Mader, "The Dyson-Schwinger Equation of a Link Variable in Lattice Landau Gauge Theory," *PoS* **LATTICE2014** (2015) 354, arXiv:1502.05945 [hep-lat].